Synthesis and characterisation of various mixed oxides catalysts for environmental applications

Reem Kourieh

N° d'ordre : 298-2012 Année 2012

THESE DE L'UNIVERSITE DE LYON

Délivrée par

L'UNIVERSITE CLAUDE BERNARD LYON 1

ECOLE DOCTORALE DE CHIMIE

Pour l'obtention du

DIPLOME DE DOCTORAT
(arrêté du 7 août 2006)

soutenue publiquement le 14 Décembre 2012

par

Reem KOURIEH

TITLE : **Synthesis and characterisation of various mixed oxides catalysts for environmental applications.**

TITRE : **Synthèse et caractérisation de catalyseurs de type oxydes mixtes pour des applications environnementales.**

Directeur de thèse : Mme Aline AUROUX

JURY

Mme. A. AUROUX	Directeur de thèse
Mme. S. BENNICI	Co-encadrant
Mme. A.GERVASINI	Rapporteur
Mme. V. RAKIC	Rapporteur
Mr. J.M. LANCELIN	Examinateur
Mr. J.C. VEDRINE	Examinateur
Mme. A. GIROIR-FENDLER	Membre invité

Thèse préparée au sein de
L'Institut de Recherches sur la Catalyse et l'Environnement de Lyon
(IRCELYON)
2 avenue Albert Einstein, 69626 - Villeurbanne Cedex. France

UNIVERSITE CLAUDE BERNARD - LYON 1

Président de l'Université	**M. François-Noël GILLY**
Vice-président du Conseil d'Administration	M. le Professeur Hamda BEN HADID
Vice-président du Conseil des Etudes et de la Vie Universitaire	M. le Professeur Philippe LALLE
Vice-président du Conseil Scientifique	M. le Professeur Germain GILLET
Secrétaire Général	M. Alain HELLEU

COMPOSANTES SANTE

Faculté de Médecine Lyon Est – Claude Bernard	Directeur : M. le Professeur J. ETIENNE
Faculté de Médecine et de Maïeutique Lyon Sud – Charles Mérieux	Administrateur provisoire : M. le Professeur G. KIRKORIAN
UFR d'Odontologie	Directeur : M. le Professeur D. BOURGEOIS
Institut des Sciences Pharmaceutiques et Biologiques	Directeur : Mme la Professeure C. VINCIGUERRA.
Institut des Sciences et Techniques de la Réadaptation	Directeur : M. le Professeur Y. MATILLON
Département de formation et Centre de Recherche en Biologie Humaine	Directeur : M. le Professeur P. FARGE

COMPOSANTES ET DEPARTEMENTS DE SCIENCES ET TECHNOLOGIE

Faculté des Sciences et Technologies	Directeur : M. le Professeur F. De MARCHI
Département Biologie	Directeur : M. le Professeur F. FLEURY
Département Chimie Biochimie	Directeur : Mme le Professeur H. PARROT
Département GEP	Directeur : M. N. SIAUVE
Département Informatique	Directeur : M. le Professeur S. AKKOUCHE
Département Mathématiques	Directeur : M. le Professeur A. GOLDMAN
Département Mécanique	Directeur : M. le Professeur H. BEN HADID
Département Physique	Directeur : Mme S. FLECK
Département Sciences de la Terre	Directeur : Mme la Professeure I. DANIEL
UFR Sciences et Techniques des Activités Physiques et Sportives	Directeur : M. C. COLLIGNON
Observatoire de Lyon	Directeur : M. B. GUIDERDONI
Polytech Lyon	Directeur : M. P. FOURNIER
Ecole Supérieure de Chimie Physique Electronique	Directeur : M. G. PIGNAULT
Institut Universitaire de Technologie de Lyon 1	Directeur : M. C. VITON
Institut Universitaire de Formation des Maîtres	Directeur : M. R. BERNARD
Institut de Science Financière et d'Assurances	Directeur : Mme la Professeure V. MAUME-DESCHAMPS

To my parents - - -

To my brothers - - -

To the soul of aunt Souad - -

To the soul of aunt Hind - -

Acknowledgements

This work has been accomplished from September 2009 to December 2012, carrying out the research work in Institut de Recherches sur la Catalyse et l'Environnement de Lyon (IRCELYON). I am grateful to Mr. Michel Lacroix, directeur de IRCELYON, for welcoming me in IRCELYON during my PhD.

First I would gratefully acknowledge the University of Aleppo-Syria, department of chemistry, for the financial support provided for my PhD studies.

I would like to thank my advisor Mme. Aline Auroux, directeur de recherche, in IRCELYON, leader of clean and renewable energies group. She has taught me how good research can be done. She has shown me different ways to approach a research problem and the need to be persistent to accomplish any goal. I appreciate all her contributions of time, ideas, and guidance to make my PhD experience fruitful.

I gratefully thank Dr. Simona Bennici who shared her valuable knowledge, experience and technical expertise with me during the experiments as well as valuable discussions.

Thanks also to Prof. Vesna Rakic from University of Belgrade who provided me with constant advice and encouragements as well as valuable experiences and discussions.

I also wish to express my thanks to Prof. Antonella Gervasini and Dr. Matteo Marzo from University of Milano for performing the catalytic test of cellobiose hydrolysis in this work.

I gratefully thank Dr. Anne Giroir-Fendler and Mrs. Laurence Retailleau-Mével from IRCELYON – University Lyon 1 for performing the selective catalytic reduction of NO_x in this work.

I gratefully thank Dr. A. Gervasini, Dr. A. Giroir-Fendler, Dr. V. Rakic, Dr. J.M. Lancelin (University Lyon 1) and Dr. J.C. Védrine (University Paris VI) for accepting to refer and judge this manuscript as members of my PhD jury.

I must also express my deepest gratitude and thanks to the scientific and technical services of IRCELYON for their contribution to the analyses of my samples, particularly to:

Mr. Swamy Prakash, for so much help and valuable discussions in using the FTIR apparatus.

Mrs. Laurence Massin, for XPS measurements and her valuable experience and discussions.

Mrs. Marlène Daniel, who taught me the operating of Raman spectroscopy apparatus and gave me much guidance about this technique.

Mrs. Laurence Burel, who provided TEM analysis, helping me for studying the morphology properties of my samples.

I had a real pleasure to work with my colleagues who were in the Energy Group at IRCELYON during my stay in France: Dusan Stosic, Adrien Mekki-Berrada, Hao Yu, Dr. Georgeta Postole, Sirena Bassil, Jingxuan Cai, Otman Otman, Emeline Lefebvre and Amira Jabbari-Hichri. Let me say "Thank you" to all of you for your continually unselfish help and all the happy time working together.

I also owe my earnest gratitude to all my friends both in France and in Syria who gave me their help and encouragement.

Last, but not least, I would like to thank my parents (Adonis and Raghida) who raised me with a love of science and supported me unconditionally in all my pursuits, and my brothers Aboud and Mouhannad.

Contents

List of Publications

The result of this thesis have been published or submitted to publication in several international journals which are listed below:

I. R. Kourieh, S. Bennici, A. Auroux, "Study of acidic commercial WO_x/ZrO_2 catalysts by adsorption microcalorimetry and thermal analysis technique", Journal of Thermal Analysis and Calorimetry 99 (2010) 849-853.

II. R. Kourieh, S. Bennici, A. Auroux, "Acid and redox properties of tungstated zirconia catalysts", Reaction Kinetics, Mechanism and Catalysis 105 (2012)101-111.

III. R. Kourieh, S. Bennici, M. Marzo, A. Gervasini, A. Auroux, "Investigation of the WO_3/ZrO_2 surface acidic properties for the aqueous hydrolysis of cellobiose", Catalysis Communications 19 (2012) 119-126.

IV. R. Kourieh, V. Rakic, S. Bennici, A. Auroux, "Relation between surface acidity and reactivity in fructose conversion into 5-HMF using tungstated zirconia catalysts", Catalysis Communications 30 (2013) 5-13.

V. R. Kourieh, L. Retailleau, S. Bennici, A. Giroir-Fendler, A. Auroux, "Infulence of the acidic properties of ZrO_2 based mixed oxides catalysts in the selective reduction of NO_x with n-decane", Catalysis Letters. DOI: 10.1007/s10562-012-0945-7

VI. R. Kourieh, S. Bennici, A. Auroux, "Tuning of the acid-base properties of primary Me_2O_3 (Me = Al, Ga, In) and binary (ZrO_2-Me_2O_3) (Me = B, Al, Ga, In) oxides by adding WO_3: a calorimetric study", submitted to Thermochimica Acta.

List of Communications

I. Conference of Solid Compounds of Transition Elements (SCTE 2010), 05-10th Sep., 2010: Annecy, France, "Influence of the preparative route on the properties of WO_x-ZrO_2 catalysts", R. Kourieh, S. Bennici, A. Auroux, Poster.

II. EUROPACAT X Congress, 28th Aug. – 02th Sep., 2011: Glascow, Scotland, "Influence os surface acid-base properties of tungstated zirconia catalysts on the conversion of fructose to 5-HMF", R. Kourieh, V. Rakic, S. Bennici, A. Auroux, Poster.

III. EUROPACAT X Congress, 28th Aug. – 02th Sep., 2011: Glascow, Scotland, "Catalytic hydrolysis of cellobiose to glucose on tungstated zirconia catalysts", R. Kourieh, S. Bennici, M. Marzo, A.Gervasini, A. Auroux, Poster.

IV. EUROPACAT X Congress, 28th Aug. – 02th Sep., 2011: Glascow, Scotland, "ZrO_2 based mixed oxides as catalysts for the selective reduction of NO by n-decane", R. Kourieh, L. Retailleau, S. Bennici, A. Giroir-Fendler, A. Auroux, Poster.

V. 12th European Meeting on Environmental Chemistry (EMEC 12), 7-10th Dec., 2011: Clermont-Ferrand, France, "Influence of the acid-base properties of oxide catalysts in fructose dehydration to 5-HMF", R. Kourieh, D. Stosic, V. Rakic, S. Bennici, A. Auroux, Oral presentation.

VI. Calorimetry and Thermal Effects in Catalysis (CTEC 2012), 26-29th June, 2012: Lyon, France, "Synthesis and acid-base properties of WO_3-Me_2O_3 (Me = Al, Ga, In) and WO_3/ZrO_2-Me_2O_3 (Me = B, Al, Ga, In) catalysts", R. Kourieh, S. Bennici, A. Auroux, Poster.

VII. 7th International Conference on Environmental Catalysis (ICEC 2012), 02-06th Sep., 2012: Lyon, France, "Selective Catalytic reduction of NO by n-decane on ZrO_2-Me_2O_3 (Me = B, Al, Ga, In) and $WO_3/(ZrO_2$-$Al_2O_3)$ catalysts", R. Kourieh, S. Bennici, A. Giroir-Fendler, L. Retailleau, A. Auroux, Poster.

1. Background and Introduction

It is widely acknowledged that there is a growing need for more environmentally acceptable processes in the chemical industry. This trend towards what has become known as 'Green Chemistry' [1–5] or 'Sustainable Technology' necessitates a shift from traditional concepts of process efficiency, that focus largely on chemical yield, to one that assigns economic value to eliminating waste at source and avoiding the use of toxic and/or hazardous substances. A definition of green chemistry can be formulated as follows [6]: *Green chemistry efficiently utilizes (preferably renewable) raw materials, eliminates waste and avoids the use of toxic and/or hazardous reagents and solvents in the manufacture and application of chemical products*.

My PhD work is related to the topic "Green chemistry", in particular the application of the following three main principles: (i) the role of catalysts, (ii) renewable raw materials (the conversion of renewable feedstock mainly carbohydrates) and (iii) the decrease of hazardous and toxic materials (selective catalytic reduction of NO_x by hydrocarbons).

1.1 The role of catalysis

Acid-catalyzed processes constitute one of the most important areas for the application of heterogeneous catalysis. Hundreds of solid acids have been developed in the last decades; these solid acids have been applied as catalysts for various reactions. Solid acids are used also as supports of catalysts such as metals, oxides, salts, etc. Now, solid acid catalysis is one of the economically and ecologically important fields in catalysis. The solid acid catalysts have many advantages over liquid acid catalysts. They are noncorrosive and environmentally benign, presenting fewer disposal problems. Their repeated use is possible and their separation from liquid products is much easier. Furthermore, they can be designed to give higher activity, selectivity, and longer catalyst life. Therefore, the replacement of the homogeneous catalysts with the heterogeneous ones is becoming even more important in chemical and life science industry.

Zirconia is a versatile oxide and useful catalyst support, it is amphoteric being able to show both mildly acidic and basic properties. These acid properties could be adjusted by adding a second component such as WO_3, B_2O_3, Al_2O_3, Ga_2O_3 and In_2O_3. Tungsten oxide species dispersed on zirconia support (WO_x/ZrO_2) are an interesting class of solid acids [7]. Interest in

tungstated zirconia increased since Arata and Hino showed that they could isomerize *n*-alkanes when prepared according to specific synthesis procedures [8]. Their catalytic behavior was studied for several reactions such as alcohol decomposition [9-11], alkane hydroisomerization in the presence of platinum [12-14]. Oxides such as Al_2O_3, SiO_2-Al_2O_3, TiO_2 and ZrO_2 are active in the selective catalytic reduction of NO_x by hydrcarbons [15-18]. Ga_2O_3 and In_2O_3 supported on acidic supports (Al_2O_3 - TiO_2 - SiO_2/Al_2O_3) have also been reported to present a remarkable de-NO_x catalytic activity [19-21].

1.2 Renewable raw materials

The necessity to switch from nonrenewable fossil resources to renewable raw materials, such as carbohydrates and triglycerides derived from biomass, was an important conclusion of the Report of the Club of Rome in 1972 [22]. This switch to 'renewables' is desirable for various reasons, such as biocompatibility, biodegradability and lower toxicity, i.e. renewable raw materials leave a smaller environmental footprint [23]. Monosaccharides that can be found in biomass, glucose and fructose, can be used to produce liquid fuels – bioethanol and biodiesel. Recent efforts have been focused on converting the monosaccharides to one derivative of furan (5-hydroxymethylfurfural) since direct production of biofuels from C_5- and C_6-sugars is difficult. 5-HMF is a compound which has been found to be a key intermediate between biomass-based carbohydrates and desired products such as chemicals and biofuels. It has been found that 5-HMF can serve as a precursor to numerous products and chemical intermediates related to fuel, polymer, and pharmaceutical industries [24-28].

Renewable raw materials can contribute to the sustainability of chemical products in two ways:

(i) By developing greener, biomass-derived products which replace existing oil-based products, e.g. a biodegradable plastic.

(ii) Greener processes for the manufacture of existing chemicals from biomass instead of from fossil feedstocks. These conversion processes should, of course, be catalytic in order to maximize atom efficiencies and minimize waste (E factors).

Recently, several solid catalysts known to express surface acidity have been tested in dehydration of monosaccharides; for example, sulphated alumina zirconia [29], sulphated zirconia [30], titania zirconia mixed oxide [31], and zirconium phosphate [32].

1.3 Less hazardous/toxic chemicals

The removal of NOx from engine exhaust gas is highly important due to its detrimental impact on the environment resulting in acid rains, ground-level ozone, as well as degradation of the visibility and human health (i.e.lung infections and respiratory allergies) [33,34]. As a result of the negative impact of NO_x, the regulation of its emission is becoming stricter, regardless of the region, including Asia, Europe and USA [35]. The next NO_x limits (Euro 6 in Europe, see Fig. 1.3.1) will require the introduction of sophisticated after-treatment techniques from the diesel manufacturers [36].

The selective reduction of NO_x to nitrogen ($DeNO_x$) is a known technology for eliminating this pollutant from both stationary and mobile sources, but it is still a relevant target in catalysis research and an open problem to meet the future exhaust emission regulation, in particular, for emission from diesel engines.

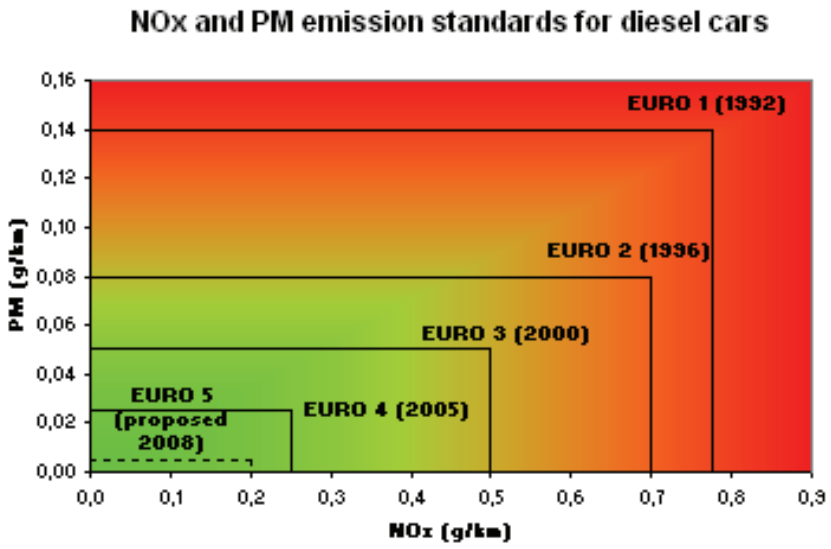

Fig.1.3.1 NO_x and PM (particulate matter) emission standards for diesel cars [37]

A suitable active commercial catalyst is needed to achieve a good NO_x conversion [38]; this catalyst should show good stability, activity and selectivity over a wide range of operation temperatures. The oxides such as Al_2O_3, SiO_2-Al_2O_3, TiO_2 and ZrO_2 are active in this selective reduction [39-42]. The oxides of group III elements have received much attention recently as they have been tested in various catalytic reactions of environmental interests. Ga_2O_3 and

In_2O_3 supported on acidic supports (Al_2O_3 - TiO_2 - SiO_2/Al_2O_3) have been reported to present a remarkable de-NO_x catalytic activity [43-45].

To summarize, the objectives of my PhD work can be depicted as follows:

(1) Characterization of the acidic and redox properties of four different commercial tungstated zirconia catalysts with W loadings of about 12–13 wt%. The samples were characterized in terms of their micro-structural and surface properties by BET, X-ray diffraction, temperature programmed reduction, elemental chemical analysis and adsorption microcalorimetry of NH_3.

(2) Design and preparation of two series of tungstated zirconia catalysts by coprecipitation and incipient wetness impregnation with various tungsten oxide loadings (1-20) wt%; to investigate how both the preparation method and the WO_3 content impact the acidic and redox properties. The obtained materials were thoroughly characterized by complementary physico-chemical techniques (BET, XRD, Raman, XPS, TGA, redox properties). NH_3 and SO_2 adsorption calorimetry and pyridine adsorption FTIR were used to investigate the acidic properties. The catalytic activity of tungstated zirconia prepared by coprecipitaion was tested in the hydrolysis of cellobiose disaccharide, while the series prepared by impregnation was tested in the reaction of fructose dehydration to 5-HMF.

(3) Mixed oxides of zirconia with boria, alumina, gallia, india and tungsta, were prepared by coprecipitation and impregnation methods. The central theme in this research was to understand how the different guest metal oxides could influence the acidic, redox and catalytic properties of these catalysts. The structural properties were characterized by BET, XRD, XPS. The redox properties were investigated by TPR, while the acid-base properties were studied by ammonia and sulphur dioxide adsorption calorimetry. The selective catalytic reduction of NO_x by decane ($C_{10}H_{22}$-SCR) has been studied over these mixed oxides.

(4) Two series of binary oxides WO_3-Me_2O_3 (Me = Al, Ga and In) and ternary oxides $WO_3/(ZrO_2$-$Me_2O_3)$ (Me = B, Al, Ga and In) were prepared by coprecipitation and impregnation methods and characterized in terms of their structural, textural, and surface properties, including the acid and redox features, by a variety of techniques (BET, XRD, TG, TPR) and microcalorimetry. The acid-base properties were estimated by the adsorption of NH_3 and SO_2 as probe molecules, respectively.

The aim of this work was to tune and predict catalyst acid-base properties by varying the composition of the mixed oxides.

WO_3 being an acidic component has been chosen as the main guest oxide to increase the acidity of amphoteric supports such as zirconia, alumina, gallia or india.

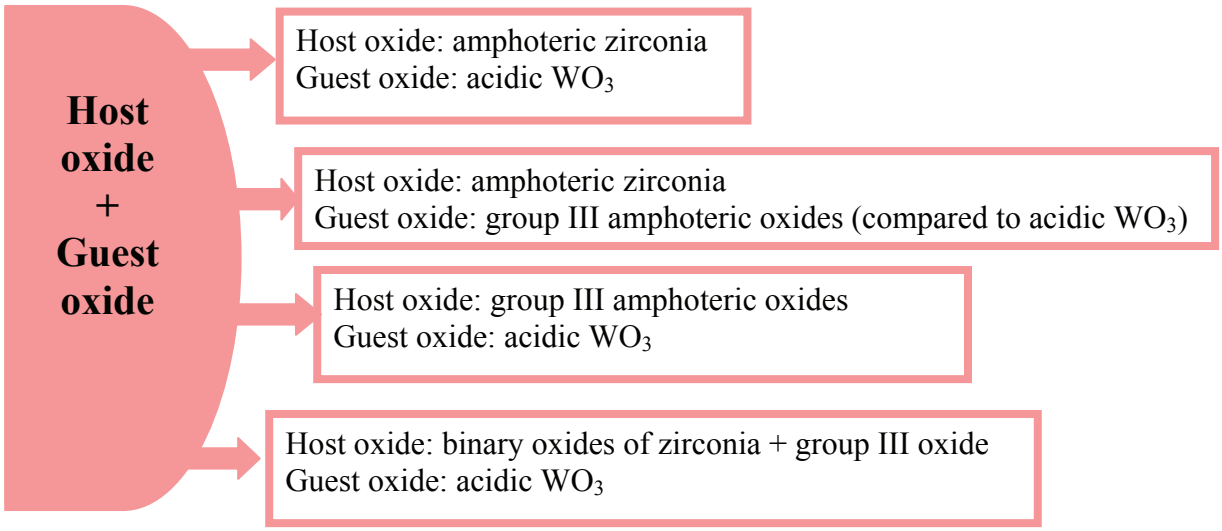

The acidity of zirconia based binary oxides (mixed with group III oxides) was also tuned by adding tungsta. The acid-base properties of these samples have been characterized mainly using adsorption microcalorimetry of ammonia and sulphur dioxide probes and their efficiency was tested in "green chemistry" reactions such as carbohydrates conversion (dehydration of fructose and hydrolysis of cellobiose) and in the selelctive catalytic reduction of NOx by n-decane. The scheme below summerizes the interconnection between the various steps which involve the complete study of WO_3 based catalysts from synthesis to catalytic test.

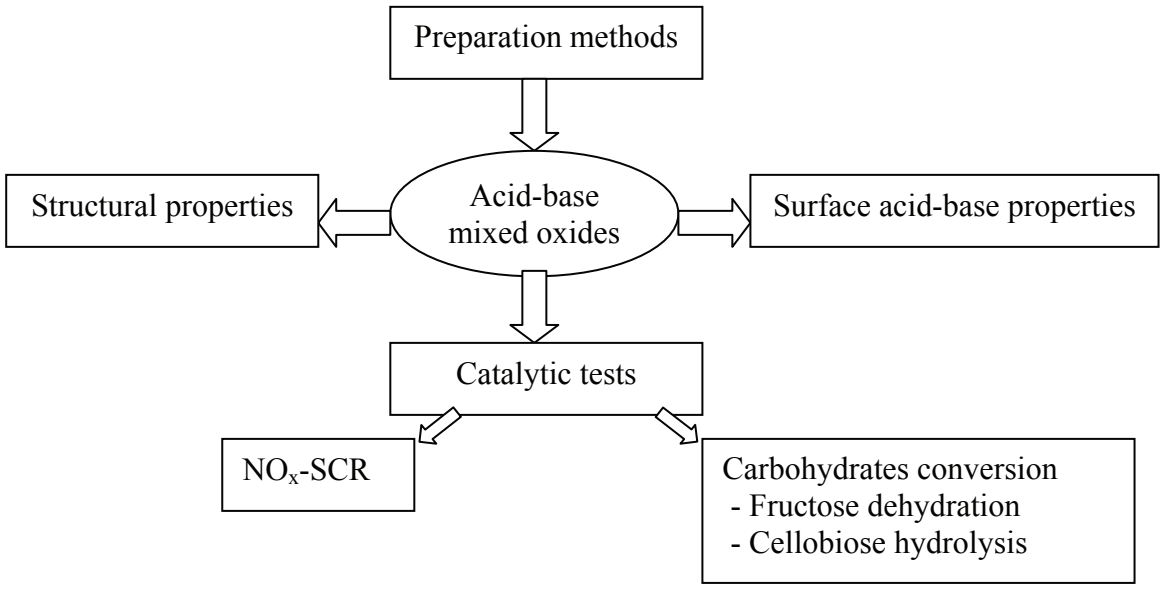

2. Experimental Description

The following chapter describes the preparation methods of catalysts and experimental techniques used in this work.

2.1 Catalyst preparation

2.1.1 Commercial tungsted zirconia catalysts and zirconium oxide

Four tungstated zirconia supported catalysts (labeled XZO- 1903-1, XZO-1903-2, XZO-1903-3, XZO-1251-01) and a $Zr(OH)_4$ support (ZO), supplied by MEL-Chemicals, have been calcined at 700 °C under air flow for 4 h (see Table 1) .

2.1.2 Tungsted zirconia catalysts prepared by various methods

Two different synthesis routes were followed for obtaining two series of catalysts with various tungsten oxide loadings (1-20 wt.%), each one composed of five samples.

2.1.2.1 Preparation by coprecipitation

An amount of $ZrOCl_2 \cdot 8H_2O$ was dissolved under stirring in distilled water. Then a solution containing concentrated NH_4OH, distilled H_2O, an amount of ammonium metatungstate hydrate [$(NH_4)_6H_2W_{12}O_{40} \cdot nH_2O$, Fluka, ≥ 99.0% WO_3] to have a WO_3 loading ranging from (1-20) wt.%, was added dropwisely over a 30–45 min period. The pH of the final solution was adjusted to approximately 9 by the addition of concentrated ammonium hydroxide. This slurry was then put in polypropylene bottles and placed in a steambox (100 °C) for 72 h. The product formed was recovered by filtration, washed with excess water, and dried overnight at 85 °C. The catalysts were calcined in flowing air for 4h, at 700 °C. The final WO_x/ZrO_2 catalysts were labelled as wt%-WO_3/ZrO_2-Cop (see Table 2).

2.1.2.2 Preparation by incipient wetness impregnation

WO_3/ZrO_2 catalysts were prepared by wetness impregnation method. $Zr(OH)_4$ was impregnated with an ammonium metatungstate hydrate solution, to have a WO_3 loading ranging from 1 to 20 wt.%. The resulting materials were air dried overnight at 85 °C, then calcined in flowing air for 4 hours at 700 °C. This calcination temperature has been chosen on the basis of TG measurements, performed using Labsys-TG from Setaram. The crude samples (~50 mg) were heated from 25 to 900 °C with a heating rate of 5 °C min^{-1} in a flow of air, which was chosen as a soft oxidizing agent for calcination. The pure zirconia sample was also calcined at 700 °C (see Table 2). The prepared solids are denoted by m-WO_3/ZrO_2, where m indicates the percentage of WO_3 wt%.

2.1.3 Preparation of ZrO_2-Me_2O_3 (Me: B, Al, Ga, In, W) and $WO_3/(Al_2O_3–ZrO_2)$ catalysts by coprecipitation and incipient wetness impregnation

Zirconia mixed oxides with Me_2O_3 (Me: B, Al, Ga, In, W) were prepared by coprecipitation. The compounds used as Me_2O_3 precursors were boric acid (H_3BO_3, Merck), the nitrates of aluminum, gallium, and indium: $Al(NO_3)_3.9H_2O$ (≥99%, Fluka), $Ga(NO_3)_3.5H_2O$ (99.9% Alfa Aesar), $In(NO_3)_3.5H_2O$ (99.9%, Aldrich) and ammonium metatungstate $(NH_4)_6H_2W_{12}O_{40}\cdot nH_2O$ (≥ 99.0% WO_3 Fluka). The precursor for the zirconia phase was zirconium oxychloride $ZrOCl_2\cdot 8H_2O$ (≥ 99.5%, Sigma-Aldrich). The required quantities of the group III metal oxide and zirconia precursors were dissolved in deionized water at room temperature. The solutions were mixed with a continuous monitoring of pH. Concentrated ammonia (32% wt/wt) was added gradually dropwise to this mixture of two solutions with vigorous stirring, until the precipitation was achieved (pH 9).

Pure zirconia was obtained by precipitation from a solution of $ZrOCl_2\cdot 8H_2O$ by ammonia in the same way. All precipitates were filtrated, washed with water and dried overnight in an oven at 100 °C and calcined at 450 °C under air flow.

$WO_3/(Al_2O_3–ZrO_2)$ was prepared by incipient wetness impregnation on the uncalcined $Al_2O_3–ZrO_2$ precursor prepared as reported just above, starting from aqueous solution of ammonium metatungstate. After drying at 100°C for 24 h and calcination at 450 °C, the tungsten oxide loading was 16.7 wt.%.

The calcination temperature of 450 °C was chosen on the basis of thermogravimetry (TG) measurements, performed with a Labsys-TG from Setaram. The crude samples (~50 mg) were

heated from 25 to 900 °C with a heating rate of 5 °C min^{-1} in a flow of air, which was chosen as a soft oxidizing agent for calcination (see Table 3).

2.1.4 Preparation of WO_3-Me_2O_3 (Me = Al, Ga, In) and WO_3/(Me_2O_3–ZrO_2) (Me = B, Al, Ga, In) catalysts by coprecipitation and incipient wetness impregnation

Pure hydroxides of zirconium, aluminum, gallium and indium were obtained by precipitation. The required quantities of the nitrates of aluminum, gallium, indium: $Al(NO_3)_3 \cdot 9H_2O$ (≥99%, Fluka), $Ga(NO_3)_3 \cdot 5H_2O$ (99.9% Alfa Aesar), $In(NO_3)_3 \cdot 5H_2O$ (99.9%, Aldrich) and zirconium oxychloride $ZrOCl_2 \cdot 8H_2O$ (≥ 99.5%, Sigma-Aldrich) were dissolved in deionized water at room temperature, except in the case of gallium nitrate which was dissolved at 60 °C with stirring. The pH of the solutions was monitored during the addition of concentrated ammonia (32% wt/wt). Ammonia was added gradually dropwise to the precursor solution of with vigorous stirring, until the precipitation was complete (pH 9).

Zirconia hydroxide mixed with $Me(OH)_3$ (Me: B, Al, Ga, In) were prepared by coprecipitation. The required quantities of the group III metal and zirconium hydroxides precursor were dissolved in deionized water at room temperature. The solutions were mixed with a continuous monitoring of pH. Concentrated ammonia (32% wt/wt) was added gradually dropwise to this mixture of two solutions with vigorous stirring, until the precipitation was complete (pH 9). All precipitates (hydroxides) were filtrated, washed with water and dried overnight in an oven at 100 °C.

WO_3/Me_2O_3 and $WO_3/(Me_2O_3–ZrO_2)$ catalysts were prepared by incipient wetness impregnation on the uncalcined $Me(OH)_3$ and $Me(OH)_3$-$Zr(OH)_4$ precursors prepared as reported in the previous paragraph, starting from aqueous solution of ammonium metatungstate. After drying at 100°C for 24 h and calcination at 400 °C, the tungsten oxide loading was of ~ 6 wt.%.

The calcination temperature of 400 °C was chosen on the basis of thermogravimetry (TG) measurements, performed using a Labsys-TG from Setaram. The crude samples (~50 mg) were heated from 25 to 900°C with a heating rate of 5 °C min^{-1} in a flow of air, which was chosen as a soft oxidizing agent for calcination (see Table 4).

2.2 Catalyst characterization

Different techniques were used to characterize the physico-chemical properties of the catalysts which are listed as the following:

The thermogravimetric (TG) analyses were performed on a SETARAM Labsys instrument in the 30-900 °C temperature range, with a heating rate of 5 °C min^{-1}, under air flow.

Elemental analysis was performed using ICP optical emission spectroscopy (ICP-OES) with an ACTIVA spectrometer from Horiba JOBIN YVON

The surface areas, pore volumes and pore sizes were measured by nitrogen adsorption at -196 °C on a Micromeritics 2010 apparatus after heat pre-treatment under vacuum for 2 h at a temperature of 400 °C. Surface areas were determined by the BET method from the resulting isotherms. Pore volumes and pore sizes were determined by the BJH method.

The X-ray diffraction (XRD) measurements were carried out on a Bruker D5005 powder diffractometer scanning from 3° to 80° (2θ) at a rate of 0.02° s^{-1} using a Cu Kα radiation (λ = 0.15418 nm) source. The applied voltage and current were 50 kV and 35 mA, respectively.

The recording of transmission electron micrographs (TEM) was carried out using a JEOL 2010 LaB6 equipment operating at 200 kV with an energy dispersive X-ray spectrometer (EDS), (Link ISIS from Oxford Instruments). The samples were dispersed in ethanol using a sonicator and a drop of the suspension was dripped onto a carbon film supported on a copper grid and then ethanol was evaporated. EDS study was carried out using a probe size of 15 nm to analyze borders and centers of the particles and the small particles.

The X-ray photoelectron spectra (XPS) were obtained on a KRATOS AXIS Ultra DLD spectrometer equipped with a hemispherical electron analyzer and an Al anode (Al Kα = 1486.6 eV) powered at 150 W, a pass energy of 20 eV, and a hybrid lens mode. The detection area analyzed was 700 μm x 300 μm. Charge neutralization was required for all samples. The peaks were referenced to the C–(C, H) components of the C 1s band at 284.6 eV. Shirley background subtraction and peak fitting to theoretical Gaussian–Lorentzian functions were performed using an XPS processing program (Vision 2.2.6 KRATOS). The residual pressure in the spectrometer chamber was 5 x 10^{-9} mbar during data acquisition.

Raman spectroscopy measurements were performed using a LabRAM HR (Jobin Yvon) spectrometer. The excitation was provided by the 514.5 nm line of an Ar^+ ion laser (Spectra physics) employing a laser power of 100 μW. The laser beam was focused through microscope objective lenses (100 x) down to a 1 μm spot on the sample. For each solid, the spectra were recorded at several points of the sample to ascertain the homogeneity of the sample and the average of these spectra was plotted.

Temperature programmed reduction and oxidation experiments were performed using a TPD/R/O-1100 instrument (Thermo). Redox cycles (TPR/TPO/TPR2) were realized carrying out sequentially a temperature programmed reduction (TPR1) on the oxidized sample followed by a temperature programmed oxidation (TPO) and then a second temperature programmed reduction (TPR2). The samples were initially pre-treated in O_2/He flow (20 mL min^{-1}) at 350 °C for 60 min. After cooling to room temperature, the H_2/Ar (4.96% v/v) reducing mixture flowed through the sample at 20 mL min^{-1} with the temperature increasing from 40 to 700 °C at a rate of 10 °C/min. TPO run was carried out on the reduced sample cooled at 40 °C in H_2/Ar flow. After Ar purge (10 mL min^{-1}), the O_2/He (0.99% v/v) oxidizing mixture flowed at 20 mL min^{-1} through the sample with similar experimental conditions, in terms of temperature increasing and range, to those used for TPR analysis. On the re-oxidized sample a second reduction (TPR2) was performed in the same conditions as TPR1 but increasing the temperature up to 1000 °C instead of 700 °C.

Pyridine adsorption FTIR spectra were recorded at room temperature with a Bruker Vector 22 FTIR spectrophotometer (DTGS detector) operating in the 4000–400 cm^{-1} range, with a resolution of 2 cm^{-1} and 100 acquisition scans. In each pyridine adsorption FTIR measurement, the self-supporting wafer (50-60 mg, 18 mm diameter) was first activated in situ at a temperature of 350 °C in oxygen flow for 14 h, then evacuated at the same temperature for 2 h and then exposed to pyridine (Air Liquide, 99.8%, vapor pressure 3.3 kPa) at room temperature for 5 min. The desorption was carried out by evacuation for 30 min each at room temperature, 100, 200, 300, 400 °C respectively . The spectra were recorded at room temperature after adsorption and desorption at each temperature (see scheme Fig.2.2.1).

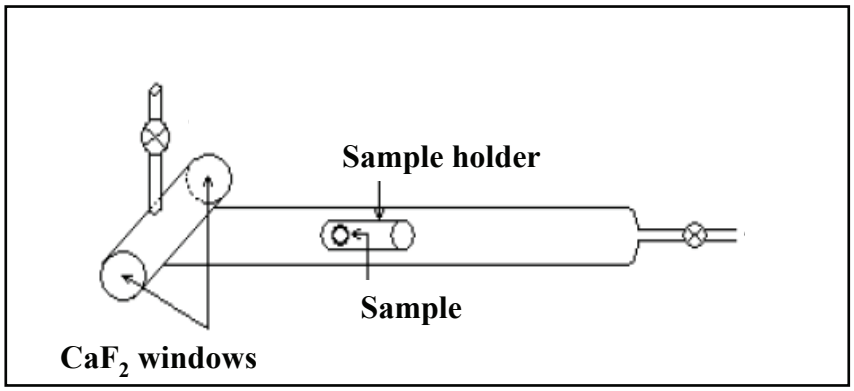

Fig.2.2.1 Scheme of the in-situ cell for adsorption FTIR (IRCELYON)

Adsorption microcalorimetry measurements were performed at 80 °C in a heat flow calorimeter (C80 from Setaram) linked to a conventional volumetric apparatus equipped with a Barocel capacitance manometer for pressure measurements. The probes (ammonia and sulphur dioxide) used for measurements (Air Liquide, purity > 99.9%) were purified by successive freeze–pump–thaw cycles. About 100 mg of sample was pre-treated in the calorimetric quartz cell overnight at 400 °C, and then evacuated at the same temperature for 1h prior to the measurements. The differential heats of adsorption were measured as a function of coverage by repeatedly introducing small doses of the adsorbate onto the catalyst, until an equilibrium pressure of about 66 Pa was reached. The sample was then outgassed for 30 min at the same temperature, and a second adsorption was performed at 80 °C until an equilibrium pressure of about 27 Pa was attained in order to calculate the irreversibly chemisorbed amount of the probe molecules at this pressure (see scheme Fig.2.2.2).

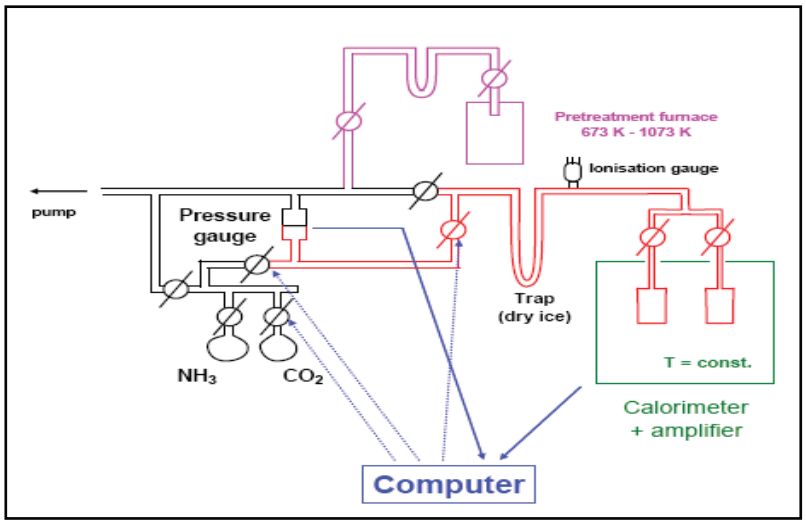

Fig.2.2.2. Scheme of adsorption microcalorimetry system (IRCELYON)

2.3 Catalytic reactions

2.3.1 Cellobiose hydrolysis

D-(+)-cellobiose (Fluka, ≥99.0% purity) was used as substrate. The kinetic tests of cellobiose catalytic dehydration to glucose were performed in water in a glass batch thermostated reactor at atmospheric pressure and at a constant temperature of 97 °C (reaction temperature ± 1°C) under strong magnetic stirring. The reactions were followed for a period of 32 h.

A weighted amount of calcined catalyst sample of about 100 mg was crushed and sieved in 300 μm particle size and put into the reactor without any pre-treatment. Preliminary tests of WO_3 leaching in hot water (50 °C) were performed on the 9.9-WO_3/ZrO_2 catalyst, chosen as representative sample. The tests indicated the absence of any amount of tungsten in the solution at this temperature.

Aqueous cellobiose solution (total volume of 10 mL) of 0.1 g·mL^{-1} (corresponding to 0.3 M) was prepared for each run. The reaction temperature was attained in approximately 15 min. Starting from 30 min, amounts of solution (0.5 mL) were taken off from the reactor at fixed time on stream (TOS) (typically at 0.5, 8, 24, and 32 h). The sampling was filtered before analysis (0.45 μm nylon filter).

Analyses were performed in a liquid-chromatography apparatus (HPLC) consisting of an injector (Waters U6K), pump (Waters 510), and a refractive index detector (Waters 410). A Carbohydrate Analysis column (Waters) operating at room temperature and eluted with an acetonitrile:water 80:20 solution was used. Cellobiose and glucose were quantitatively determined from previous calibration measurements employing solutions of known concentration of both products.

In parallel, some analyses were also repeated employing an enzymatic kit of analysis (D-Glucose / D-Fructose UV-method, Biopharm) for the determination of the glucose concentration by using a Beckman spectrophotometer (mod. DU 640).

2.3.2 Fructose dehydration

The reaction of fructose dehydration was performed in a batch catalytic system. Experiments were performed in a 100 mL stainless steel autoclave at 130 °C. In a typical procedure 600 mg of fructose was dissolved in 60 mL of water and then 80 mg of solid

catalyst was added [46,47]. Water was chosen as a green and appropriate solvent for dehydration of fructose to 5-HMF. In the analysis, starting time of the reaction was taken when the reaction mixture reached 130 °C. Samples were withdrawn from the reaction mixture at 1 h intervals; the changes of fructose, 5-HMF, formic and levulinic acids concentration with time were followed by collecting ^{1}H NMR spectra, using liquid NMR technique (Bruker AVANCE 250 spectrometer equipped with a multinuclear 10mm Probe). The concentration of the various species has been obtained by the integration of areas under the peaks after calibration (integration perfomed using Mnova 7 software).

Reactant conversion (mol%), yield of 5-HMF (mol%), and product selectivity (%) were defined as follows:

Conversion (mol%) = (moles of fructose that reacted)/(moles of fructose initial) × 100% (1)

Yield (mol%) = (moles of X produced)/(moles of fructose initial) × 100% (2)

Selectivity (%) = (moles of X produced)/(moles of fructose reacted) × 100% (3)

2.3.2 Selective catalytic reduction of NO_x by n-decane ($C_{10}H_{22}$-SCR)

The selective catalytic reduction of NO_x by n-decane ($C_{10}H_{22}$-SCR) was carried out in a U-shaped quartz reactor with 0.2 g of catalyst. The reactor was heated and the temperature of the catalyst was monitored using a K-type thermocouple. The reaction mixture was composed of 400 ppm NO, 240 ppm $C_{10}H_{22}$ and 9 vol.% O_2 in He as carrier gas in the presence of H_2O (1.5 vol.%). The total flow rate was 120 mL.min^{-1}, corresponding to a space velocity of about 35,000 h^{-1}. Reaction products were analyzed by micro-gaschromatography (μGC: TCD detector) for N_2 (molecular sieve 5A), by gas chromatography (FID detector) for $C_{10}H_{22}$, and by IR-UV for CO_2, NO, NO_2 and N_2O (see scheme Fig.2.2.3). After stabilization, the temperature-programmed reaction began at 100 °C by increasing the catalyst temperature at a rate of 2 °C min^{-1} until 500 °C was obtained. At the end of the ramp, the temperature was maintained 30 min at 500 °C and then decreased at a rate of 1 °C min^{-1} down to 100 °C. All the data presented in this paper were recorded during the cooling ramp. The N_2, N_2O, NO_2, global NO_x, total $C_{10}H_{22}$ yields, nitrogen balance were calculated by the following equations from (1) to (6):

Equation (1): $$Y_{NOx-N2} = 100 \times \frac{2[N_2]}{[NO]_0 + [NO_2]_0}$$

Equation (2): $$Y_{NOx-N2O} = 100 \times \frac{2[N_2O]}{[NO]_0 + [NO_2]_0}$$

Equation (3): $Y_{NOx-NO2} = 100 \times \frac{[NO_2]}{[NO]_0 + [NO_2]_0}$

Equation (4): $Y_{NOxglobal} = 100 \times \left(\frac{([NO]_0 + [NO_2]_0) - ([NO] + [NO_2])}{[NO]_0 + [NO_2]_0} \right)$

Equation (5): $Y_{C10H22} = 100 \times \left(\frac{\frac{1}{10}[CO_2]}{[C_{10}H_{22}]_0} \right)$

Equation (6): $N\ balance : [NO]_0 + [NO_2]_0 = [NO] + [NO_2] + 2[N_2] + 2[N_2O]$

Equation (7): $S_{N2} = 2[N_2] / 2[N_2] + 2[N_2O] + [NO_2]$

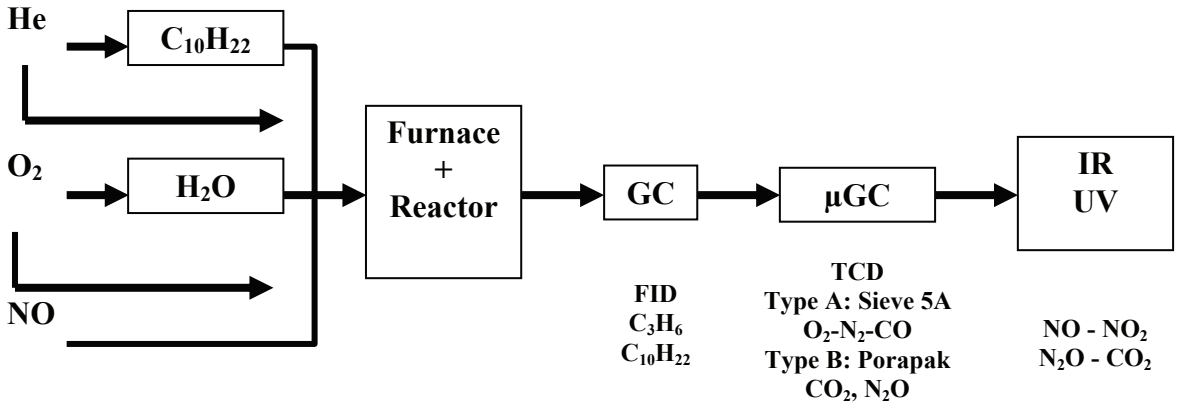

Fig.2.2.3. Scheme of the SCR reaction setup and analysis

A substantial amount of NO_2 was formed in homogeneous phase in the pipes of the apparatus; before and after the reactor, as previously observed for studies on selective catalytic reduction of NO by propene in the presence of oxygen performed in the same equipment [48]. Indeed, the thermodynamic equilibrium of the following reaction leads to the formation of NO_2 at room temperature [49]:

$$NO + 1/2O_2 \rightarrow NO_2$$

The quantity of NO_2 formed in the pipes was subtracted from the total NO_2 amount before the conversion of NO_x into NO_2 was calculated.

3. List of Catalysts

Table 1 WO_3/ZrO_2 commercial catalysts used in this work

Catalyst	Component	Preparation method	Precursors	Calcination Temp[b] /°C	Publication
ZrO_2 (ZO)	-	Commercial, supplied by Mel-Chemicals	-	700 °C	I, II, III, IV
W/ZrO_2-1 (XZO- 1903-01)	15.40% WO_3-ZrO_2	Commercial, supplied by Mel-Chemicals	-	700 °C	I, II
W/ZrO_2-2 (XZO- 1903-02)	15.90% WO_3-ZrO_2	Commercial, supplied by Mel-Chemicals	-	700 °C	I, II
W/ZrO_2-3 (XZO- 1903-03)	15.50% WO_3-ZrO_2	Commercial, supplied by Mel-Chemicals	-	700 °C	I, II
W/ZrO_2-4 (XZO- 1251-01)	16.60% WO_3-ZrO_2	Commercial, supplied by Mel-Chemicals	-	700 °C	I, II

[b] all catalysts were calcined in air

Table 2 WO_3/ZrO_2 prepared by coprecipitation and incipent wetness impregnation catalysts used in this work

Catalysts	Component	Preparation method	Precursors	Calcination Temp[b] /°C	Publication
0.9-WO_3/ZrO_2-Cop	0.90% WO_3-ZrO_2	Coprecipitation	$(NH_4)_6H_2W_{12}O_{40}\cdot nH_2O$, $ZrOCl_2\cdot 8H_2O$	700 °C	III
4.7-WO_3/ZrO_2-Cop	4.72% WO_3-ZrO_2	Coprecipitation	$(NH_4)_6H_2W_{12}O_{40}\cdot nH_2O$, $ZrOCl_2\cdot 8H_2O$	700 °C	III
9.9-WO_3/ZrO_2-Cop	9.97% WO_3-ZrO_2	Coprecipitation	$(NH_4)_6H_2W_{12}O_{40}\cdot nH_2O$, $ZrOCl_2\cdot 8H_2O$	700 °C	III
15.2-WO_3/ZrO_2-Cop	15.22% WO_3-ZrO_2	Coprecipitation	$(NH_4)_6H_2W_{12}O_{40}\cdot nH_2O$, $ZrOCl_2\cdot 8H_2O$	700 °C	III
19-WO_3/ZrO_2-Cop	19.00% WO_3-ZrO_2	Coprecipitation	$(NH_4)_6H_2W_{12}O_{40}\cdot nH_2O$, $ZrOCl_2\cdot 8H_2O$	700 °C	III
1.2-WO_3/ZrO_2	1.21% WO_3-ZrO_2	incipient wetness impregnation	$(NH_4)_6H_2W_{12}O_{40}\cdot nH_2O$, $Zr(OH)_4$	700 °C	IV
5.1-WO_3/ZrO_2	5.09% WO_3-ZrO_2	incipient wetness impregnation	$(NH_4)_6H_2W_{12}O_{40}\cdot nH_2O$, $Zr(OH)_4$	700 °C	IV
9.8-WO_3/ZrO_2	9.86% WO_3-ZrO_2	incipient wetness impregnation	$(NH_4)_6H_2W_{12}O_{40}\cdot nH_2O$, $Zr(OH)_4$	700 °C	IV
16.8-WO_3/ZrO_2	16.85% WO_3-ZrO_2	incipient wetness impregnation	$(NH_4)_6H_2W_{12}O_{40}\cdot nH_2O$, $Zr(OH)_4$	700 °C	IV
20.9-WO_3/ZrO_2	20.93% WO_3-ZrO_2	incipient wetness impregnation	$(NH_4)_6H_2W_{12}O_{40}\cdot nH_2O$, $Zr(OH)_4$	700 °C	IV

[b] all catalysts were calcined in air

Table 3 Me_2O_3-ZrO_2 (Me = B, Al, Ga, In) prepared by coprecipitation, WO_3/ZrO_2 and $WO_3/(Al_2O_3$-$ZrO_2)$ prepared by incipent wetness impregnation catalysts used in this work

Catalyst	Component	Preparation method	Precursors	Calcination Temp[b] /°C	Publication
ZrO_2	-	Precipitation	$ZrOCl_2 \cdot 8H_2O$	450 °C	V
B_2O_3- ZrO_2	30.21 % B_2O_3- ZrO_2	Coprecipitation	H_3BO_3, $ZrOCl_2 \cdot 8H_2O$	450 °C	V
Al_2O_3-ZrO_2	34.80 % Al_2O_3-ZrO_2	Coprecipitation	$Al(NO_3)_3.9H_2O$, $ZrOCl_2 \cdot 8H_2O$	450 °C	V
Ga_2O_3-ZrO_2	21.32 % Ga_2O_3-ZrO_2	Coprecipitation	$Ga(NO_3)_3.5H_2O$, $ZrOCl_2 \cdot 8H_2O$	450 °C	V
In_2O_3-ZrO_2	27.00 % In_2O_3-ZrO_2	Coprecipitation	$In(NO_3)_3.5H_2O$, $ZrOCl_2 \cdot 8H_2O$	450 °C	V
WO_3/ZrO_2	16.85 % WO_3-ZrO_2	incipient wetness impregnation	$(NH_4)_6H_2W_{12}O_{40} \cdot nH_2O$, $Zr(OH)_4$	450 °C	V
$WO_3/(Al_2O_3$-$ZrO_2)$	16.70 % $WO_3/(34.8$ % Al_2O_3 - $ZrO_2)$	incipient wetness impregnation and coprecipitation	$(NH_4)_6H_2W_{12}O_{40} \cdot nH_2O$, $Al(OH)_3$-$Zr(OH)_4$	450 °C	V

[b] all catalysts were calcined in air

Table 4 WO_3/Me_2O_3 (Me = Al, Ga, In) prepared by coprecipitation and $WO_3/(Me_2O_3\text{-}ZrO_2)$ (Me = B, Al, Ga, In) prepared by incipient wetness impregnation catalysts used in this work

Catalyst	Component	Preparation method	Precursors	Calcination Temp[b] /°C	Publication
WO_3/ZrO_2	4.30 % WO_3-ZrO_2	Coprecipitation	$(NH_4)_6H_2W_{12}O_{40}\cdot nH_2O$, $ZrOCl_2\cdot 8H_2O$	400 °C	VI
WO_3/Al_2O_3	6.82 % WO_3-ZrO_2	Coprecipitation	$(NH_4)_6H_2W_{12}O_{40}\cdot nH_2O$, $Al(NO_3)_3.9H_2O$	400 °C	VI
WO_3/Ga_2O_3	7.71 % WO_3-ZrO_2	Coprecipitation	$(NH_4)_6H_2W_{12}O_{40}\cdot nH_2O$, $Ga(NO_3)_3.5H_2O$	400 °C	VI
WO_3/In_2O_3	9.32 % WO_3-ZrO_2	Coprecipitation	$(NH_4)_6H_2W_{12}O_{40}\cdot nH_2O$, $In(NO_3)_3.5H_2O$	400 °C	VI
$WO_3/(B_2O_3\text{-}ZrO_2)$	6.50 % WO_3/(30.21 % B_2O_3- ZrO_2)	incipient wetness impregnation and coprecipitation	$(NH_4)_6H_2W_{12}O_{40}\cdot nH_2O$, $B(OH)_3$-$Zr(OH)_4$	400 °C	VI
$WO_3/(Al_2O_3\text{-}ZrO_2)$	4.80 % WO_3/(34.80 % Al_2O_3-ZrO_2)	incipient wetness impregnation and coprecipitation	$(NH_4)_6H_2W_{12}O_{40}\cdot nH_2O$, $Al(OH)_3$-$Zr(OH)_4$	400 °C	VI
$WO_3/(Ga_2O_3\text{-}ZrO_2)$	5.93 % WO_3/(21.32 % Ga_2O_3-ZrO_2)	incipient wetness impregnation and coprecipitation	$(NH_4)_6H_2W_{12}O_{40}\cdot nH_2O$, $Ga(OH)_3$-$Zr(OH)_4$	400 °C	VI
$WO_3/(In_2O_3\text{-}ZrO_2)$	6.13 % WO_3/(27.00 % In_2O_3-ZrO_2)	incipient wetness impregnation and coprecipitation	$(NH_4)_6H_2W_{12}O_{40}\cdot nH_2O$, $In(OH)_3$-$Zr(OH)_4$	400 °C	VI

[b] all catalysts were calcined in air

References

[1] P. Anastas, J.C. Warner (Eds.), Green Chemistry: Theory and Practice, Oxford University Press, Oxford, 1998

[2] P.T. Anastas, M.M. Kirchhoff, Acc. Chem. Res. 35 (2002) 686-693

[3] P.T. Anastas, L.G. Heine, T.C. Williamson (Eds.), Green Chemical Syntheses and Processes, American Chemical Society, Washington DC, 2000

[4] J.H. Clark, D.J. Macquarrie, Handbook of Green Chemistry and Technology, Blackwell, Abingdon, 2002

[5] J.H. Clark (Ed.), The Chemistry of Waste Minimization, Blackie, London, 1995

[6] R.A. Sheldon, C.R. Acad. Sci. Paris, IIc, Chimie/Chemistry 3 (2000) 541–551

[7] D.G. Barton, M.Shtein, R.D. Wilson, S.L. Soled, E. Iglesia, J. Phys. Chem. B, 103 (1999) 630-640

[8] M. Hino, K.J. Arata, Chem. Soc. Chem. Commun. 18 (1988) 1259-1260

[9] P. Afanasiev, C. Geantet, M. Breysse, G. Coudurier, J.C. Vedrine, J. Chem. Soc. Faraday Trans. 90 (1994) 193-202

[10] G. Larsen, E. Lotero, L. M. Petkovic, D. S. Shobe, J. Catal. 169 (1997) 67-75

[11] C.D. Baertsch, K.T. Komala, Y.H. Chua, E. Iglesia, J. Catal. 205 (2002) 44-57

[12] E. Iglesia, D.G. Barton, S.L. Soled, S. Miseo, J.E. Baumgartner, W.E. Gates, G.A. Fuentes, G.D. Meitzner, Stud. Surf. Sci.Catal. 101(1996) 533-542

[13] G. Larsen, E. Lotero, S. Raghavan, R.D. Parra, C.A. Querini, Appl. Catal. A 139 (1996) 201-211

[14] S.R. Vaudagna, S.A. Canavese, R.A. Comelli, N.S. Figoli, Appl. Catal. A 168 (1998) 93-111

[15] Y. Kintaichi, H. Hamada, M. Tabata, M. Sasaki, T. Ito, Catal. Lett. 6 (1990) 239-244

[16] G. Delahay, B. Coq, E. Ensuque, F. Figueras, Catal. Lett. 39 (1996) 105-109

[17] M. Sasaki, H. Hamada, Y. Kintaichi, T. Ito, Catal. Lett. 15 (1992) 297-304

[18] R.T. Yang, W.B. Li, N. Chen, Appl. Catal. A 169 (1998) 215-225

[19] P.T. Wierzchowski, L. Zatorski, Appl. Catal. B 44 (2003) 53-56

[20] M. Haneda, E. Joubert, J.C. Menezo, D. Duprez, J. Barbier, N. Bion, M. Daturi, J. Saussey, J.L. Lavalley, H. Hamada, Phys. Chem. Chem. Phys. 3 (2001) 1366-1370

[21] A.L. Petre, J.A. Perdigon-Melon, A. Gervasini, A. Auroux, Top. Catal. 19 (2002) 271-281

[22] D.H. Meadows, D.I. Meadows, J. Randers, W.W. Behrens, Limits to Growth, New American Library, New York, 1972
[23] B. E. Dale, J. Chem. Technol. Biotechnol. 78 (2003) 1093-1103
[24] P. Gupta, S.K. Singh, A. Pathak, B. Kundu, Tetrahedron. 58 (2002) 10469-10474
[25] E.L. Kunkes, D.A. Simonetti, R.M. West, J.C. Serrano-Ruiz, C.A. Gartner, J.A. Dumesic, Science 322 (2008) 417-421
[26] J. Lewkowski, Arkivoc 2 (2001) 17-54
[27] B.F.M. Kuster, Starch 42 (1990) 314-321
[28] Y. Roman-Leshkov, J.N. Chheda, J.A. Dumesic, Science 312 (2006) 1933-1937
[29] Y. Yang, X. Xiang, D. Tong, C.W. Hu, M.M. Abu-Omar, Bioresource Technol. 116 (2012) 302-306
[30] X. Qi, M. Watanabe, T.M. Aida, R.L. Smith Jr., Green Chem. 11 (2009) 1327-1331
[31] M. Watanabe, Y. Aizawa, T. Iida, R. Nishimura, H. Inomata, Appl. Catal. A. 295 (2005) 150-156
[32] F.S. Asghari, H. Yoshida, Carbohyd. Res. 341 (2006) 2379-2387
[33] A. Fritz, V. Pitchon, Appl. Catal. B 13 (1997) 1–25
[34] M.V. Twigg, Appl. Catal. B 70 (2007) 2–15
[35] S. Fischer, K. Rusch, B. Amon, Asian vehicule Emission Control Conference, Beijing, China, 27-29 April, 2004
[36] J. Rodriguez-Fernandez, A. Tsolakis, M. Ahmadinejad, S. Sitshebo, Energ. Fuel. 24 (2010) 992-1000
[37] http://en.wikipedia.org/wiki/European_emission_standards
[38] R. Foo, N. Cortes Felix, Platinum Metals Rev. 53 (2009) 164-171
[39] Y. Kintaichi, H. Hamada, M. Tabata, M. Sasaki, T. Ito, Catal. Lett. 6 (1990) 239-244
[40] G. Delahay, B. Coq, E. Ensuque, F. Figueras, Catal. Lett. 39 (1996) 105-109
[41] M. Sasaki, H. Hamada, Y. Kintaichi, T. Ito, Catal. Lett. 15 (1992) 297-304
[42] R.T. Yang, W.B. Li, N. Chen, Appl. Catal. A 169 (1998) 215-225
[43] P.T. Wierzchowski, L. Zatorski, Appl. Catal. B 44 (2003) 53-56
[44] M. Haneda, E. Joubert, J.C. Menezo, D. Duprez, J. Barbier, N. Bion, M. Daturi, J. Saussey, J.L. Lavalley, H. Hamada, Phys. Chem. Chem. Phys. 3 (2001) 1366-1370
[45] A.L. Petre, J.A. Perdigon-Melon, A. Gervasini, A. Auroux, Top. Catal. 19 (2002) 271-281
[46] T. Armaroli, G. Busca, C. Carlini, M. Guittari, A.M. Raspolli Galletti, G. Sbrana, J. Mol. Catal. A 151 (2000) 233-243

[47] C. Carlini, M. Giuttari, A.M. Raspolli Galletti, G. Sbrana, T. Armaroli, G. Busca, Appl. Catal. A 183 (1999) 295-302
[48] P. Denton, A. Giroir-Fendler, H. Praliaud, M. Primet, J. Catal. 189 (2000) 410-420
[49] S. Benard, L. Retailleau, F. Gaillard, P. Vernoux, A. Giroir-Fendler, Appl. Catal. B 55 (2005) 11-21

4. Published Results

Publication I

J Therm Anal Calorim (2010) 99:849–853
DOI 10.1007/s10973-009-0407-7

Study of acidic commercial WO_x/ZrO_2 catalysts by adsorption microcalorimetry and thermal analysis techniques

R. Kourieh · S. Bennici · A. Auroux

MEDICTA2009 Conference

Abstract In this work we report about the characterization of the acidic and redox properties of four different commercial tungstated zirconia catalysts with W loadings of about 12–13 mass%. The samples have been characterized in terms of their micro-structural and surface properties by BET, X-ray diffraction, temperature programmed reduction, elemental chemical analysis and adsorption microcalorimetry of NH_3. Improved acidity has been detected upon addition of WO_3 to zirconia and differences between the samples were pointed out thanks to the results obtained by the complementary physicochemical techniques used in this study.

Keywords Tungsten oxide · Zirconia supported catalysts · Surface acidity · Adsorption microcalorimetry

Introduction

Tungstated zirconia (WO_x/ZrO_2) has received considerable attention due to its potential catalytic application in hydrocarbon conversion reactions in the petrochemical industry [1–4].

The challenge to obtain solid acid catalysts with acid sites of comparable strength to those in sulfuric acid is still open in an attempt to eliminate environmentally concerns caused by the use, regeneration, transportation and storage of liquid acids [5]. Moreover, in the last years the growing interest towards biodiesel, a clean fuel source which is viewed as a viable alternative for dwindling petroleum-based diesel resources, has led to renewed interest in acid catalysts [6]. Better yet, if solid acid catalysts could replace liquid acids, the corrosion and environmental problems associated with them could be avoided and product purification protocols could be significantly reduced, simplifying various hydrocarbons transformation reactions, and thus reducing their costs. Moreover heterogeneous catalysts are preferable because offering easy separation from the reactants and products which are either liquids or gases.

It is known that catalytic activity of oxides can be related to the cooperative action of an oxidizing function and an acidic function. From this perspective, the determination of both redox and acidic properties of the catalytic centers becomes of fundamental importance in the present study.

Adsorption of a basic probe molecule (NH_3) will be used in adsorption calorimetry, one of the most powerful techniques for the determination of the number, strength and strength distribution of surface acid sites of catalysts [7]. Besides the redox character will be determined using thermoprogrammed reduction and oxidation experiments.

Experimental

Four tungstated zirconia supported catalysts (labeled XZO-1903-1, XZO-1903-2, XZO-1903-3, XZO-1251-01) and a $Zr(OH)_4$ support (ZO), supplied by MEL-Chemicals, have been calcined at 700 °C under air flow for 4 h.

Elemental analysis was performed using ICP atomic emission spectroscopy (ICP-AES) with a flame Perkin-Elmer M1100 spectrometer.

R. Kourieh · S. Bennici · A. Auroux (✉)
CNRS, UMR 5256, IRCELYON, Institut de recherches sur la catalyse et l'environnement de Lyon, Université Lyon 1, 2 Avenue Albert Einstein, 69626 Villeurbanne, France
e-mail: aline.auroux@ircelyon.univ-lyon1.fr

The surface areas and pore sizes were measured by nitrogen adsorption at −196 °C on a Micromeritics 2010 apparatus after heat pretreatment under vacuum for 2 h at a temperature of 400 °C.

The X-ray diffraction (XRD) measurements were carried out on a Bruker D5005 powder diffractometer scanning from 3° to 80° (2θ) at a rate of 0.02° s^{-1} using a Cu Kα radiation ($\lambda = 0.15418$ nm) source. The applied voltage and current were 50 kV and 35 mA, respectively.

The thermogravimetric (TG) analyses were performed on a SETARAM Labsys instrument in the 303–1,073 K temperature range, with a heating rate of 5 °C min^{-1}, under air flow.

Temperature programmed reduction and oxidation experiments were performed using a TPD/R/O-1100 instrument (Thermo). Redox cycles (TPR/TPO/TPR2) were realized carrying out sequentially a temperature programmed reduction (TPR1) on the oxidized sample followed by a temperature programmed oxidation (TPO) and then a second temperature programmed reduction (TPR2). The samples were initially pre-treated in O_2/He flow (20 mL min^{-1}) at 350 °C for 60 min. After cooling to room temperature, the H_2/Ar (4.96% v/v) reducing mixture flowed through the sample at 20 mL min^{-1} with the temperature increasing from 40 to 700 °C at a rate of 10 °C/min. TPO run was carried out on the reduced sample cooled at 40 °C in H_2/Ar flow. After Ar purge (10 mL min^{-1}), the O_2/He (0.99% v/v) oxidizing mixture flowed at 20 mL min^{-1} through the sample with similar experimental conditions, in terms of temperature increasing and range, to those used for TPR analysis. On the re-oxidized sample a second reduction (TPR2) was performed in the same conditions as TPR1 but increasing the temperature up to 1,000 °C instead of 700 °C.

Ammonia ($pK_a = 9.24$ and PA (proton affinity) = 857.7 kJ mol^{-1}), dried on 3A zeolite spheres, was used as a basic probe molecule to titrate the surface acid sites of the samples. Calorimetric and volumetric gas–solid titrations were carried out concomitantly in a volumetric line linked to a heat-flow microcalorimeter (Tian-Calvet type, C80 from Setaram). The chosen adsorption temperature was 80 °C to limit physisorption. About 0.1 g of powder sample previously calcined at 700 °C was pretreated under vacuum at 400 °C overnight (about 12 h) and then evacuated at the same temperature for 1 h prior to the measurements. Small successive NH_3 injections were sequentially sent onto the sample, up to a final NH_3 pressure of about 60 kPa. The equilibrium pressure relevant to each adsorbed amount was measured by means of a differential Barocel capacitance manometer (Datametrics). At the end of the adsorption, a second adsorption was performed after desorption (1 h at 80 °C) of the NH_3 amount weakly retained on the surface. The difference between the first and second isotherms at 27 kPa represented the strongly chemisorbed NH_3 amount, the so-called irreversible amount (V_{irr}).

Results and discussion

More or less significant differences in the surface properties between the WO_3 containing catalysts and the bare ZrO_2 support emerged from the various techniques used for characterizing the samples.

The chemical analysis values (expressed as W mass%) and the BET surface areas (in m^2 g^{-1}) of the zirconium-tungsten mixed oxides as well as of the zirconia are presented in Table 1. The tungsten amount was always close to 12–13 mass% which is slightly above the monolayer coverage (10.7 mass%) [8] assuming a surface concentration of tungsten of 3.5 W-atom·nm^{-2} for the monolayer. Even after calcination at 700 °C the catalysts maintained a remarkable surface area (between 80 and 105 m^2 g^{-1}), while the bare calcined zirconia decreased its surface down to 37 m^2 g^{-1}.

The XRD patterns of the un-calcined samples as received from Mel Chemicals (Fig. 1) show the same amorphous phase (for this reason only one sample is shown). The calcination of the catalysts at 700 °C resulted in the appearance of the tetragonal ZrO_2 phase only, as shown by the X-ray diffractograms reported in Fig. 1. At the same calcination temperature, the ZO support gave rise to the well known segregation into a mixture of tetragonal and monoclinic ZrO_2 with the specific reflections of the monoclinic phase at 28.3° and 31.6 2θ [9–11]. It is known that at a given W concentration, the BET surface area and the tetragonal content in ZrO_2 decrease with calcination temperatures higher than 500 °C [12]. The presence of WO_x species in fact inhibits the sintering and the transformation to monoclinic ZrO_2 crystallites, as demonstrated from the XRD and BET results of the four samples containing W. Moreover, no specific diffraction peak of WO_3 crystallites ($2\theta = 23.2°$, 23.7°, and 24.3°) has been detected in any of the catalysts.

TG analyses were carried out to provide information about any decomposition of the sample and also to help in determining a more accurate calcination temperature of the un-calcined samples.

Typical TG curves of the materials before calcination are shown in Fig. 2. All samples showed basically one event of mass loss that can be attributed to the releasing of physisorbed and structural water molecules. The decomposition of the precursor (mostly $Zr(OH)_4$) occurred mainly between 70–500 °C, with a mass loss which could attain up to the 39% of the initial mass. The residue at 700 °C corresponds essentially to WO_x/ZrO_2 oxides, as shown by chemical analysis and XRD.

Table 1 Physicochemical characteristics of pure zirconia and tungstated zirconia catalysts

Sample	W content/ mass%	BET surface area/m^2 g^{-1}	Acidity		
			Q_{init}/kJ mol^{-1}	$V_{tot}/\mu mol_{NH_3}$ g^{-1}	$V_{irr}/\mu mol_{NH_3}$ g^{-1}
XZO- 1903-01	12.2	88	180	234	147
XZO- 1903-02	12.6	101	158	291	199
XZO- 1903-03	12.3	111	175	321	214
XZO- 1251-01	13.2	105	170	285	173
ZO	–	37	178	124	68

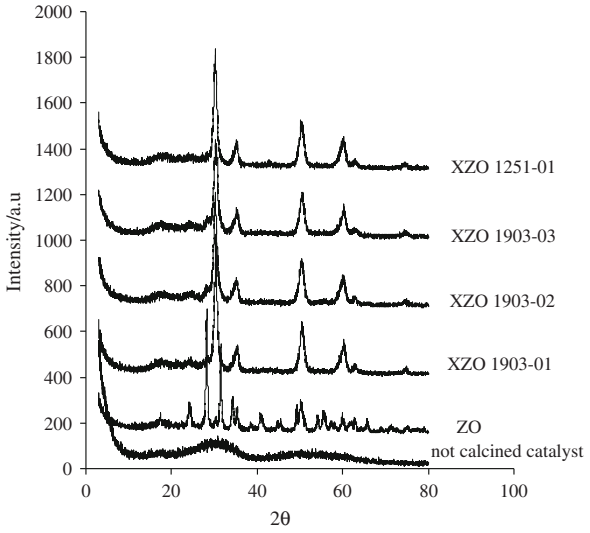

Fig. 1 XRD of WO_x/ZrO_2 commercial catalysts calcined at 700 °C, un-calcined, and of the bare ZrO_2

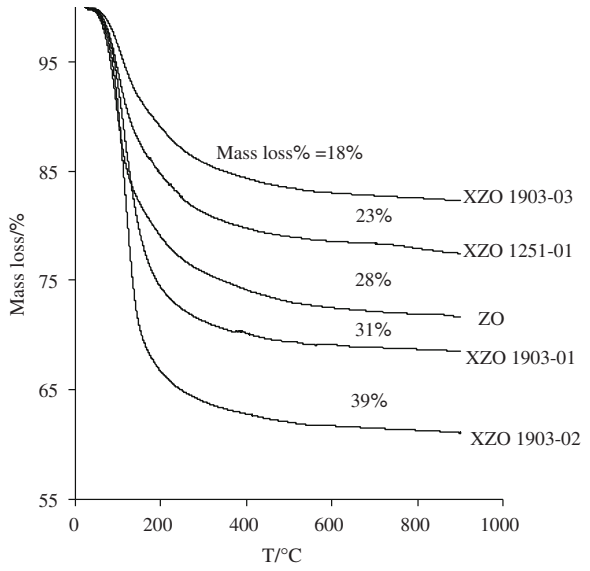

Fig. 2 TG curves of the un-calcined catalysts and zirconium hydroxide

The water loss due to the thermal treatment of the manufactured samples caused several changes in the zirconia which means decreasing surface area and formation of crystallites. Upon analysing the TG curves the decision to calcine all catalysts at 700 °C has been taken with the aim to remove most of the OH groups physically or chemically adsorbed on the surface, to decompose any precursor eventually still present, and to facilitate the adhesion and condensation of tungstate species on the ZrO_2 surface [13].

To verify the existence of species capable to participate in a red-ox cycle TPR/TPO/TPR2 analyses have been performed (see Fig. 3a) as described in the experimental section. A first reduction (TPR) has been carried out up to a maximum temperature of 700 °C, corresponding to the calcination temperature required to avoid structural changes in the catalyst structure before to achieve the red-ox cycle. TPR1 analysis showed for all the catalysts a reduction peak centered around 460 °C, that was completely re-oxidized during the TPO treatment and that could be attributed to the reduction of WO_3 crystallites, too small to be revealed by XRD.

The WO_3 species reduced at 460 °C can be re-oxidized and again reduced as evidenced by the reduction peak present in the TPR2 curve at the same temperature. In the TPR2 analysis, presented in Fig. 3b, the temperature was increased up to 1,000 °C. The TPR2 curves exhibited a broad reduction peak with a maximum temperature centered around 880 °C, which can be related to the reduction of tetrahedrally coordinated species anchored to the zirconia [14].

Because the XRD results did not indicate the presence of WO_3 crystalline structure, we can assume that the broad peak detected at temperature higher than 700 °C is related to the reduction of WO_x species (amorphous and non-stoichiometric oxides) strongly anchored to the support. No quantitative evaluation of the amount of H_2 consumed was done due to the experimental conditions (TPR2 T_{max} = 1,000°C) that did not allow to complete the high temperature peak.

The amounts of NH_3 adsorbed at 80 °C and the corresponding interaction energies with the bare ZO sample and the tungstated zirconia catalysts were determined by means of a volumetry–calorimetry coupled technique.

The equilibrium isotherms and differential heats of NH_3 adsorption are reported in Fig. 4a and b, respectively.

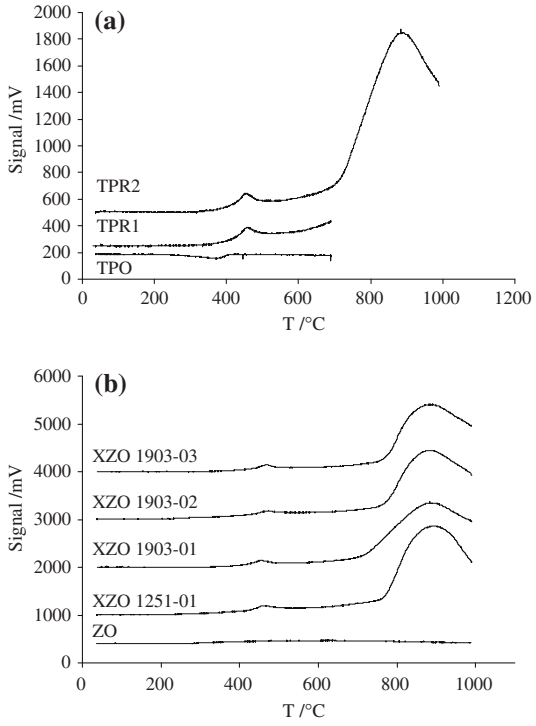

Fig. 3 **a** TPR1/TPO/TPR2 profiles for the XZO-1903-02 catalyst and **b** TPR2 profiles for the catalysts and zirconia

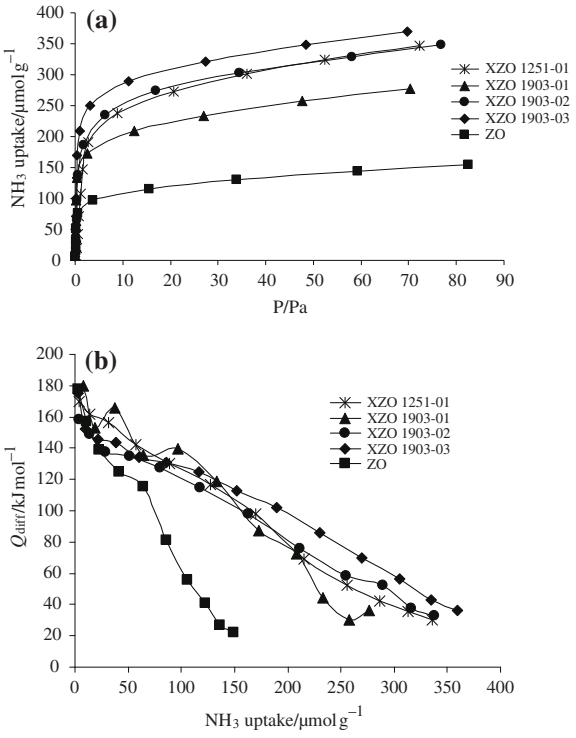

Fig. 4 **a** Ammonia adsorption isotherms and **b** differential heats of ammonia adsorption vs. coverage at 80 °C on WO_3/ZrO_2 catalysts and pure ZrO_2 calcined at 700 °C

The volumetric adsorption isotherms of the studied samples displayed in all cases an initial vertical section proportional to the amount of strongly chemisorbed NH_3 [15]. The heats of adsorption showed a decreasing trend upon increasing coverage, as usually observed for heterogeneous surfaces [7, 16, 17]. For WO_x/ZrO_2 catalysts the contribution from Lewis acidity may be influenced by the nature of the second oxide. The heterogeneity of the studied materials is due to the presence of acidic sites of different natures (i.e. Lewis acid sites from WO_x and both Brönsted and Lewis sites from zirconia) and presenting various strengths [18]. The tungsten oxide catalysts showed a higher capacity to adsorb NH_3, if compared to pure ZrO_2.

According to its adsorption properties towards NH_3 and CO_2, tungsten oxide was classified as acidic oxide while zirconia was assigned to the amphoteric group [19]. However, it was found that many oxides in the anphoteric group adsorbed more NH_3 and with a higher heat than some of the ones in the acidic group. Also the ZrO_2 sample adsorbed NH_3 with a heat of 150 kJ mol^{-1}, comparable to WO_3 [19]. Depending in their preparative procedures zirconia samples can display very different adsorption heats [20]. It should be noted that in the case of pure zirconia, the smaller surface area associated to our sample suggests a more complicated picture in ranking solid acids.

The slight increase in the total number of acid sites and the small decrease in the initial heat when going from sample XZO -1901-01 to sample 03 might be related to a difference in history and aging as they are issuing from the same initial batch.

Moreover our results are very comparable to those obtained by Vartuli et al. [21] who reported a total acidity of 308 μmol_{NH_3} g^{-1}, an initial heat of 155 kJ mol^{-1} and an overall average integral heat of adsorption of 107 kJ mol^{-1} for a WO_x/ZrO_2 catalyst prepared by coprecipitation (62 m^2 g^{-1}, 15.9 W mass%) and calcined at 700 °C.

Conclusions

Coupling WO_x species with ZrO_2 gives rise to improved materials both in terms of surface acidity and structure stability. The loss of surface area of pure zirconia is significantly inhibited by the presence of WO_x species. A calcination at 700 °C has been shown to be high enough to ensure the complete elimination of the synthesis precursor as well as the physisorbed and structural water, and low enough to avoid the sintering of the WO_x crystallites.

The combination of different thermal, calorimetric and structural analysis has permitted to deeply analyze samples that can be potentially applied as acidic catalysts in different environmental friendly reactions such as biodiesel-forming transesterifications.

References

1. Kim T, Burrows A, Kiely CJ, Wachs IE. Molecular/electronic structure—surface acidity relationships of model supported Tungsten oxide catalysts. J Catal. 2007;246:370–81.
2. Wachs IE, Kim T, Ross EI. Catalysis science of the solid acidity of model supported Tungsten oxide catalysts. Catal Today. 2006;116:162–8.
3. Busca G. Acid catalysts in industrial hydrocarbon chemistry. Chem Rev. 2007;107:5366–410.
4. Ji W, Hu J, Chen Y. The structure and surface acidity of zirconia-supported tungsten oxides. Catal Lett. 1998;53:15–21.
5. Kogelbauer A, Vassena D, Prins R, Armor J. Solid acids as substitutes for sulfuric acid in the liquid phase nitration of toluene to nitrotoluene and dinitrotoluene. Catal Today. 2000;55:151–60.
6. Lotero E, Liu Y, Lopez DE, Suwannakarn K, Bruce DA, Goodwin JG. Synthesis of biodiesel via acid catalysis. Ind Eng Chem Res. 2005;44:5353–63.
7. Bennici S, Auroux A. Thermal analysis and calorimetric methods. In: Jackson SD, Hargreaves SJ, editors. Metal oxide catalysis. : Wiley-VCH Verlag GmbH & Co; 2009. p. 391–442.
8. Naito N, Katada N, Niwa M. Tungsten oxide monolayer loaded on zirconia: determination of acidity generated on the monolayer. J Phys Chem B. 1999;103:7206–13.
9. Di Gregorio F, Keller V. Activation and isomerization of hydrocarbons over WO_3/ZrO_2 catalysts: I. Preparation, characterization, and X-ray photoelectron spectroscopy studies. J Catal. 2004;225:45–55.
10. Arata K. Preparation of superacids by metal oxides for reactions of butanes and pentanes. Appl Catal A Gen. 1996;146:3–32.
11. Kuba S, Concepcion Heydorn P, Grasselli RK, Gates BC, Che M, Knozinger H. Redox properties of tungstated zirconia catalysts: relevance to the activation of n-alkanes. Phys Chem Chem Phys. 2001;3:146–54.
12. Barton DG, Soled SL, Iglesia E. Solid acid catalysts based on supported tungsten oxides. Top Catal. 1998;6:87–99.
13. Garrido Pedrosa AM, Souza MJB, Melo DMA, Araujo AS. Thermo-programmed reduction study of Pt/WO_x-ZrO_2 materials by thermogravimetry. J Therm Anal Calorim. 2007;87:351–5.
14. Garrido Pedrosa AM, Souza MJB, Lima SH, Melo DMA, Souza AG, Araujo AS. Influence of the synthesis method on THE DTG-TPR profiles of Pt/WO_x-ZrO_2 bifunctional catalysts. J Therm Anal Calorim. 2007;87:703–7.
15. Sprinceana D, Caldararu M, Ionescu NI, Auroux A. Calorimetric study of the acidity and interface effects of tin dioxide layers deposited on another metal oxide. J Therm Anal Calorim 1999;56:109-15.
16. Auroux A. Acidity characterization by microcalorimetry and relationship with reactivity. Top Catal. 1997;4:71–89.
17. Busco C, Barbaglia A, Broyer M, Bolis V, Foddanu GM, Ugliengo P. Characterisation of Lewis and Brønsted acidic sites in H-MFI and H-BEA zeolites: a thermodynamic and ab initio study. Thermochim Acta. 2004;418:3–9.
18. Desmartin-Chomel A, Flores JL, Bourane A, Clacens JM, Figueras F, Delahay G, et al. Calorimetric and FTIR study of the acid properties of sulfated titanias. J Phys Chem B. 2006;110:858–63.
19. Auroux A, Gervasini A. Microcalorimetric study of the acidity and basicity of metal oxide surfaces. J Phys Chem. 1990;94:6371–9.
20. Solinas V, Ferrino I. Microcalorimetric characterisation of acid-basic catalysts. Catal Today. 1998;41:179–89.
21. Vartuli JC, Santiesteban JG, Traverso P, Cardona-Martinez N, Chang CD, Stevenson SA. Characterization of the acid properties of tungsten/zirconia catalysts using adsorption microcalorimetry and n-pentane isomerization activity. J Catal. 1999;187:131–8.

Publication II

Reac Kinet Mech Cat (2012) 105:101–111
DOI 10.1007/s11144-011-0385-1

Acid and redox properties of tungstated zirconia catalysts

R. Kourieh · S. Bennici · A. Auroux

Received: 18 May 2011 / Accepted: 1 October 2011 / Published online: 21 October 2011

Abstract Various tungstated zirconia catalysts with a WO_3 loading of about 16 wt% were characterized both in their acid and oxidation properties. The samples have been characterized in their micro-structural and surface properties by BET, X-ray diffraction, Raman spectroscopy, temperature programmed reduction, elemental chemical analysis. The surface acidity was determined by the techniques of NH_3 adsorption microcalorimetry and pyridine infrared spectroscopy (FT-IR). Improved acidity has been detected upon addition of WO_3 to zirconia by both techniques. The global acid strength and the total number of acid sites increased greatly with the formation of WO_x clusters on the zirconia support. This acidity increase can be attributed to the creation of Brønsted acid sites generated by the well dispersed WO_x domains, as observed by FT-IR pyridine desorption.

Keywords Tungstated zirconia catalysts · Surface acidity · FT-IR spectroscopy · Adsorption microcalorimetry

Introduction

Solid acids have numerous important industrial applications and supported metal oxides are considered as an important class among them. Zirconia supported WO_x catalysts have received considerable attention due to their potential catalytic application in hydrocarbon conversion reactions in the petrochemical industry [1–4]. They present also interesting applications in the selective catalytic reduction of NO_x to N_2 [5, 6]. Moreover, these catalysts represent an important model for the acid catalytic material in general [7].

R. Kourieh · S. Bennici · A. Auroux (✉)
IRCELYON, Institut de recherches sur la catalyse et l'environnement de Lyon, UMR 5256, CNRS, Université Lyon 1, 2 avenue Albert Einstein, 69626 Villeurbanne, France
e-mail: aline.auroux@ircelyon.univ-lyon1.fr

The challenge to obtain solid acid catalysts with acid sites of comparable strength to those in sulfuric acid is still open in an attempt to eliminate environmental concerns caused by the use, regeneration, transportation and storage of liquid acids [8]. Moreover, in the last years, the growing interest towards biodiesel, a clean fuel source which is viewed as a viable alternative for dwindling petroleum-based diesel resources, has led to renewed interest in acid catalysts [9]. Better yet, if solid acid catalysts could replace liquid acids, the corrosion and environmental problems associated with them could be avoided and product purification protocols could be significantly reduced, simplifying various hydrocarbons transformation reactions, and thus reducing their costs. Moreover, heterogeneous catalysts are preferable because offering easy separation from the reactants and products which are either liquids or gases.

It is known that catalytic activity of oxides can be related to the cooperative action of an oxidizing function and an acidic function. From this perspective, the determination of both redox and acidic properties of the catalytic centers becomes of fundamental importance in the present study which concerns tungstated zirconia samples with a high WO_x surface density. In addition, adsorption microcalorimetry and FT-IR desorption of basic probe molecules complete each other to supply the necessary information to map the acid sites in terms of strength, number and type of acid sites.

The acidity of solid catalysts is an important factor that determines their application as industrial catalysts, and, consequently, many of their catalytic properties can be directly related to their acidity. In the present work adsorption of a basic probe molecule (NH_3) was used in adsorption calorimetry, one of the most powerful techniques for the determination of the number, strength and strength distribution of the surface acid sites of catalysts [10]. IR spectroscopy of pyridine adsorption was used to distinguish the nature of the different types of surface acid sites [11]. Besides, the redox character was determined using temperature-programmed reduction experiments. The acid–base properties of the samples have been related to the presence of WO_x clusters on the zirconia support [12].

Experimental

Materials

Four commercial hydrated tungstated zirconia powders and a pure $Zr(OH)_4$ powder, all supplied by MEL-Chemicals, have been calcined at 700 °C under air flow for 4 h. The calcined samples were labeled as W/ZrO_2-1, W/ZrO_2-2, W/ZrO_2-3, W/ZrO_2-4 and ZrO_2 respectively and characterized as explained below.

Characterization

Elemental analysis was performed using ICP optical emission spectroscopy (ICP-OES) with an ACTIVA spectrometer from Horiba Jobin–Yvon.

The surface areas and pore sizes were measured by nitrogen adsorption at −196 °C on a Micromeritics 2010 apparatus after heat treatment under vacuum for 2 h at a temperature of 400 °C.

The X-ray diffraction (XRD) measurements were carried out on a Bruker D5005 powder diffractometer scanning from 3° to 80° (2θ) at a rate of 0.02°/s using Cu K_α radiation ($\lambda = 0.15418$ nm) source. The applied voltage and current were 50 kV and 35 mA.

Raman spectroscopy measurements were performed using a LabRAM HR (Jobin–Yvon) spectrometer. The excitation was provided by the 514.5 nm line of an Ar^+ ion laser (Spectra physics) employing a laser power of 100 μW. The laser beam was focused through microscope objective lenses (100×) down to a 1 μm spot on the sample.

The thermogravimetric (TG) analyses were performed on a SETARAM Labsys instrument in the 30–900 °C temperature range, with a heating rate of 5 °C min^{-1}, under air flow.

Temperature-programmed reduction (TPR) was performed using a TPD/R/O-1100 instrument (ThermoFisher). Prior to the TPR run, the fresh sample was treated in a stream of O_2/He (0.998% v/v, flowing at 20 mL min^{-1}), ramping the temperature at 10 °C min^{-1} from 40 to 350 °C and maintaining it for 60 min, and then cooled to RT. The TPR measurement was carried out using H_2/Ar (4.98% v/v) as reducing gas mixture, flowing at 20 mL min^{-1}. The heating rate was 10 °C min^{-1} from 40 to 1,000 °C. The sample mass was around 0.060 g in order to maintain the characteristic K factor [13] around 60 s.

Acidity

The pyridine adsorption infrared spectra were recorded with a Bruker Vector 22 FT-IR spectrophotometer (DTGS detector), in the 4,000–400 cm^{-1} range, with a resolution of 2 cm^{-1} and using 100 scans. The self-supporting wafer (50–60 mg, 18 mm diameter) was first activated in situ at 400 °C in oxygen flow for 14 h, then evacuated at the same temperature for 2 h and then exposed to pyridine (Air Liquide, 99.8%, vapor pressure 3.3 kPa) at room temperature for 5 min. The desorption was carried out by evacuation for 30 min each at room temperature, 100, 200, and 300 °C. The spectra were recorded at room temperature after desorption at each temperature.

Ammonia ($pK_a = 9.24$ and PA (proton affinity) = 857.7 kJ mol^{-1}), dried on 3A zeolite spheres, was used as a basic probe molecule to titrate the surface acid sites of the samples. Calorimetric and volumetric gas–solid titrations were carried out concomitantly in a volumetric line linked to a heat-flow microcalorimeter (Tian-Calvet type, C80 from Setaram). The chosen adsorption temperature was 80 °C to limit physisorption. About 0.1 g of powder sample was pretreated at 400 °C overnight (about 12 h) in air and then evacuated at the same temperature for 1 h prior to the measurements. Small successive NH_3 doses were sequentially sent onto the sample, up to a final NH_3 pressure of about 60 kPa. The equilibrium pressure relevant to each adsorbed amount was measured by means of a differential Barocel capacitance manometer (Datametrics). At the end of the adsorption, a second

adsorption was performed after desorption (1 h at 80 °C) of the NH_3 amount weakly retained on the surface. The difference between the first and second isotherms at 27 kPa represents the strongly chemisorbed NH_3 amount, the so-called irreversible amount (V_{irr}).

Results and discussion

Characterization

TG analyses (in Fig. 1) were carried out to help in determining the most accurate calcination temperature of the commercial sample precursors necessary to ensure a total removal of water while maintaining a high surface area and avoiding the transformation of zirconia from tetragonal to monoclinic phase.

All the samples showed the same behavior, which is basically a single event of weight loss that can be attributed to the releasing of physisorbed and structural water molecules. The decomposition of the precursor (mostly $Zr(OH)_4$) occurred mainly between 70 and 500 °C, with a weight loss which could attain up to the 39% of the initial weight. The weight loss can be associated to the release of physically bound water and to dehydroxylation of hydroxyl bridges to form oxide nuclei in order to obtain the final tungstated zirconia samples [14]. The resulting materials at 700 °C correspond to WO_x/ZrO_2 oxides, as shown by chemical analysis and XRD.

The water loss due to the thermal treatment of the manufactured zirconia precursor caused several changes which means decreasing surface area and formation of crystallites. Table 1 shows the weight loss at 200, 400, 700, 900 °C respectively. Analyzing the TGA results, a calcination temperature of 700 °C confirms that most of the OH groups physically or chemically adsorbed on the surface were removed and that this temperature is high enough to decompose any

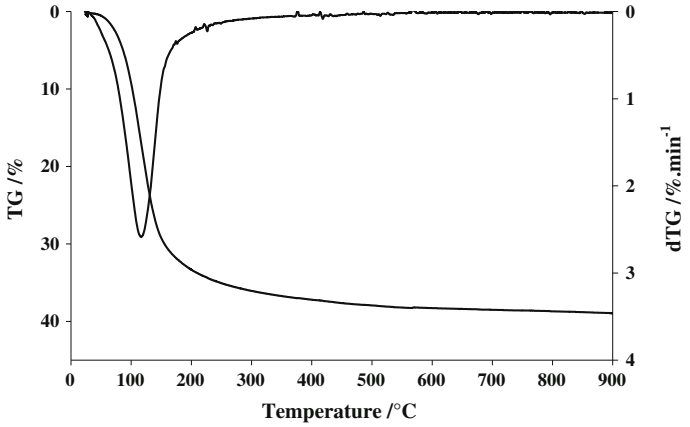

Fig. 1 TG and dTG curves of the commercial un-calcined sample precursor (W/ZrO_2-3 reported as example)

Table 1 Samples weight loss at 400, 700, and 900 °C upon thermogravimetric (TG) analysis

Sample	Weight loss %			
	200 °C	400 °C	700 °C	900 °C
ZrO_2	21	26	28	28
W/ZrO_2-1	26	30	31	31
W/ZrO_2-2	33	37	39	39
W/ZrO_2-3	11	16	17	18
W/ZrO_2-4	15	20	22	23

precursor eventually still present, and facilitate the adhesion and condensation of tungstated species on the ZrO_2 surface [15].

More or less significant differences in the surface properties between the tungstated zirconia samples and the bare ZrO_2 support emerged from the various techniques used for characterizing the samples.

The chemical analysis values (expressed as WO_3 wt%) and the BET surface areas (in $m^2\ g^{-1}$) of the tungstated zirconia samples as well as of the pure zirconia are presented in Table 2. The tungsta amount was always close to 15–16 wt% which is close to the monolayer coverage (15.4 WO_3 wt% for a 100 m^2/g sample) assuming a W surface concentration of about 4 W-atom·nm^{-2} for the monolayer [16]. Even after calcination at 700 °C the catalysts maintained a remarkable surface area (between 80 and 105 $m^2\ g^{-1}$), while the bare calcined zirconia displayed a much lower surface area (37 $m^2\ g^{-1)}$ at such high temperature.

The XRD patterns showed that the calcination of the catalysts at 700 °C resulted in the appearance of the tetragonal ZrO_2 phase only. At the same calcination temperature, the ZrO_2 sample gave rise to the well known segregation into a mixture of tetragonal and monoclinic ZrO_2 with the specific reflections of the monoclinic phase at 28.3° and 31.6° 2θ [17–19]. It is known that at a given W concentration, the BET surface area and the tetragonal ZrO_2 phase content decrease with calcination temperatures higher than 500 °C [20]. The presence of WO_x species in fact inhibits

Table 2 Physicochemical characteristics of pure zirconia and tungstated zirconia samples

Sample	WO_3 content/wt%	BET surface area/$m^2\ g^{-1}$	Acidity			
			Q_{int} [a]/ J g^{-1}	V_{tot} [b]/ $\mu mol_{NH3}\ m^{-2}$	V_{irr} [c]/ $\mu mol_{NH3}\ m^{-2}$	V_{irr} [c]/ $\mu mol_{NH3}\ g^{-1}$
ZrO_2	–	37	13.1	3.35	1.82	68
W/ZrO_2-1	15.4	88	26.5	2.65	1.67	147
W/ZrO_2-2	15.9	101	29.5	2.88	1.97	199
W/ZrO_2-3	15.5	111	34.3	2.89	1.92	214
W/ZrO_2-4	16.6	105	30.1	2.71	1.64	173

[a] Total heat evolved at 27 Pa of NH_3 equilibrium pressure upon NH_3 adsorption

[b] Total amount of NH_3 retained as determined at 27 Pa of equilibrium pressure

[c] Irreversibly adsorbed amount of NH_3 as determined from the difference between the amounts adsorbed in the first and second adsorptions at 27 Pa

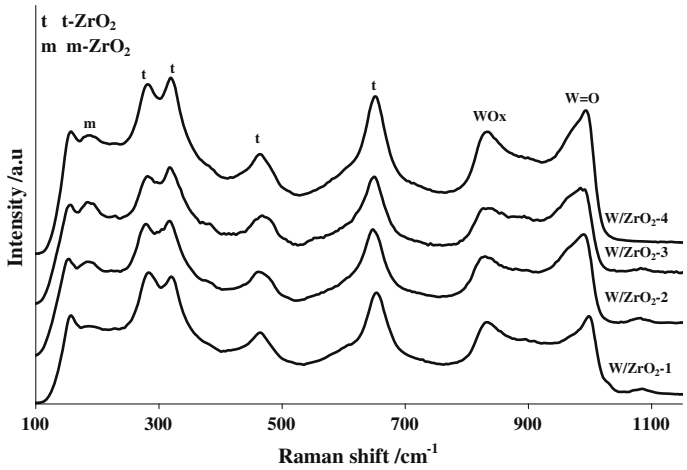

Fig. 2 RAMAN spectra of tungstated zirconia samples

the sintering and the transformation of tetragonal zirconia to monoclinic ZrO_2 crystallites, as demonstrated from the XRD and BET results of the four samples containing W. Moreover, no specific diffraction peak of WO_3 crystallites ($2\theta =$ 23.2°, 23.7°, and 24.3°) has been detected in any of the catalysts.

The surface structure of tungsten oxide and zirconia species on the tungstated zirconia samples was examined by Raman spectroscopy, from 1,600 to 200 cm^{-1}, as shown in Fig. 2. In agreement with the XRD results, the Raman spectra for the series of samples show that the zirconia is predominantly present in its tetragonal form [14, 21, 22]. We also observed a peak located around 181 cm^{-1} indicating the presence of the monoclinic phase which was not revealed by the XRD technique. A broad peak located at approximately 980 cm^{-1} was observed for the series of catalysts; this peak can be attributed to terminal W=O bonds [23]. Besides W–O–W linkages present in two-dimensional and three-dimensional extended WO_x, oligomers were observed at 807 cm^{-1} [12].

The reduction behavior of the catalysts was studied by TPR, in order to locate the reduction features within the temperature range covered by the experiment (room temperature to 1,000 °C). Reduction profiles reported in Fig. 3 show a reduction peak centered around 480 °C which could be attributed to the first step of WO_3 reduction, while the other broad reduction peak centered around 910 °C can be related to the complete reduction of WO_3 and to the reduction of tetrahedrally coordinated WO_x species (amorphous and non-stoichiometric oxides) strongly anchored to the zirconia surface [24].

Acidity

The amounts of NH_3 adsorbed at 80 °C and the corresponding interaction energies with the bare ZrO_2 sample and the tungstated zirconia catalysts were determined by means of a volumetry–calorimetry coupled technique.

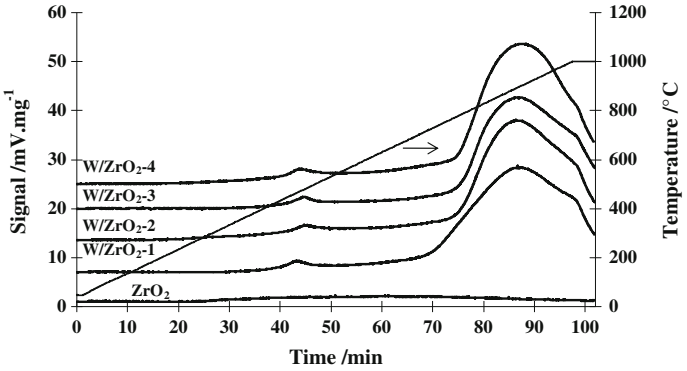

Fig. 3 TPR curves for the tungstated zirconia samples and pure ZrO_2 calcined at 800 °C

The equilibrium isotherms (ammonia uptake in μmol m^{-2} vs. equilibrium pressure) and differential heats of NH_3 adsorption (heats in kJ mol^{-1} vs. ammonia uptake in μmol g^{-1}catalyst) are reported in Fig. 4A, B, respectively. The volumetric adsorption isotherms of the studied samples displayed in all cases an initial vertical section proportional to the amount of strongly chemisorbed NH_3 [25]. The heats of adsorption showed a decreasing trend upon increasing coverage, as usually observed for heterogeneous surfaces [10, 26, 27]. For tungstated zirconia samples, the contribution from Lewis or Brønsted acidity may be influenced by the nature of the second oxide. The heterogeneity of the studied materials is due to the presence of acidic sites of different nature and presenting various strengths [28]. Table 2 gives the total number of acid sites as well as the number of strong acid sites (corresponding to the irreversibly adsorbed amount of NH_3 expressed both in μmol m^{-2} and in μmol g^{-1}), together with the corresponding integral heats. The tungstated zirconia samples showed a higher capacity to adsorb NH_3 (see Table 2, column 7) than pure zirconia.

According to its adsorption properties towards NH_3 and CO_2, tungsten oxide was classified as acidic oxide while zirconia was assigned to the amphoteric group [29]. However, it was found that many oxides in the amphoteric group adsorbed more NH_3 and with a higher heat than some oxides located in the acidic group. The ZrO_2 sample adsorbed NH_3 with an initial heat of 178 kJ mol^{-1}, comparable to bulk WO_3 (around 175 kJ mol^{-1}) as reported in the literature Ref. [29]. Depending on their preparative procedures zirconia samples can display very different adsorption heats [30].

Fig. 5 shows the acid site distributions of all the catalysts which means the number of sites of a given strength. No specific trend was evidenced for the population of sites with high strength ($Q_{diff} > 150$ kJ mol^{-1}) when compared to pure zirconia. Besides a remarkable increase of the sites of medium and weak acid strength ($150 > Q_{diff} > 50$ kJ mol^{-1}) can be observed for all tungstated zirconia samples. The difference in the acid sites population can be attributed to a difference in history and aging as they are issuing from the same initial batch [31].

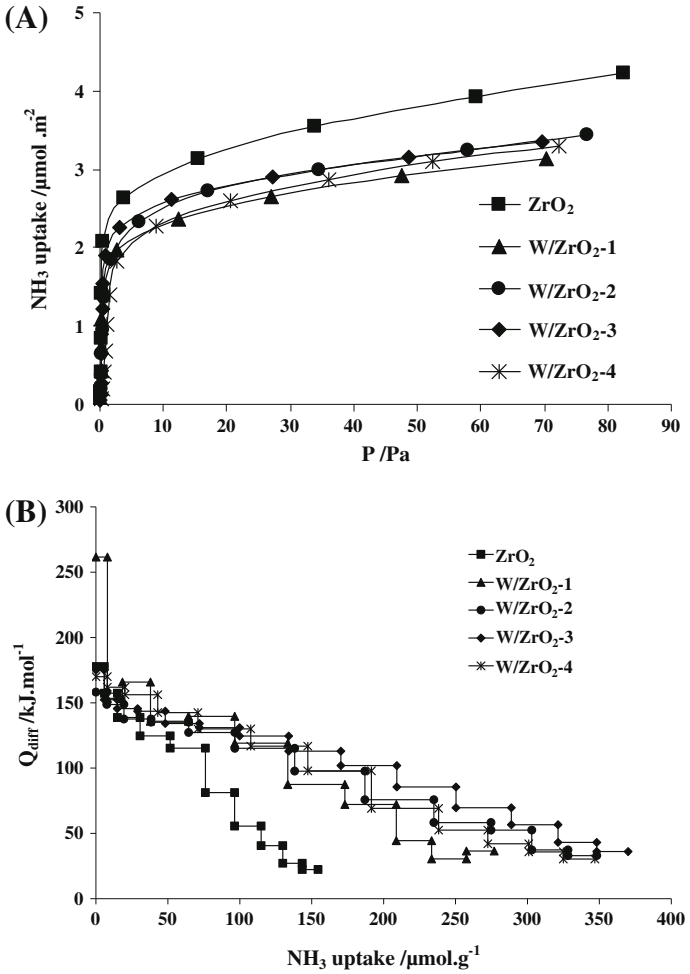

Fig. 4 **A** Ammonia adsorption isotherms and **B** differential heats of ammonia adsorption versus coverage at 80 °C for WO_x/ZrO_2 catalyst and pure ZrO_2

Moreover our results are comparable to those obtained by Vartuli et al. [32] who reported a total acidity of 308 μmol_{NH3} g^{-1}, an initial heat of 155 kJ mol^{-1} and an overall average heat of adsorption of 107 kJ mol^{-1} for a tungstated zirconia catalyst prepared by coprecipitation (62 m^2 g^{-1}, 15.9 W wt%) and calcined at 700 °C.

The study by FT-IR of pyridine desorption as a base probe molecule is one of the most applied methods for characterizing the nature of the surface acid sites. The band at 1,455–1,438 cm^{-1} is characteristic of Lewis acid sites, while the band at around 1,540 cm^{-1} can be attributed to Brønsted acid sites [33–35].

Fig. 6A–B present the IR spectra of ZrO_2 and W/ZrO_2-3 sample (as examples), after desorption of pyridine at different temperatures. On pure zirconia, pyridine molecules bonded to Lewis acid sites correspond to the bands observed at 1,444,

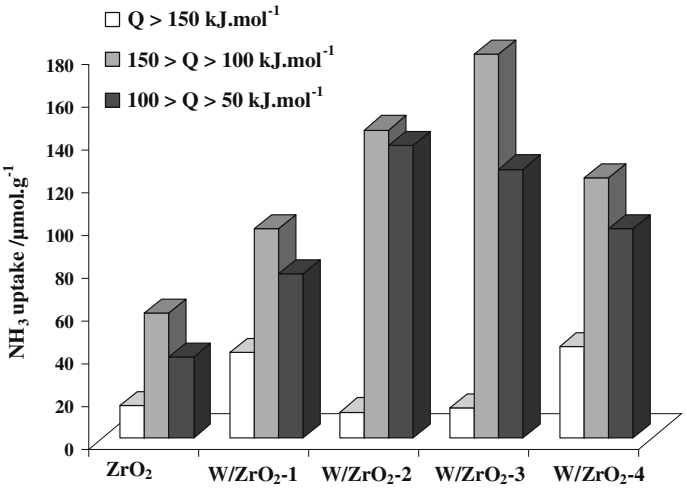

Fig. 5 Acid sites strength distribution of tungstated zirconia and ZrO_2 samples

1,575 and 1,609 cm^{-1}. These results are comparable to those obtained by Ouyang et al. [36]. The W/ZrO_2-3 sample showed the same bands of Lewis acid sites as pure zirconia, but also displayed absorbance at 1,540 and 1,639 cm^{-1} which corresponds to pyridinium ions bonded to Brønsted acid sites. The appearance of Brønsted acid sites on the W/ZrO_2 sample can be related to the presence of dispersed WO_x domains, composed of two-dimensional polytungstate allowing protons to remain accessible at external surfaces [12]. The band present at 1,489 cm^{-1} for both samples, is a combined band generated from pyridine bonded to both Brønsted and Lewis sites [35]. A considerable decrease in intensity is observed for both Lewis and Brønsted sites assigned bands, in both samples after desorption at 300 °C. It has been reported in the literature [35] that pure zirconia presents a medium to weak acidity corresponding to Lewis sites, while WO_3 shows significant to very strong Brønsted acidity.

Conclusion

Coupling WO_x species with ZrO_2 gave rise to improved materials both in terms of surface acidity and structure stability. The loss of surface area of pure zirconia is significantly inhibited by the presence of WO_x species by stabilization of the tetragonal phase. The ammonia adsorption microcalorimetry and FT-IR pyridine desorption studies have shown an obvious difference of surface acidity between the zirconia and the tungstated zirconia samples. The appearance of strong Brønsted sites on all the tungstated zirconia samples studied in this work can be associated to the presence of WO_x clusters on the surface.

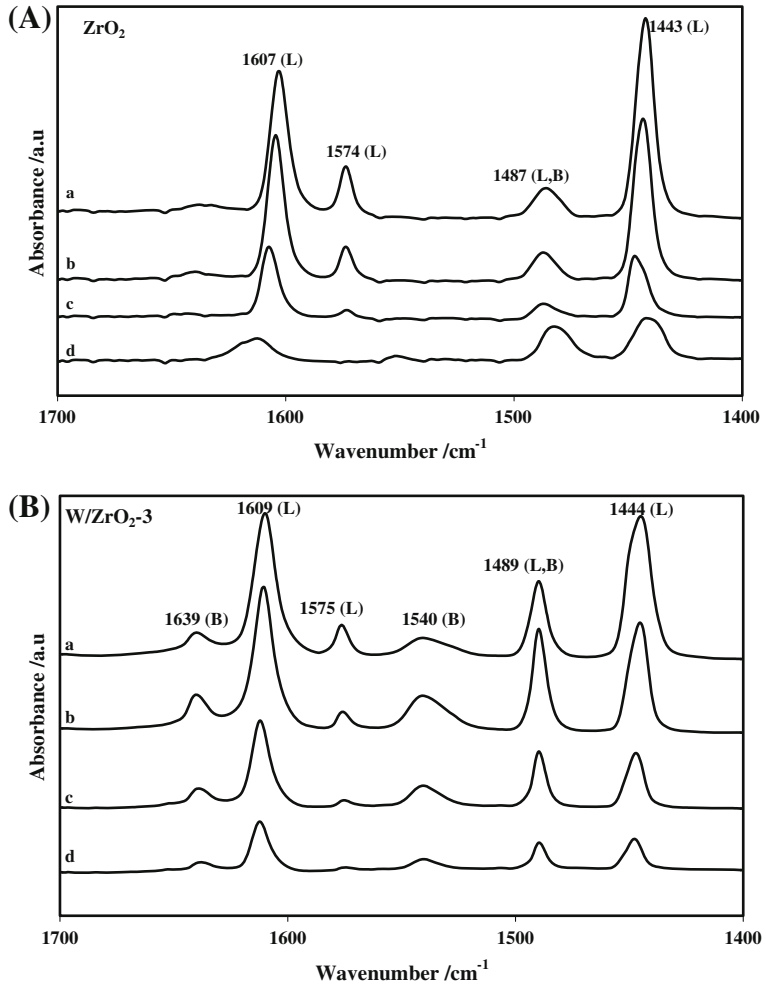

Fig. 6 FT-IR spectra for pyridine desorption on **A** ZrO_2 and **B** W/ZrO_2-3 sample at different temperatures: **a** room temperature, **b** 100 °C, **c** 200 °C, **d** 300 °C

The combination of various IR, calorimetric and structural analyses has permitted to deeply characterize samples that can be potentially applied as acidic catalysts in different environment-friendly reactions such as biodiesel-forming transesterifications.

References

1. Kim T, Burrows A, Kiely CJ, Wachs IE (2007) J Catal 246:370–381
2. Wachs IE, Kim T, Ross EI (2006) Catal Today 116:162–168
3. Busca G (2007) Chem Rev 107:5366–5410
4. Ji W, Hu J, Chen Y (1998) Catal Lett 53:15–21

5. Chang CD, Santiesteban JG, Shihabi DS, Stevenson SA (1995) U.S. Patent No. 5,401,478
6. Chang CD, Santiesteban JG, Shihabi DS, Stern DL, Vartuli JC (1996) U.S. Patent No. 5,552,128
7. Soultanidis N, Zhou W, Psarras AC, Gonzalez AJ, Lliopoulou EF, Kiely CJ, Wachs IE, Wong MS (2010) J Am Chem Soc 132:13462–13471
8. Kogelbauer A, Vassena D, Prins R, Armor JN (2000) Catal Today 55:151–160
9. Lotero E, Liu Y, Lopez DE, Suwannakarn K, Bruce DA, Goodwin JG (2005) Ind Eng Chem Res 44:5353–5363
10. Bennici S, Auroux A (2009) In: Jackson SD, Hargreaves SJ (ed) Metal oxide catalysis. WILEY-VCH Verlag GmbH, Weinheim
11. Bordoloi A, Mathew NT, Devassy BM, Mirajkar SP, Halligudi SB (2006) J Mol Catal A Chem 247:58–64
12. Macht J, Iglesia E (2008) J Phys Chem Phys 10:5331–5343
13. Monti D, Baiker A (1983) J Catal 83:323–335
14. Li M, Feng Z, Xiong G, Ying P, Xin Q, Li C (2001) J Phys Chem B 105:8107–8111
15. Garrido Pedrosa AM, Souza MJB, Melo DMA, Araujo AS (2007) J Therm Anal Calorim 87:349–353
16. Naito N, Katada N, Niwa M (1999) J Phys Chem B 103:7206–7213
17. Di Gregorio F, Keller V (2004) J Catal 225:45–55
18. Arata K (1996) Appl Catal A Gen 146:3–32
19. Kuba S, Concepcion Heydorn P, Grasselli RK, Gates BC, Che M, Knozinger H (2001) Phys Chem Chem Phys 3:146–154
20. Barton DG, Soled SL, Iglesia E (1998) Top Catal 6:87–99
21. Lopez DE, Suwannakarn K, Bruce DA, Goodwin JG Jr (2007) J Catal 247:43–50
22. Zhao B, Xu X, Gao J, Fu Q, Tang Y (1996) J Raman Spectrosc 27:549–554
23. Vaidyanathan N, Hercules DM, Houalla M (2002) Anal Bioanal Chem 373:547–554
24. Garrido Pedrosa AM, Souza MJB, Lima SH, Melo DMA, Souza AG, Araujo AS (2007) J Therm Anal Calorim 87:703–707
25. Sprinceana D, Caldararu M, Ionescu NI, Auroux A (1999) J Therm Anal Calorim 56:109–115
26. Auroux A (1997) Top Catal 4:71–89
27. Busco C, Barbaglia A, Broyer M, Bolis V, Foddanu GM, Ugliengo P (2004) Thermochim Acta 418:3–9
28. Desmartin-Chomel A, Flores JL, Bourane A, Clacens JM, Figueras F, Delahay G, Giroir-Fendler A, Lehaut-Bornoul C (2006) J Phys Chem B 110:858–863
29. Auroux A, Gervasini A (1990) J Phys Chem 94:6371–6379
30. Solinas V, Ferrino I (1998) Catal Today 41:179–189
31. http://www.zrchem.com/
32. Vartuli JC, Santiesteban JG, Traverso P, Cardona-Martinez N, Chang CD, Stevenson SA (1999) J Catal 187:131–138
33. Sohn JR, Park MY (1998) Langmuir 14:6140–6145
34. Cortés-Jacome MA, Angeles-Chaves C, Lopez-Salinas E, Navarret J, Toribio P, Toledo JA (2007) J Appl Catal A Gen 318:178–189
35. Busca G (1999) Phys Chem Chem Phys 1:723–736
36. Ouyang F, Nakayama A, Tabada K, Suzuki E (2000) J Phys Chem B 104:2012–2018

Publication III

Catalysis Communications 19 (2012) 119–126

Contents lists available at SciVerse ScienceDirect

Catalysis Communications

journal homepage: www.elsevier.com/locate/catcom

Short Communication

Investigation of the WO_3/ZrO_2 surface acidic properties for the aqueous hydrolysis of cellobiose

R. Kourieh [a], S. Bennici [a], M. Marzo [b], A. Gervasini [b], A. Auroux [a,*]

[a] Université Lyon 1, CNRS, UMR 5256, IRCELYON, Institut de recherches sur la catalyse et l'environnement de Lyon, 2 avenue Albert Einstein, F-69626 Villeurbanne, France
[b] Dipartimento di Chimica Fisica ed Elettrochimica, Università degli Studi di Milano, Via Golgi 19, 20133 Milano, Italy

ARTICLE INFO

Article history:
Received 10 June 2011
Received in revised form 13 December 2011
Accepted 21 December 2011
Available online 29 December 2011

Keywords:
Tungsten oxide
Zirconia supported catalysts
Surface acidity
Adsorption microcalorimetry
Cellobiose hydrolysis

ABSTRACT

A series of WO_x/ZrO_2 with various tungsten oxide loadings (1–20) wt.% was prepared by co-precipitation. The catalysts were characterized by XRD, BET, XPS, Raman spectroscopy, TPR, ammonia adsorption microcalorimetry and pyridine FT-IR spectroscopy. XRD and Raman results showed that the ZrO_2 support is predominantly present in the monoclinic phase when the WO_3 loading was less than 5 wt.% and predominantly in the tetragonal phase above 10 wt.%. No formation of bulk WO_3 was detected for the catalysts calcined at 700 °C, which is also the case for the highest loaded samples. TPR results revealed that isolated WO_3 species are easier to reduce than amorphous WO_x. The ammonia adsorption microcalorimetric study evidenced acid sites with adsorption heats in the range $90 < Q_{diff} < 130$ kJ.mol^{-1}, in amounts which increase with increasing WO_3 loading until reaching the monolayer. Concerning the acid site nature, a progressive increase of the amount of Brønsted sites with the WO_3 loading was observed. The catalytic reaction of cellobiose disaccharide hydrolysis showed a better catalytic performance on the highest WO_3 loaded catalysts, associated to the presence of Zr-stabilized WO_x clusters and a strong protonic acidity.

1. Introduction

In the last few years, a great deal of attention has been given to supported metal oxides for their interesting catalytic behavior depending on the kind of support, the content of active component, and the preparation method. The challenge to obtain solid acid catalysts with acid sites of comparable strength to those present in sulphuric acid is still open, in an attempt to eliminate environmental concerns caused by the use, regeneration, transportation and storage of liquid acids [1,2]. Tungstated zirconia catalysts have a remarkable catalytic activity for acid-catalyzed reactions in particular paraffin isomerization, cracking, alkylation, liquid-phase Beckmann rearrangement of cyclohexanone oxime and biodiesel synthesis (esterification and transesterification of fatty acids) [3–6]. This catalytic activity is related to the surface acidic functions and for such catalysts, new applications in emerging catalytic fields like biomass exploitation, are desirable. Tungstated zirconia possesses advantages due to the formation of acid sites, which depends strongly on the preparation conditions and calcination temperatures. Higher calcination temperatures are required for the stabilization of the zirconia tetragonal phase and the anchorage of WO_x species on the surface, thereby leading to the creation of strong acid sites [7]. From this perspective, the determination of the acidic properties of catalytic centers becomes of fundamental interest.

A fundamental understanding of the WO_3 dispersed phase evolution on zirconia has been presented in the literature by many authors and recently reviewed by Iglesia [8] with particular attention to the evaluation of the catalytic consequences of the size and structural composition. Evolution of the W – O – W to W═O ratio affects the catalytic activity in given reactions, such as isomerization reactions and alcohol dehydration. The presence of oxygen-deficient domains attributed to a very poor dispersion of WO_x structures, contributes to low Brønsted acid site densities, while higher Brønsted acidity was observed on well dispersed WO_x domains on oxygen-rich supports.

Many investigations have been done to measure the acid strength of tungstated zirconia materials, and the direct measurement of the strength of a solid acid is not as straightforward as in a liquid acid. Issues such as heterogeneity of the surface and accessibility of acid sites, make the determination of acid strength of solid acids difficult. In addition, when the catalyst is used for liquid–solid heterogeneous reactions, the solvating ability of protic and polar liquids, in particular, toward the Lewis acid and highly polarized Brønsted sites, can modify the *intrinsic* acidity of the surface, thus reducing the amount or modifying the nature of its acid sites [9]. This causes more difficulty in establishing valid property-activity relationships.

In addition, it has been demonstrated that in the case of WO_x/ZrO_2 catalysts, the density of strong acid sites responsible for their remarkable catalytic activity is extremely low, ~4 μmol H^+/g catalyst [10]. This low density of sites causes difficulties in the characterization of the sites relevant to catalysis. Typically, the acid strength of a solid catalyst is measured from the interaction of the acid site with a base

* Corresponding author. Tel.: +33 472 445398; fax: +33 472 445399.
E-mail address: aline.auroux@ircelyon.univ-lyon1.fr (A. Auroux).

1566-7367/$ – see front matter © 2011 Elsevier B.V. All rights reserved.
doi:10.1016/j.catcom.2011.12.030

probe molecule such as NH_3 in adsorption calorimetry or pyridine in FT-IR adsorption spectroscopy, which are among the most powerful techniques for the determination of the number, strength and strength distribution of surface acid sites of catalysts [4,11]. In the present work we have prepared tungstated zirconia catalysts by coprecipitation and with various tungsten oxide loadings and fully characterized them in their structural and surface acid/base properties. To complete the study, the test reaction of cellobiose hydrolysis (the disaccharide obtained from cellulose hydrolysis) was studied to obtain new information on the performance of WO_3 surface acid properties in reactions running in protic solvent, like water. Cellobiose is a disaccharide derived from the condensation of two glucose molecules linked by a $\beta(1\rightarrow4)$ bond. It can be obtained by enzymatic or acid inorganic hydrolysis of cellulose and cellulose rich materials such as cotton, jute, or paper. Its hydrolysis is not easy to perform due to strong inter- and intra-molecular hydrogen bonds which are formed from the eight free alcohol (COH) groups, and three ether linkages of the molecule. Concerning the inorganic acids able to hydrolyze cellobiose, cationic ion exchange resins and zeolites in particular conditions [12,13] are reported in the literature. In any case, only catalysts with strong protonic acidity (Brønsted sites) are good candidates for this task. Moreover, when the heterogeneous catalytic reaction occurs in water, the catalyst has to maintain its acidity even in this protic and polar solvent, which is known to quench the acidity of many good solid acids, such as zeolites.

Up to now, as very few solid acids are known to be effective for this reaction [9,12–14], high temperatures (140–180 °C) are often needed to observe appreciable glucose production from cellobiose hydrolysis. Interesting results have been reported on sulphated zirconia modified SBA-15 [15] for which a glucose yield of 60% was observed after 90 min of reaction at 160 °C. Layered transition metal oxides, such as $HNbMoO_6$ oxides have been successfully used as solid-acid catalysts for glucose production from saccharides [16]. Cellobiose has been hydrolyzed on $HNbMoO_6$ with a higher rate than Amberlyst-15 and Nafion. This high catalytic activity has been attributed to the strong acidity, water tolerance, and facile intercalation ability of saccharides in this catalytic material. Other promising catalytic material is the mesoporous Nb–W mixed oxide [17], with activity in disaccharide hydrolysis exceeding the maximum performance of any other catalytic materials comparatively tested (ion-exchanged resins, niobic acid, zeolites). In view of the importance of reactions of biomass exploitation, the discovery of new acid catalysts working in mild conditions is thoroughly required for this kind of application. WO_x/ZrO_2 catalysts, well known for their high acid surface chemistry, could potentially be good candidates for this near-boiling water phase biomass reaction.

2. Experimental

2.1. Catalyst preparation

An amount of $ZrOCl_2\cdot 8H_2O$ was dissolved under stirring in distilled water. A solution containing concentrated NH_4OH, distilled H_2O, an amount of ammonium metatungstate hydrate [$(NH_4)_6H_2W_{12}O_{40}\cdot nH_2O$, Fluka, ≥99.0% WO_3] to have a WO_3 loading ranging from (1–20) wt.%, was added dropwisely over a 30–45 min period. The pH of the final solution was adjusted to approximately 9 by the addition of concentrated ammonium hydroxide. This slurry was then put in polypropylene bottles and placed in a steambox (100 °C) for 72 h. The product formed was recovered by filtration, washed with excess water, and dried overnight at 85 °C. The catalysts were calcined in flowing air for 4 h, at 700 °C. The final WO_x/ZrO_2 catalysts were labeled as wt.%-WO_3/ZrO_2-Cop.

2.2. Catalyst characterization

Elemental analysis was performed using ICP optical emission spectroscopy (ICP-OES) with an ACTIVA spectrometer from Horiba Jobin Yvon.

The surface areas, pore volumes and pore sizes were measured by nitrogen adsorption at −196 °C on a Micromeritics 2010 apparatus after heat pretreatment under vacuum for 2 h at a temperature of 400 °C.

The X-ray diffraction (XRD) measurements were carried out on a Bruker D5005 powder diffractometer scanning from 3° to 80° (2θ) at a rate of $0.02°\,s^{-1}$ using a Cu Kα radiation (λ = 0.15418 nm) source. The applied voltage and current were 50 kV and 35 mA, respectively.

The X-ray photoelectron spectra (XPS) were obtained on a KRATOS AXIS Ultra DLD spectrometer equipped with a hemispherical electron analyzer and an Al anode (Al Kα = 1486.6 eV) powered at 150 W, a pass energy of 20 eV, and a hybrid lens mode. The detection area analyzed was 700 μm × 300 μm. Charge neutralization was required for all samples. The peaks were referenced to the C–(C, H) components of the C 1s band at 284.6 eV. Shirley background subtraction and peak fitting to theoretical Gaussian–Lorentzian functions were performed using an XPS processing program (Vision 2.2.6 KRATOS). The residual pressure in the spectrometer chamber was 5×10^{-9} mbar during data acquisition.

Raman spectroscopy measurements were performed using a LabRAM HR (Jobin Yvon) spectrometer. The excitation was provided by the 514.5 nm line of an Ar+ ion laser (Spectra physics) employing a laser power of 100 μW. The laser beam was focused through microscope objective lenses (100×) down to a 1 μm spot on the sample.

Temperature-programmed reduction (TPR) was performed using a TPD/R/O-1100 instrument (ThermoFisher). Prior to the TPR run, the fresh sample was treated in a stream of O_2/He (0.998% v/v, flowing at 20 mL min^{-1}), ramping the temperature at 10 °C min^{-1} from 40 °C to 350 °C and maintaining it for 60 min, and then cooled to RT. The TPR measurement was carried out using H_2/Ar (4.98% v/v) as reducing gas mixture, flowing at 20 mL min^{-1}. The heating rate was 10 °C min^{-1} from 40 °C to 1000 °C. Mass of catalyst samples was varied from 0.050 to 0.065 g to have approximately the same amount of WO_3 moles for all the analyzed samples.

Adsorption microcalorimetry measurements were performed at 80 °C in a heat flow calorimeter (C80 from Setaram) linked to a conventional volumetric apparatus equipped with a Barocel capacitance manometer for pressure measurements. The probe (ammonia) used for measurements (Air Liquide, purity > 99.9%) was purified by successive freeze–pump–thaw cycles. About 100 mg of sample was pretreated in the calorimetric quartz cell overnight at 400 °C, and then evacuated at the same temperature for 1 h prior to the measurements. The differential heats of adsorption were measured as a function of coverage by repeatedly introducing small doses of the adsorbate onto the catalyst until an equilibrium pressure of about 66 Pa was reached. The sample was then outgassed for 30 min at the same temperature, and a second adsorption was performed at 80 °C until an equilibrium pressure of about 27 Pa was attained in order to calculate the irreversibly chemisorbed amount of the probe molecule at this pressure.

The pyridine adsorption FTIR spectra were recorded at room temperature with a Bruker Vector 22 FTIR spectrophotometer (DTGS detector) operating in the 4000–400 cm^{-1} range, with a resolution of 2 cm^{-1} and 100 acquisition scans. In each pyridine adsorption FTIR measurement, the self-supporting wafer (about 50 mg, 18 mm diameter) was first activated in situ at 400 °C in oxygen flow for 14 h, then evacuated at the same temperature for 2 h and then exposed to pyridine (Air Liquide, 99.8%, vapor pressure 3.3 kPa) at room temperature for 5 min. The desorption was carried out by evacuation for 30 min each at room temperature, 100 °C, 200 °C, and 300 °C, respectively. The spectra were recorded at room temperature after adsorption and desorption at each temperature.

2.3. Kinetic measurements of cellobiose hydrolysis

D-(+)-cellobiose (Fluka, ≥99.0% purity) was used as substrate. The kinetic tests of cellobiose catalytic dehydration to glucose were

Table 1
Physico-chemical characteristics of WO_x/ZrO_2 samples prepared by co-precipitation method.

Sample	WO_3 content/wt.%	W content/wt.%	BET surface area/$m^2\ g^{-1}$	W surface density/ W-atom nm^{-2}	Acidity		
					Q_{init}/[a] kJ mol^{-1}	V_{tot}/[b] $mol_{NH3}\ g^{-1}$	V_{irr}/[c] $mol_{NH3}\ g^{-1}$
ZrO_2	–	–	37	–	178	124	68
0.9-WO_3/ZrO_2-Cop	0.90	0.71	50	0.5	176	162	98
4.7-WO_3/ZrO_2-Cop	4.72	3.74	56	2.1	162	173	107
9.9-WO_3/ZrO_2-Cop	9.97	7.91	78	3.3	175	240	156
15.2-WO_3/ZrO_2-Cop	15.22	12.08	104	3.8	193	296	185
19-WO_3/ZrO_2-Cop	19.00	15.06	104	4.7	174	278	180

[a] Heat evolved from the first NH_3 dose.
[b] Total amount of NH_3 retained as determined at 27 Pa of equilibrium pressure.
[c] Irreversibly adsorbed amount of NH_3 as determined from the difference between the amounts adsorbed in the first and second adsorptions at 27 Pa.

performed in water in a glass batch thermostated reactor at atmospheric pressure and at a constant temperature of 97 °C (reaction temperature ± 1 °C) under strong magnetic stirring. The reactions were followed for a period of 32 h.

A weighted amount of calcined catalyst sample of about 100 mg was crushed and sieved in 300 μm particle size and put into the reactor without any pre-treatment. Preliminary tests of WO_3 leaching in hot water (50 °C) were performed on the 9.9-WO_3/ZrO_2 catalyst, chosen as representative sample. The tests indicated the absence of any amount of tungsten in the solution at this temperature.

Aqueous cellobiose solution (total volume of 10 mL) of 0.1 $g\cdot mL^{-1}$ (corresponding to 0.3 M) was prepared for each run. The reaction temperature was attained in approximately 15 min. Starting from 30 min, amounts of solution (0.5 mL) were taken off from the reactor at fixed time on stream (TOS) (typically at 0.5, 8, 24, and 32 h). The sampling was filtered before analysis (0.45 m nylon filter).

Analyses were performed in a liquid-chromatography apparatus (HPLC) consisting of an injector (Waters U6K), pump (Waters 510), and a refractive index detector (Waters 410). A Carbohydrate Analysis column (Waters) operating at room temperature and eluted with an acetonitrile:water 80:20 solution was used. Cellobiose and glucose were quantitatively determined from previous calibration measurements employing solutions of known concentration of both products.

In parallel, some analyses were also repeated employing an enzymatic kit of analysis (D-Glucose/D-Fructose UV-method, Biopharm) for the determination of the glucose concentration by using a Beckman spectrophotometer (mod. DU 640).

3. Results and discussion

3.1. Structural properties

The chemical analysis values (expressed as W and WO_3 wt.%), the BET surface areas (in $m^2\ g^{-1}$) and theoretical W surface concentration of the zirconium–tungsten mixed oxides are presented in Table 1.

Surface area values increased as the WO_3 (wt.%) content increased. The catalysts with WO_3 loading higher than 10 wt.% maintained a surface area between 78 and 104 $m^2\cdot g^{-1}$. It seems likely that the interaction between tungsten oxide and ZrO_2 reduced the surface mobility of zirconia thanks to formation of WO_x overlayer [18,19]. Yet further increase in WO_3 loading above 15 wt.% did not lead to higher surface area. The maximum surface area (104 $m^2.g^{-1}$) obtained at the given calcination temperature of 700 °C can be attributed to the surface stabilization of the ZrO_2 support by direct interaction with the WO_x surface species [20]. From the measured surface area, the surface concentration of tungsten was calculated as follows;

$$WO_3\,\text{concentration}\left(W-\text{atom}\cdot nm^{-2}\right)=\frac{mWO_3\times 10^{-2}\times N_A}{M_{WO_3}\times S_{BET}\times 10^{18}}$$

where; mWO_3 is the WO_3 wt.% loading, $M_{WO3}=231.8\ g\cdot mol^{-1}$ is the WO_3 molecular weight, N_A is the Avogadro number, 6.023×10^{23}, S_{BET} is the surface area of the catalyst in $m^2\cdot g^{-1}$.

Assuming a W surface concentration of (3.5–4) W-atom·nm^{-2} for the monolayer [21,22], a maximum surface area is obtained for this coverage.

The X-ray diffraction patterns of the m-WO_3/ZrO_2-Cop catalysts are shown in Fig. 1. The XRD patterns of the catalysts with WO_3 loading lower than 10 wt.% showed diffraction peaks characteristic of tetragonal ZrO_2 at $2\theta=30.17°$, 35.31°, 49.79°, and 60° [3,5], and monoclinic ZrO_2 was observed at $2\theta=28.3°$ and 31.6° [3,23,24]. For catalysts with WO_3 loading higher than 10 wt.% the XRD patterns show only the specific reflections of the tetragonal phase of zirconia. The presence of WO_x species at a certain WO_3 concentration (≥10 wt.%), in fact inhibits the sintering and the transformation to monoclinic ZrO_2 crystallites. No crystalline WO_3 phase ($2\theta=23.2°$, 23.7°, and 24.3°) appeared even for a WO_3 content close to 20 wt.%, thus indicating that tungsten oxide was present in a highly dispersed manner. However, the presence of WO_3 crystallites with size less than 4 nm, which is beyond the detection capacity of the powder XRD technique, cannot be excluded.

The surface structure of tungsten oxide and zirconia species on the m-WO_x/ZrO_2-Cop catalysts was examined by Raman spectroscopy, from 1600 to 200 cm^{-1}, as shown in Fig. 2. In agreement with the XRD results, the Raman spectra for the series of catalysts shows that the zirconia is predominantly present in the tetragonal form for the catalysts with WO_3 loading higher than 10 wt.% [5,25,26]. A broad peak located at approximately 980 cm^{-1} is observed for the catalysts with a WO_3 loading ≥5 wt.%; this peak can be attributed to surface W═O interaction species [27]. This Raman band shifts from 977 to

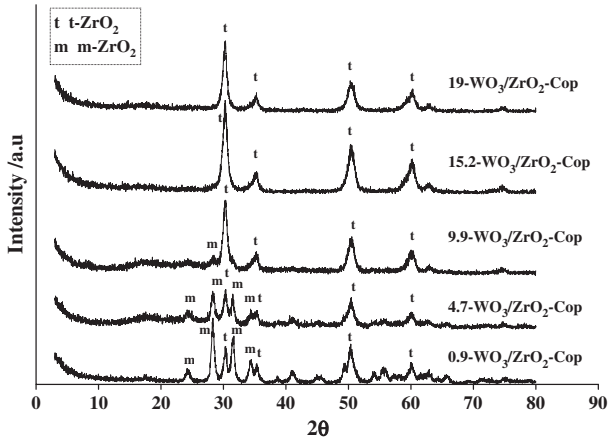

Fig. 1. XRD of WO_x/ZrO_2 catalysts prepared by co-precipitation and calcined at 700 °C.

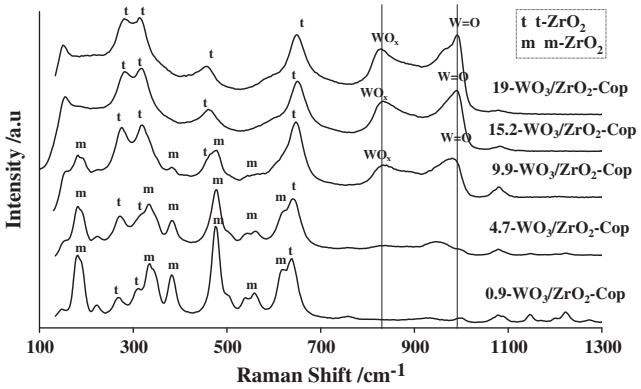

Fig. 2. RAMAN spectra of WO_x/ZrO_2 catalysts prepared by co-precipitation.

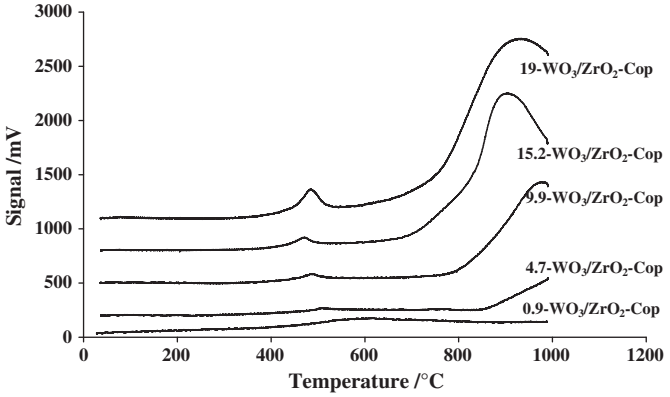

Fig. 3. TPR profiles of WO_x/ZrO_2 catalysts prepared by co-precipitation.

990 cm^{-1} with increasing surface WO_x coverage reflecting the transformation of surface monotungstate to polytungstate species. This shift has been also observed by other authors [28,29]. Crystalline WO_3 species are present for sample with 9.97 WO_3 wt.% or higher surface density evidenced by Raman bands at 820 cm^{-1}. WO_x domains grow with WO_x surface density leading to these WO_3 crystallites. For samples with high W surface concentration the strong and complex Raman spectrum of the zirconia makes the tungsten bands with a position lower than 800 cm^{-1} almost undetectable.

Table 2 presents the binding energies (BE) of Zr $3d_{5/2}$ and W $4f_{7/2}$. The BE of Zr 3d value was shifted to higher BE as the WO_3 loading increased and this indicates the flow of electron density from zirconia phase into WO_x phase through Zr–O–W linkages. These values are close to the corresponding BE of Zr^{4+} in bulk zirconia (182.1 eV) [30] while the BEs of the W $4f_{7/2}$ are close to the reported value of W^{6+} (35.5 eV) [31]. The surface W/Zr ratio increases roughly linearly as the loading of WO_3 increases. Tungsten surface enrichment is observed for all samples indicating that the activation treatment at 700 °C was effective in expelling tungsten from the bulk to the surface of the co-precipitated m-WO_x/ZrO_2-Cop [32].

The reduction behavior of the catalysts was studied by TPR, in order to locate the reduction features within the temperature range covered by the experiment (room temperature to 1000 °C). Fig. 3 shows the reduction profiles for the co-precipitated catalysts in the temperature range in which features due to tungsten reduction appear (>400 °C). As observed, a reduction peak centered around 480 °C could be attributed to first step of WO_3 reduction. Another broad reduction peak with a maximum temperature centered around 910 °C can be observed, which can be related to complete reduction of WO_3 and to the reduction of tetrahedrally coordinated WO_x species anchored to the zirconia [33]. Moreover, the total H_2 consumption rises, and the maximum shifts toward lower temperature with increased WO_3 loading. These findings indicate that the larger and more interconnected WO_x clusters formed at increasing WO_3 loading are easier to reduce than the smaller and more isolated ones prevailing at low WO_3 loading [32].

Table 2
Binding energy of WO_x/ZrO_2 samples prepared by co-precipitation method.

Sample	Binding energy/eV		Atomic ratio
	Zr $3d_{5/2}$	W $4f_{7/2}$	W/Zr
0.9-WO_3/ZrO_2-Cop	181.9	35.1	0.008
4.7-WO_3/ZrO_2-Cop	182.0	35.4	0.05
9.9-WO_3/ZrO_2-Cop	182.2	35.5	0.09
15.2-WO_3/ZrO_2-Cop	182.7	35.9	0.13
19-WO_3/ZrO_2-Cop	182.5	35.7	0.16

3.2. Acidic properties

The acidity of the catalysts was determined by ammonia adsorption microcalorimetry [34]. The initial heats of adsorption (denoted by Q_{init}) and the amount of ammonia adsorbed under an equilibrium pressure of 27 Pa are presented in Table 1. Fig. 4 displays the ammonia adsorption isotherms obtained in the first run of adsorption while Fig. 5 displays the differential heats as a function of coverage for the m-WO_x/ZrO_2-Cop catalysts. Moreover the re-adsorption isotherm for sample 19-WO_3/ZrO_2 is also plotted in Fig. 4 as an example to explain the calculation of the irreversibly adsorbed volume which determines the number of strong sites of chemisorption.

According to its adsorption properties toward NH_3 and CO_2, tungsten oxide was classified as acidic oxide while zirconia was assigned to the amphoteric group [35]. However, it was observed that many oxides in the amphoteric group adsorbed more NH_3 and with a higher heat than some of those of the acidic group [36].

The volumetric adsorption isotherms of the studied samples displayed in all cases an initial vertical section at very low pressure corresponding to the amount of strongly chemisorbed NH_3 [37]. The heats of adsorption showed a decreasing trend upon increasing coverage, as usually observed for heterogeneous surfaces [11,34,38]. The heterogeneity of the studied materials is due to the presence of acidic sites of different natures (i.e. Lewis acid sites from zirconia and both Brönsted and Lewis sites from WO_x) and presenting various strengths.

The initial heat values changed slightly as the WO_3 content increased. Additionally, the amount of irreversibly absorbed ammonia (V_{irr}), corresponding to strong chemisorption, increased with increasing WO_3 content up to 15 wt.%, which corresponds to the monolayer coverage and maximum surface area. As observed from Table 1 there is not much difference in the acidic properties of samples with WO_3 contents of 15 and 19 wt.%.

Fig. 6 shows the acid site distribution of all the catalysts. For the m-WO_3/ZrO_2-Cop samples, the population of medium strength acid sites ($90<Q_{diff}<130$ kJ.mol^{-1}) and weak acid sites ($50<Q_{diff}<90$ kJ.mol^{-1}) increased with increasing amount of WO_3 up to 15 wt.%, while the amount of strong acid sites with $Q_{diff}>130$ kJ.mol^{-1} reached a maximum for sample 9.9-WO_3/ZrO_2 and started to decrease when the WO_3 loading was higher than 10 wt.%. Sites with $Q_{diff}>130$ kJ.mol^{-1} can be attributed to Lewis acid sites while sites with $130>Q_{diff}>90$ kJ.mol^{-1} can be assigned to mainly Brønsted acidity [36].

Pyridine was the probe chosen for studying the nature of acid sites by FT-IR analysis. Fig. 7 shows FT-IR spectra of pyridine adsorption in the 1700–1400 cm^{-1} range on the 4.7-WO_3/ZrO_2-Cop, 15.2-WO_3/ZrO_2-Cop, and 19-WO_3/ZrO_2-Cop catalysts.

The band around 1445 cm^{-1} was assigned to pyridine coordinated to surface Lewis acid sites, as well as the band at 1610 cm^{-1}. The

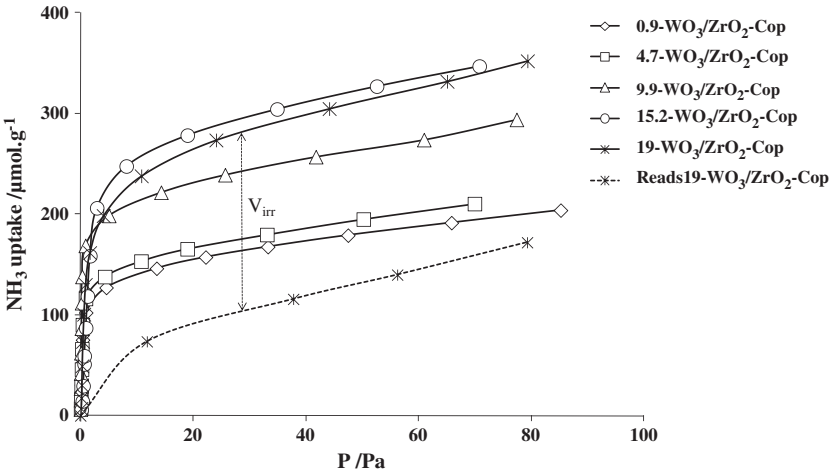

Fig. 4. Adsorption isotherms for ammonia adsorption carried out at 80 °C on WO_x/ZrO_2 catalysts prepared by co-precipitation. The readsorption isotherm for sample 19-WO_3/ZrO_2 is reported in dashed line.

band at 1489 cm^{-1} was assigned to combination of pyridine on Lewis and Brønsted acid sites, while the absorption around 1540 cm^{-1}, accompanied by another peak in the 1640–1620 cm^{-1} region, was assigned to pyridine adsorbed on Brønsted acid sites [39]. In this spectral region, hydrogen bonded pyridine, which typically adsorbs at 1440 and 1490 cm^{-1} can also show its contribution [40].

At RT, the bands at 1640 and 1540 cm^{-1} are clearly visible on the 15.2-WO_3/ZrO_2-Cop, and 19-WO_3/ZrO_2-Cop samples and not detectable on the sample containing only 4.7 wt.% of WO_3. These two peaks clearly identify the pyridinium ion, showing that the 15.2-WO_3/ZrO_2-Cop, and 19-WO_3/ZrO_2-Cop catalysts possess Brønsted acid sites strong enough to protonate adsorbed pyridine [39].

To complete this study, experiments were also performed after outgassing the samples at increasing temperatures in the 100–300 °C range. Only 19-WO_3/ZrO_2-Cop sample displayed a shoulder at 1452 cm^{-1} which disappeared at temperature higher than 200 °C. For temperature higher than 200 °C only the band centered at 1444 cm^{-1} (assigned to pyridine molecules adsorbed on Lewis acid sites) was still present.

The adsorption bands at 1444 and 1609 cm^{-1} were observed for all the samples outgassed at 25 °C, and were still present after outgassing at 300 °C. These two bands can be assigned to the probe molecule adsorbed as hydrogen-bonded pyridine [40].

3.3. Catalytic properties

Activity in the cellobiose hydrolysis over the WO_3/ZrO_2 catalysts and also with the zirconia support in quite mild conditions: ca. 97 °C of reaction temperature and 1:10 for the catalyst to cellobiose mass ratio were observed. Within the chosen conditions, the extent of reaction was not higher than 10–12% at the longer reaction times (differential conditions). Because only the first part of reaction was studied, the decrease of cellobiose concentration with time on stream (TOS) was linear (Fig. 8). Selectivity to glucose was total with absence of any by-products detectable by HPLC analysis. It was observed that glucose, too, linearly increased with TOS (Fig. 9). The mass balance indicated a loss of 5–7% of carbon for the longest reaction times, observed in particular for the most active catalysts. This could be due to formation of oligosaccharides which deposited on the catalyst surface which tended to become pale colored. No obvious deactivation was observed during a reaction time of 30 h. It cannot be excluded that at a longer reaction time the formation of oligosaccharides or the poisoning of the surface by reaction products may cause some deactivation of the catalyst surface [41,42].

Table 3 lists the obtained results in terms of average reaction rates and first-order kinetic constants calculated from the slopes of the straight lines plotted in Fig. 8. In the table, the calculated reaction

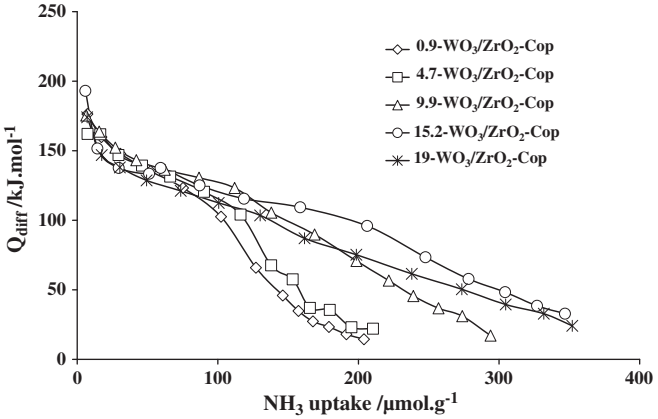

Fig. 5. Differential heats for ammonia adsorption carried out at 80 °C on WO_x/ZrO_2 prepared by co-precipitation.

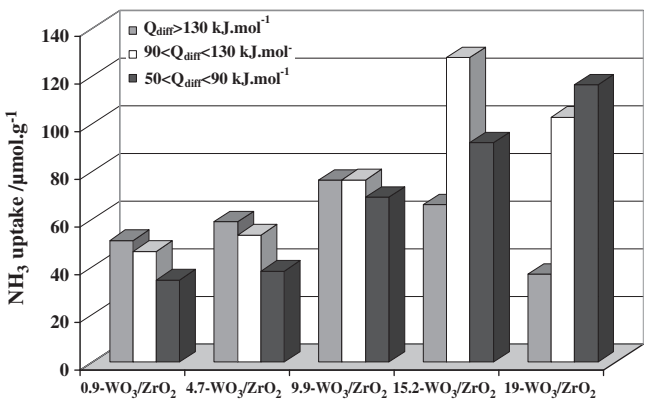

Fig. 6. Acid site strength distribution of WO_x/ZrO_2 catalysts prepared by co-precipitation.

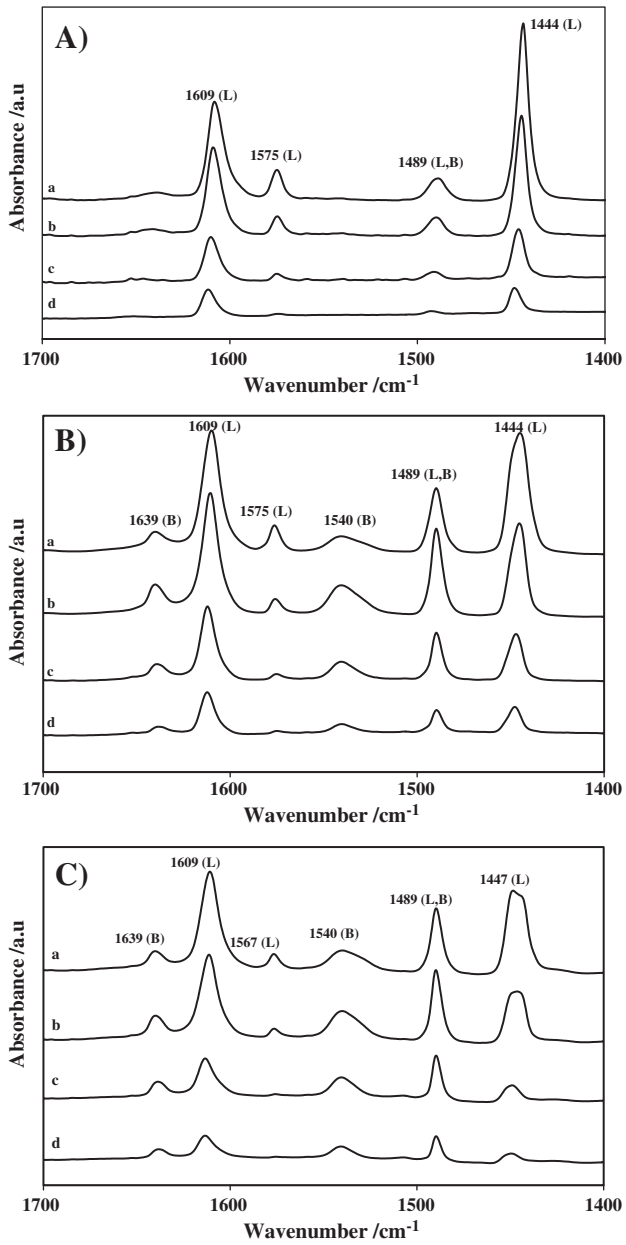

Fig. 7. FT-IR spectra for pyridine desorption on (A) 4.7-WO_3/ZrO_2, (B) 15.2-WO_3/ZrO2, and (C) 19-WO_3/ZrO_2 at different temperatures: (a) room temperature, (b) 100 °C, (c) 200 °C, (d) 300 °C.

rates have been reported both per unit catalyst mass and per unit catalyst surface. The partial transformation from tetragonal to monoclinic phase of the bare zirconia at 700 °C undergoes a much lower specific surface area and renders any comparison between the predominantly monoclinic zirconia and the stabilized WO_3/tetragonal ZrO_2 samples difficult.

Zirconia displayed good activity (high reaction rate and kinetic constant), higher than that of catalysts loaded with 0.9 to 9.9 WO_3 wt.%. For higher WO_3 loadings, the hydrolysis activity of the catalysts increased and overcame that of zirconia. The observed trend is depicted in Fig. 10; the minimum of activity was observed over 4.7-WO_3/ZrO_2. Clearly, the partial coverage of active zirconia surface by monomeric WO_x species led to a loss of activity. The amount of loaded WO_3 phase was not high enough to develop the typical WO_3 structure with protonic acid sites. Higher WO_3 loadings gave rise to well active catalysts thanks to the formation of interconnected WO_x clusters which possess strong acid sites [43]. These data are in agreement with the results from the characterization study above described. As observed by FT-IR of pyridine adsorption, the absence of Brønsted acid sites on the 4.7-WO_3/ZrO_2-Cop sample, as well as the presence of Brønsted acid sites (bands at 1540 and 1639 cm^{-1}) on the 15.2-WO_3/ZrO_2-Cop and 19-WO_3/ZrO_2-Cop catalysts is helpful to interpret the catalytic results. The increasing rate of reaction with increasing amount of WO_3 in the samples, can be in fact related to the formation (once the catalyst is put in aqueous solution) of hydroxyl groups able to further enhance the Brønsted acidity [8,39]. It has to be pointed out that the presence of water molecules could play an important role by interacting with the WO_x surface species thus causing prominent changes in the Raman spectra, as already observed [29]. Moreover, it has been shown that well dispersed structures become more reactive in acid catalysis with increasing domain size [8].

It seems also that the population of very strong acid sites (mainly Lewis acid sites with $Q_{diff} > 130$ kJ.mol^{-1}) plays a minor role in the reaction. Only sites with strength around 100 kJ.mol^{-1} (that could be assigned to Brønsted acidity) are responsible of an increase in activity in cellobiose hydrolysis (see Fig. 6).

In the literature, some hypotheses on the heterogeneous catalysis mechanism for cellobiose hydrolysis over protonic zeolites and phosphate salt catalysts are proposed [44,45]. In any case, the mechanism involves disaccharide chemisorption and subsequent activation via interactions with surface acid/base sites. The adsorption phenomena are of fundamental importance leading to favorable interaction of oxygen lone pairs of the sugar species with the electron-deficient sites present on the solid surface; not only protonic species are involved in the catalytic action but acid–base pairs seem to play an active role. This could explain our observations concerning the activity of the bare zirconia surface.

Concerning the catalyst stability in hot water, additional tests were performed on 15.2-WO_3/ZrO_2-Cop sample to ascertain the exclusive heterogeneous hydrolysis of cellobiose, with the absence of any homogeneous metal-ion catalysis deriving from a WO_3 leaching. After catalyst separation at about 8 h of TOS, only light increase of cellobiose conversion was observed in the filtrate. The reaction rate, in terms of cellobiose disappearance, evaluated in the filtrate mixture and measured after further 24 h of TOS was as low as 0.388 $g_{CELL}/(g_{cat} \cdot L \cdot h)$ (Table 3). Furthermore, the 15.2-WO_3/ZrO_2-Cop catalyst after 32 h of use at 97 °C was filtered, dried and analyzed by ICP-OES to check the remaining W-concentration. Results indicated a moderate decrease of 3 W wt.% which is in agreement with the low reaction rate of cellobiose observed above for the filtrate mixture.

4. Conclusion

Coupling WO_x species with ZrO_2 gives rise to improved materials both in terms of surface acidity and structure stability. WO_x species inhibited zirconia crystallite sintering and stabilized tetragonal ZrO_2 crystallites during high-temperature oxidative treatments. A calcination at 700 °C has been shown to be high enough to ensure the complete elimination of the synthesis precursor as well as the physisorbed and structural water, and low enough to avoid the formation of WO_x crystallites at higher surface densities near to monolayer coverage on ZrO_2. The calorimetry results show that the strength of the acid sites of the catalysts was rather heterogeneous. The heterogeneity of the studied materials is proportional to increasing WO_3 (wt.%) loading, and is due to the presence of acidic sites of different natures, Brønsted and Lewis acid sites, presenting various strengths.

In the present work, thus is confirmed the importance of the presence of protonic species (Brønsted acidity) on the surface of tungstated solids. Samples with 15.2 and 19.0 wt.% of WO_3 present a lower amount of strong acid sites (with NH_3 adsorption heats >130 kJ.mol^{-1}) and a higher amount of medium strength acid sites (with $130 > Q_{diff} > 90$ kJ.mol^{-1}) than the samples with very low

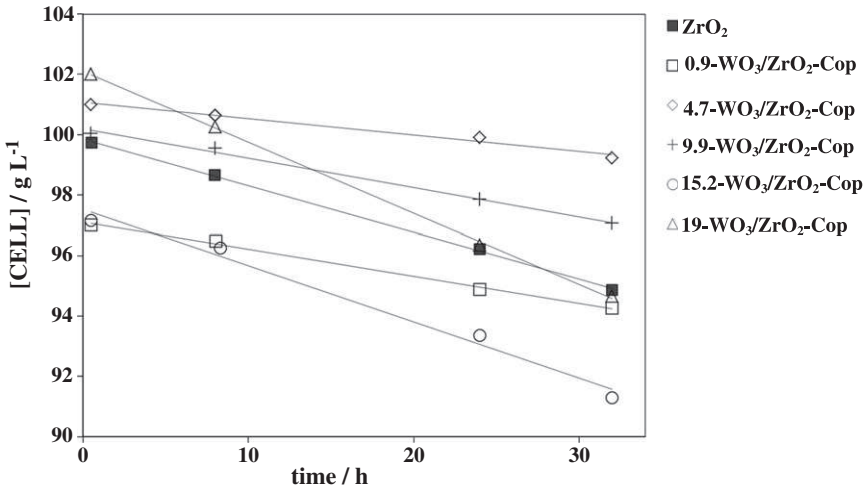

Fig. 8. Extent of the hydrolysis of cellobiose reaction on the WO_3/ZrO_2 catalysts: decay of cellobiose concentration as a function of TOS (time on stream).

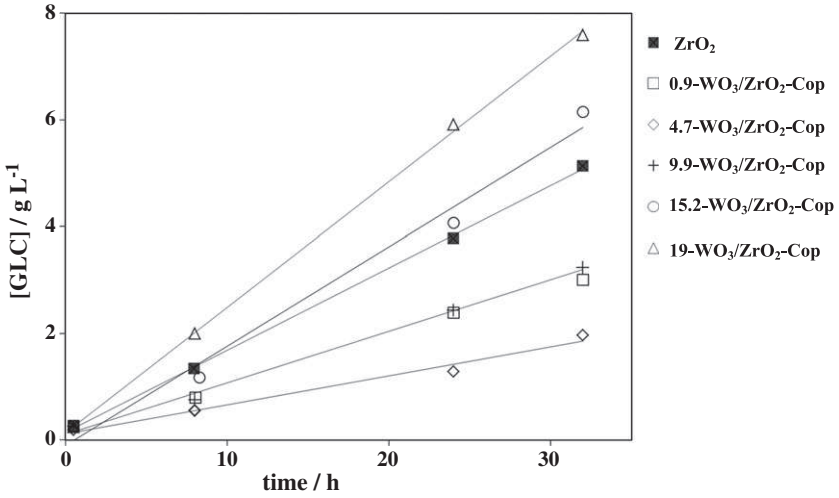

Fig. 9. Extent of the hydrolysis of cellobiose reaction on the WO_3/ZrO_2 catalysts: increase of glucose concentration as a function of TOS (time on stream).

amounts of WO_3 (see Fig. 6). The major difference between these two categories of samples is to be ascribed to the presence of Brønsted acid sites at high WO_3 loading. From the NH_3 isotherms it can be roughly estimated that, at the completion of the monolayer, the population of Brønsted acid sites (expressed in $mol_{NH3}.g^{-1}$) is ca. 40% more abundant than on the low loaded samples.

The WO_x clusters of the tungstated surface which act as an entity that prevails over the Lewis acid sites of the zirconia calcined at 700 °C enable the creation of a large number of Brønsted acid sites in the immediate vicinity of the disaccharide reactant, thus favorizing the adsorption of cellobiose and hydrolysis of the glycosidic bonds.

Table 3
Kinetic results obtained from the catalytic hydrolysis of cellobiose over the WO_3/ZrO_2 catalysts at 97 °C.

Catalyst	Average rate [a]		Rate constant
	$g_{CELL}/(g_{cat}\cdot L\cdot h)$	$g_{CELL}/(m^2_{cat}\cdot L\cdot h)$	$10^3\ k/(h^-)^1$
0.9-WO_3/ZrO_2	0.897	0.0180	0.947 ± 0.027
4.7-WO_3/ZrO_2	0.546	0.00975	0.464 ± 0.033
9.9-WO_3/ZrO_2	0.946	0.0122	0.970 ± 0.021
15.2-WO_3/ZrO_2	1.82 (0.388)[b]	0.0175	1.83 ± 0.085
19-WO_3/ZrO_2	2.35	0.0226	2.43 ± 0.035

[a] Average rate calculated at 8, 24, and 32 h of TOS.
[b] Reaction rate of the filtrated aqueous solution without solid catalysts (see text).

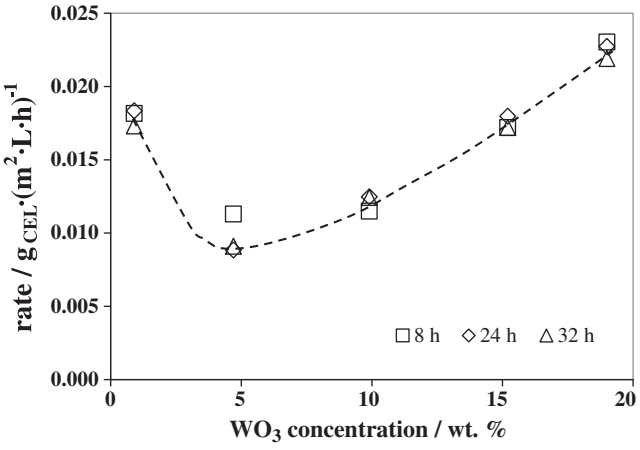

Fig. 10. Reaction rates, expressed as $g_{CELL}/(m^2_{cat}\cdot L\cdot h)$, for the hydrolysis of cellobiose over WO_3/ZrO_2 as a function of the WO_3 concentration determined at different reaction times.

Concomitantly it was confirmed that the origin of catalytic activity of cellobiose hydrolysis from the WO_3 phase is primarily associated with the presence of Brønsted sites and a WO_3 loading close to or above the monolayer (catalysts with a WO_3 loading of 15.2 and 19.0 wt.%).

The combination of different thermal, calorimetric, and structural analyses and catalytic test has permitted to deeply analyze samples that can be potentially applied as acidic catalysts in different environmental friendly reactions such as biomass exploitation and sugar transformations to valuable products, in agreement with the modern biorefinery platform requirements.

Acknowledgments

The authors are thankful to the scientific services of IRCELYON.

References

[1] A. Kogelbauer, D. Vassena, R. Prins, J.N. Armor, Catalysis Today 55 (2000) 151–160.
[2] D.G. Barton, S.L. Soled, E. Iglesia, Topics in Catalysis 6 (1998) 87–99.
[3] F. Di Gregorio, V. Keller, Journal of Catalysis 225 (2004) 45–55.
[4] J.C. Vartuli, J.G. Santiesteban, P. Traverso, N. Cardona-Martinez, C.D. Chang, S.A. Stevenson, Journal of Catalysis 187 (1999) 131–138.
[5] D.E. Lopez, K. Suwannakarn, D.A. Bruce, J.G. Goodwin Jr., Journal of Catalysis 247 (2007) 43–50.
[6] P. Wongmaneenil, B. Jongsomijt, P. Praserthdam, Catalysis Communications 10 (2009) 1079–1084.
[7] N.R. Shiju, M. AnilKumar, W.F. Hoelderich, D. Brown, Journal of Physical Chemistry 113 (2009) 7735–7742.
[8] J. Macht, E. Iglesia, Physical Chemistry Chemical Physics 10 (2008) 5331–5343.
[9] P. Carniti, A. Gervasini, S. Biella, A. Auroux, Chemistry of Materials 17 (2005) 6128–6613.
[10] J.G. Santiesteban, J.C. Vartuli, S. Han, R.D. Bastian, C.D. Chang, Journal of Catalysis 168 (1997) 431–441.
[11] S. Bennici, A. Auroux, in: S.D. Jackson, S.J. Hargreaves (Eds.), Metal Oxide Catalysis, vol 1, ch.9, WILEY-VCH, Weinheim, 2009, pp. 391–441.
[12] A. Dwiatmoko, J.W. Choi, D.J. Suh, Y.-W. Suh, H.H. Kung, Applied Catalysis A 387 (2010) 209–214.
[13] C. Moreau, R. Durand, J. Duhamet, P. Rivalier, Journal of Carbohydrate Chemistry 16 (1997) 709–714.
[14] J.A. Bootsma, B.H. Shanks, Applied Catalysis A 327 (2007) 44–51.
[15] V. Degirmenci, D. Uner, B. Cinlar, B.H. Shanks, A. Yilmaz, R.A. van Santen, E.J.M. Hensen, Catalysis Letters 141 (2011) 33–42.
[16] A. Takagaki, C. Tagusagawa, K. Domen, Chemical Communications (2008) 5363–5365.
[17] C. Tagusagawa, A. Takagaki, A. Iguchi, K. Takanabe, J.N. Kondo, K. Ebitani, S. Hayashi, T. Tatsumi, K. Domen, Angewandte Chemie International Edition 49 (2010) 1128–1132.
[18] M. Kantcheva, C. Koz, Journal of Materials Science 42 (2007) 6074–6086.
[19] M. Scheithauer, R.K. Grasselli, H. Knozinger, Langmuir 14 (1998) 3019–3029.
[20] E.I. Ross-Medgaarde, W.V. Knowles, T. Kim, M.S. Wong, W. Zhou, C.J. Kiely, I.E. Wachs, Journal of Catalysis 256 (2008) 108–125.
[21] D.G. Barton, M. Shtein, R.D. Wilson, S.L. Soled, E. Iglesia, The Journal of Physical Chemistry. B 103 (1999) 630–640.
[22] N. Naito, N. Katada, M. Niwa, The Journal of Physical Chemistry. B 103 (1999) 7206–7213.
[23] T. Onfry, G. Clet, M. Houlla, The Journal of Physical Chemistry. B 109 (2005) 3345–3354.
[24] S. Kuba, P. Concepcion Heydorn, R.K. Grasselli, B.C. Gates, M. Che, H. Knozinger, Physical Chemistry Chemical Physics 3 (2001) 146–154.
[25] M. Li, Z. Feng, G. Xiong, P. Ying, Q. Xin, C. Li, The Journal of Physical Chemistry. B 105 (2001) 8107–8111.
[26] B. Zhao, X. Xu, J. Gao, Q. Fu, Y. Tang, J. Raman, Spectroscopy 27 (1996) 549–554.
[27] N. Vaidyanathan, D.M. Hercules, M. Houalla, Analytical and Bioanalytical Chemistry 373 (2002) 547–554.
[28] M.A. Vuurman, I.E. Wachs, A.M. Hirt, Journal of Physical Chemistry 95 (1991) 9928–9937;
T. Kim, A. Burrows, C.J. Kiely, I.E. Wachs, Journal of Catalysis 246 (2007) 370–381.
[29] D. Gazzoli, M. Valigi, R. Dragone, A. Marucci, G. Mattei, The Journal of Physical Chemistry. B 101 (1997) 11129–11135.
[30] S.T. Wong, C.C. Hwang, C.Y. Mou, Applied Catalysis B: Environmental 63 (2006) 1–8.
[31] M. Valigi, D. Gazzoli, I. Pettiti, G. Mattei, S. Colonna, S. De Rossi, G. Ferraris, Applied Catalysis A 231 (2002) 159–172.
[32] A. Martinez, G. Prieto, M.A. Arribas, P. Concepcion, J.F. Sanchez-Royo, Journal of Catalysis 248 (2007) 288–302.
[33] A.M. Garrido Pedrosa, M.J.B. Souza, S.H. Lima, D.M.A. Melo, A.G. Souza, A.S. Araujo, Journal of Thermal Analysis and Calorimetry 87 (2007) 703–707.
[34] A. Auroux, Topics in Catalysis 4 (1997) 71–89.
[35] A. Auroux, A. Gervasini, Journal of Physical Chemistry 94 (1990) 6371–6379.
[36] L. Damjanovic, A. Auroux, in: M.E. Brown, P.K. Gallagher (Eds.), Handbook of Thermal Analysis and Calorimetry, Vol. 5, Elsevier, Amesterdam, 2008, p. 387.
[37] D. Sprinceana, M. Caldararu, N.I. Ionescu, A. Auroux, Journal of Thermal Analysis and Calorimetry 56 (1999) 109–115.
[38] C. Busco, A. Barbaglia, M. Broyer, V. Bolis, G.M. Foddanu, P. Ugliengo, Thermochimica Acta 418 (2004) 3–9.
[39] G. Busca, Physical Chemistry Chemical Physics 1 (1999) 723–736.
[40] S.R.G. Carrazàn, C. Martin, G. Solana, V. Rives, Langmuir 17 (2001) 6968–6973.
[41] T. Armaroli, G. Busca, C. Carlini, M. Guittari, A.M. Raspolli Galletti, G. Sbrana, Journal of Molecular Catalysis A 151 (2000) 233–243.
[42] C. Carlini, M. Giuttari, A.M. Raspolli Galletti, G. Sbrana, T. Armaroli, G. Busca, Applied Catalysis A 183 (1999) 295–302.
[43] W. Zhou, E.I. Ross-Medgaarden, W.V. Knowles, M.S. Wong, I.E. Wachs, C.J. Kiely, Nature Chemistry 1 (2009) 722–728.
[44] V. Le Strat, C. Moreau, Catalysis Letters 51 (1998) 219–222.
[45] A. Charmot, A. Katz, Journal of Catalysis 276 (2010) 1–5.

Publication IV

Catalysis Communications 30 (2013) 5–13

Contents lists available at SciVerse ScienceDirect

Catalysis Communications

journal homepage: www.elsevier.com/locate/catcom

Short Communication

Relation between surface acidity and reactivity in fructose conversion into 5-HMF using tungstated zirconia catalysts

R. Kourieh [a], V. Rakic [b], S. Bennici [a], A. Auroux [a,*]

[a] Université Lyon 1, CNRS, UMR 5256, IRCELYON, Institut de recherches sur la catalyse et l'environnement de Lyon, 2 avenue Albert Einstein, F-69626 Villeurbanne, France
[b] Faculty of Agriculture, University of Belgrade, Nemanjina 6, 11080 Zemun, Serbia

ARTICLE INFO

Article history:
Received 26 April 2012
Received in revised form 27 September 2012
Accepted 9 October 2012
Available online 15 October 2012

Keywords:
Tungsten oxide
Zirconia supported catalysts
Surface acidity/basicity
Adsorption microcalorimetry
Catalytic fructose dehydration

ABSTRACT

Catalytic dehydration of fructose and its conversion to 5-hydroxymethylfurfural was studied using tungstated zirconia oxides, with various tungsten oxide loadings (1–20 wt.%). The samples were prepared by incipient wetness impregnation and thoroughly characterized using a combination of different techniques: structural, thermal and calorimetric analyses. Zirconia was predominantly present in the investigated samples in the tetragonal phase when the WO_3 loading was above 10 wt.%. The samples exhibited amphoteric characteristics, as they adsorbed both ammonia and sulfur dioxide on their surface. The number of surface acid sites increased with increasing WO_3 content. Fructose dehydration tests evidenced the formation of 5-hydroxymethylfurfural and by-products (formic and levulinic acids). The results show that the ratio of basic to acidic sites of the solid catalysts is the key parameter for the selectivity in 5-HMF, while the global fructose conversion was mainly related to the presence of acid sites of a given strength with $150 > Q_{diff} > 100$ kJ·mol$_{NH_3}^{-1}$.

1. Introduction

The demand for energy is increasing continuously at a high rate in our global society which is rapidly evolving. Since petroleum is a dwindling source of energy, and having in mind all environmental considerations (defined, for example, by Kyoto protocol), there is a strong worldwide desire to reduce dependence on crude oil. Therefore, the need to search for renewable alternative energy systems has been imposed. Some of the alternative sources (like: solar, wind, hydroelectric, nuclear…) are carbon-free; however, their application in the transportation sector appears not to be easily feasible. Consequently, there is a need for carbon-based sustainable alternatives to petroleum-derived fuels. As a result, there is a growing interest to produce so-called biofuels from vegetable biomass, which is abundant, renewable and distributed widely in nature [1,2].

Vegetable biomass is generated from carbon dioxide and water, using sunlight as an energy source and producing oxygen as a subproduct. As primary products, this process gives monosaccharides (C_5 and C_6 sugars), while further transformations produce polymerized molecules (cellulose and hemicellulose) and cross-linked polymers (lignin). Evidently, biomass can be comprehended as a source of carbohydrates that can be transformed into families of useful or potentially useful substances. Hence, in recent years, there are numerous literature reports that present biomass as a sustainable source of carbon-based precursors and/or chemical intermediates, that can give a variety of valuable chemicals and fine chemicals [1–4]. Besides, main monosaccharides that can be found in biomass, glucose and fructose, can be used to produce liquid fuels — bioethanol and biodiesel. In fact, since direct production of biofuels from C_5- and C_6-sugars is difficult, recent efforts have been focused on converting them to one derivative of furan (5-hydroxymethylfurfural, 5-HMF), a compound which has been found to be a key intermediate between biomass-based carbohydrates and desired products such as chemicals and biofuels. It has been found that 5-HMF can serve as a precursor to numerous products and chemical intermediates related to fuel, polymer, and pharmaceutical industries [5–10]. As an illustration, Dumesic et al. raised the challenge to use 5-HMF as an intermediate to produce liquid-fuel, alkanes, and hydrogen from renewable biomass resources [11–16].

It is well known that 5-HMF can be obtained by acid catalyzed dehydration of fructose, glucose, sucrose and even cellulose; these processes are usually carried out in aqueous media with an added mineral acid. In fact, current attempts to produce 5-HMF have mainly focused on fructose as a starting material, in spite of its high cost. A drawback of acid catalysis in aqueous media is production of various side reactions, including further hydrolysis of 5-HMF to levulinic acid, that lowers its yield and increases the cost of product purification [17,18]. It is known that separation of 5-HMF from levulinic acid is particularly difficult [18]. In order to facilitate the purification of furan derivatives such as 5-HMF, the procedure of phase coupling can be applied [3,19]. Recent works proved that high yields of 5-HMF can be achieved in a biphasic reactor, where one phase contains aqueous solution of fructose and acid catalyst, while the other, the extracting phase, contains low boiling partially miscible organic solvent [19].

* Corresponding author. Tel.: +33 472 445398; fax: +33 472 445399.
E-mail address: aline.auroux@ircelyon.univ-lyon1.fr (A. Auroux).

1566-7367/$ – see front matter © 2012 Elsevier B.V. All rights reserved.
http://dx.doi.org/10.1016/j.catcom.2012.10.005

Recently, many research groups have published high-yield conversion of both glucose and fructose into HMF in ionic-liquid solvents, among them Zhao et al. [18] and Yong et al. [20–22]. However, these processes have disadvantages, such as a high cost due to several separation processes, expensive solvents, and materials corrosion. Conversion of fructose to 5-HMF was probed also in highly polar organic solvents, e.g. DMSO [17,23]. In addition, highly concentrated melt systems consisting of choline chloride, carbohydrate and different acidic catalysts have been reported as systems that express low environmental impact, giving satisfactory yields of 5-HMF [24].

Apart from these attempts to perform dehydration of sugars in homogeneous systems, there is still a possibility to provide a source of needed acidity using heterogeneous catalytic systems as an environmentally benign alternative, which offers also the possibility of easy catalyst separation, regeneration, and low cost procedure. Up to now, several solid catalysts known to express surface acidity have been tested in dehydration of monosaccharides. For example, sulphated alumina zirconia has shown 56% yield of HMF from fructose at 150 °C [25] and sulphated zirconia has shown 36% yield even at high reaction temperature [23], in comparison with about 20% yield of HMF found for TiO_2/ZrO_2 at 200 °C [26], and the yield of 50% found in the case of zirconium phosphate at 230 °C [27]. Promising yields (89% from fructose, 49% from glucose, 54% from inulin and 65% from hydrolyzed juice of Jerusalem artichoke) have been obtained using hydrated niobium pentoxide as a catalyst [28]. Recently, sulfonated organic heterpolyacid salt has also been reported as promising catalysts in fructose dehydration to 5-HMF [29]. From a brief insight into the reported results, it becomes evident that the activity and selectivity of most solid acid catalysts were found to give unsatisfactory results in water, even at high reaction temperatures [23].

In the present work, we performed the dehydration of fructose using solid WO_3-based catalysts, known to possess highly acidic surface sites. In order to tune the acidity, we have prepared a series of tungstated zirconia catalysts with various tungsten oxide loadings, using incipient wetness impregnation. Importantly, it is already known that the acid site strength of the tungsten/zirconia materials is similar or slightly higher than that found in zeolites or sulfated zirconia and is comparable to sulfuric acid [30]. WO_3/ZrO_2 catalysts are commonly used in a number of industrially important reactions, including hydration of carbohydrate, selective oxidation, paraffin isomerization, cracking, alkylation, liquid-phase Beckmann rearrangement of cyclohexanone oxime and for biodiesel synthesis through esterification and transesterification of fatty acids [31–36]. For many of these catalytic applications, the acidity of the supported tungsten oxide phase plays a crucial role in the overall catalytic activity [37]. A fundamental understanding of the WO_3 dispersed phase evolution on zirconia has been presented in the literature by many authors and recently reviewed by Iglesia [38], with particular attention to the influence of the sizes and structural compositions of the active catalytic domains on the catalytic activity. It has been found that the structure, electronic properties, and consequent catalytic function of small oxide domains depend sensitively on their surface densities (size and dimensionalities), on their composition, and on their specific connectivity to less active oxides typically used as supports [38].

Solids prepared in this work were fully characterized in terms of their structural and surface acid/base properties. The influence of surface and acid/base properties on the performance of these WO_3-based catalysts in fructose dehydration is discussed; in particular correlations have been established between the number and strength of acid/base sites and the 5-HMF selectivity and fructose conversion.

2. Experimental

2.1. Materials

WO_3 was purchased from Fluka (99.9% WO_3). $Zr(OH)_4$ was supplied by MEL-Chemicals (XZO 880/01), while ammonium metatungstate hydrate $(NH_4)_6H_2W_{12}O_{40}\cdot nH_2O$ was purchased from Fluka (≥99.0% WO_3-based on calcined substance, gravimetric), 5-HMF and fructose were purchased from SAFC (≥99% purity) and SIGMA (≥99% purity), respectively. Deuterium oxide (heavy water) was purchased from ALDRICH (99.9 atom % D).

2.2. Catalyst preparation

WO_3/ZrO_2 catalysts were prepared by wetness impregnation method. $Zr(OH)_4$ was impregnated with an ammonium metatungstate hydrate solution, to have a WO_3 loading ranging from 1 to 20 wt.%. The prepared solids are denoted by m-WO_3/ZrO_2, where m indicates the percentage of WO_3 wt.%. The resulting materials were air dried overnight at 85 °C, then calcined in flowing air for 4 h at 700 °C. This calcination temperature has been chosen on the basis of TG measurements, performed using Labsys-TG from Setaram. The crude samples (~50 mg) were heated from 25 to 900 °C with a heating rate of 5 °C min^{-1} in a flow of air, which was chosen as a soft oxidizing agent for calcination. The pure zirconia sample was also calcined at 700 °C.

2.3. Catalyst characterization

Elemental analysis was performed using ICP optical emission spectroscopy (ICP-OES) with an ACTIVA spectrometer from Horiba JOBIN YVON, after the samples were dissolved by appropriate solution of $NaOH + KNO_3$.

The surface areas, pore volumes and pore sizes were measured by nitrogen adsorption at −196 °C on a Micromeritics 2010 apparatus after heat pre-treatment under vacuum for 2 h at a temperature of 400 °C. Surface areas were determined by the BET method from the resulting isotherms. Pore volumes and pore sizes were determined by the BJH method.

The X-ray diffraction (XRD) measurements were carried out on a Bruker D5005 powder diffractometer scanning from 3° to 80° (2θ) at a rate of 0.02° s^{-1} using a Cu Kα radiation (λ = 0.15418 nm) source. The applied voltage and current were 50 kV and 35 mA, respectively.

The recording of transmission electron micrographs (TEM) was carried out using a JEOL 2010 LaB6 equipment operating at 200 kV with an energy dispersive X-ray spectrometer (EDS), (Link ISIS from Oxford Instruments). The samples were dispersed in ethanol using a sonicator and a drop of the suspension was dripped onto a carbon film supported on a copper grid and then ethanol was evaporated. EDS study was carried out using a probe size of 15 nm to analyze borders and centers of the particles and the small particles.

The X-ray photoelectron spectra (XPS) were obtained on a KRATOS AXIS Ultra DLD spectrometer equipped with a hemispherical electron analyzer and an Al anode (Al Kα = 1486.6 eV) powered at 150 W, a pass energy of 20 eV, and a hybrid lens mode. The detection area analyzed was 700 μm × 300 μm. Charge neutralization was required for all samples. The peaks were referenced to the C–(C, H) components of the C 1s band at 284.6 eV. Shirley background subtraction and peak fitting to theoretical Gaussian–Lorentzian functions were performed using an XPS processing program (Vision 2.2.6 KRATOS). The residual pressure in the spectrometer chamber was 5×10^{-9} mbar during data acquisition.

Raman spectroscopy measurements were performed using a LabRAM HR (Jobin Yvon) spectrometer. The excitation was provided by the 514.5 nm line of an Ar^+ ion laser (Spectra physics) employing a laser power of 100 μW. The laser beam was focused through microscope objective lenses (100×) down to a 1 μm spot on the sample. For each solid, the spectra were recorded at several points of the sample to ascertain the homogeneity of the sample; the average of these spectra was plotted and is discussed below.

Temperature-programmed reduction (TPR) was performed using a TPD/R/O-1100 instrument (ThermoFisher). Prior to the TPR run, the fresh sample was treated in a stream of O_2/He (0.998% v/v,

flowing at 20 ml min^{-1}), ramping the temperature at 10 °C min^{-1} from 40 °C to 350 °C and maintaining it for 60 min, and then cooled to RT. The TPR measurement was carried out using H_2/Ar (4.98% v/v) as reducing gas mixture, flowing at 20 ml min^{-1}. The heating rate was 10 °C min^{-1}, the applied temperature range was from 40 °C to 1000 °C.

Adsorption microcalorimetry measurements were performed at 80 °C in a heat flow calorimeter (C80 from Setaram) linked to a conventional volumetric apparatus equipped with a Barocel capacitance manometer for pressure measurements. The probes (ammonia and sulfur dioxide) used for measurements (Air Liquide, purity > 99.9%) were purified by successive freeze–pump–thaw cycles. About 100 mg of sample was pre-treated in the calorimetric quartz cell overnight at 400 °C, and then evacuated at the same temperature for 1 h prior to the measurements. The differential heats of adsorption were measured as a function of coverage by repeatedly introducing small doses of the adsorbate onto the catalyst, until an equilibrium pressure of about 66 Pa was reached. The sample was then outgassed for 30 min at the same temperature, and a second adsorption was performed at 80 °C until an equilibrium pressure of about 27 Pa was attained in order to calculate the irreversibly chemisorbed amount of the probe molecules at this pressure.

2.4. Catalytic reaction

The reaction of fructose dehydration was performed in the batch catalytic system. Experiments were performed in a 100 ml stainless steel autoclave at 130 °C. In a typical procedure 600 mg of fructose was dissolved in 60 ml of water and then 80 mg of solid catalyst was added [39,40]. Water was chosen as a green and appropriate solvent for dehydration of fructose to 5-HMF. In the analysis, starting time of the reaction was taken when the reaction mixture reached 130 °C. Samples were withdrawn from the reaction mixture at 1 h intervals; the changes of fructose, 5-HMF, and formic and levulinic acid concentrations with time were followed by collecting ^{1}H NMR spectra, using liquid NMR technique (Bruker AVANCE 250 spectrometer equipped with a multinuclear 10 mm Probe). The concentration of the various species has been obtained by the integration of areas under the peaks after calibration (integration performed using Mnova 7 software).

Reactant conversion (mol%), yield of 5-HMF (mol%), and product selectivity (%) were defined as follows:

$$\text{Conversion (mol\%)} = (\text{moles of fructose that reacted}) / (\text{moles of fructose initial}) \times 100\% \quad (1)$$

$$\text{Yield (mol\%)} = (\text{moles of X produced}) / (\text{moles of fructose initial}) \times 100\% \quad (2)$$

$$\text{Selectivity (\%)} = (\text{moles of X produced}) / (\text{moles of fructose reacted}) \times 100\%. \quad (3)$$

3. Results and discussion

3.1. Catalyst's structural properties

The results of chemical analysis (expressed as W and WO_3 wt.%), the BET surface areas (in $m^2 \cdot g^{-1}$) and theoretical surface concentrations of tungsten in the zirconium–tungsten mixed oxides are summarized in Table 1. It can be seen that surface area values increased with tungsten oxide loading. The catalysts with WO_3 loadings higher than 10 wt.% maintained surface areas between 86 and 108 $m^2 \cdot g^{-1}$, while further increases in WO_3 loading above 15 wt.% did not lead to increased surface area. The surface concentrations of tungsten were calculated from measured surface areas using the following relation:

$$WO_3 \text{concentration}\left(W - \text{atom} \cdot nm^{-2}\right) = \frac{m WO_3 \times 10^{-2} \times N_A}{M_{WO_3} \times S_{BET} \times 10^{18}} \quad (4)$$

where m is the WO_3 wt.% loading, M_{WO_3} is the WO_3 molecular weight (231.8 $g \cdot mol^{-1}$), N_A is the Avogadro's number, and S_{BET} is the surface area of the catalyst in $m^2 \cdot g^{-1}$. It is important to notice that maximum surface area is obtained for the samples possessing W surface concentration of 4.3 and 5 W-atom $\cdot nm^{-2}$; these values are close to those theoretically found to correspond to the monolayer of WO_3 loading on ZrO_2 [32,37,41,42].

The X-ray diffraction patterns and the Raman spectra of the m-WO_3/ZrO_2 catalysts are shown in Figs. A and B in the Supporting Information. Diffraction peak characteristics of tetragonal ZrO_2 (at $2\theta = 30.17°$, 35.31°, 49.79°, and 60°) [31,32], and monoclinic ZrO_2 (at $2\theta = 28.3°$ and 31.6°) [31,43,44] are evident for the catalysts with WO_3 loading lower than 10 wt.%. For the samples with WO_3 loading higher than 10 wt.%, the XRD patterns show only the specific reflections of the tetragonal phase of zirconia. Evidently, the presence of WO_x species at a certain WO_3 concentration (≥10 wt.%) inhibits the sintering and the transformation to monoclinic ZrO_2 crystallites. It seems that the formation of WO_x and interaction between tungsten oxide and ZrO_2 reduced the surface mobility of zirconia thus avoiding the transformation of tetragonal to monoclinic ZrO_2, which is in accordance with literature data [45–47]. No crystalline WO_3 phase ($2\theta = 23.2°$, 23.7°, and 24.3°) appeared on the investigated samples, even those with WO_3 contents close to 20 wt.%, thus indicating that tungsten oxide was present in a highly dispersed manner. However, as the presence of WO_3 crystallites with sizes lower than 4 nm (which is beyond the detection capacity of the powder XRD technique) cannot be excluded, the surface structure of tungsten oxide and zirconia species on the samples was examined by Raman spectroscopy as a complementary technique. The results showed that no characteristic bands of crystalline WO_3 (at 275, 720, and 808 cm^{-1}) were detected for the samples except for a WO_3 loading ≥20 wt.%. This confirms our hypothesis of highly dispersed WO_3 on the surface of zirconium oxide. Moreover, these results have been also confirmed by electron imaging (TEM) for the two samples 16.8-WO_3/ZrO_2 and 20.9-WO_3/ZrO_2 (Fig. 1): WO_3 was homogeneously dispersed on the zirconia surface and no aggregates nor crystallites have been detected for the 16.8-WO_3/ZrO_2 sample. On the other hand very small crystallites of WO_3 (diameter lower than 5 nm) were visible on the 20.9-WO_3/ZrO_2 sample. The homogeneous dispersion of WO_3 on the support surface has been verified by EDS analysis performed on different zones of the sample surface. For the 16.8-WO_3/ZrO_2 sample W local atomic concentration was found in the range of 9–11%, while for the 20.9-WO_3/ZrO_2 sample it was in the 16–47% domain.

The surface structure of tungsten oxide and zirconia species on the m-WO_3/ZrO_2 catalysts was examined by Raman spectroscopy. In agreement with the XRD results, the Raman spectra (Fig. B in Supporting Information) show that zirconia is predominantly present in the monoclinic form for the catalysts with WO_3 loading smaller than 10 wt.% [32,48,49]. A broad peak located at approximately 980 cm^{-1} is observed for the catalysts with a WO_3 loading ≥5 wt.%; this peak can be attributed to surface W═O interaction species [50]. A shift in the Raman peak position of the W interaction species that appeared with increasing W loading has already been reported for catalysts characterized under ambient conditions and attributed to a change in the nature of the W interaction species from WO_4^{2-} to polytungstates [51]. Spectral band characteristics for crystalline WO_3 (at 275, 720, and 808 cm^{-1}) are detected only for the sample with a WO_3 loading ≥20 wt.%.

The binding energies (BE) of Zr $3d_{5/2}$ and W $4f_{7/2}$ are presented in Table 1. The BE of Zr 3d value was shifted to higher values as the WO_3 loading increased, which indicates a flow of electron density from zirconia phase into WO_x phase through Zr–O–W linkages. Values found in this work are close to the corresponding BE of Zr^{4+} in bulk zirconia (182.1 eV) [52] while the BEs of the W $4f_{7/2}$ are close to the reported value of W^{6+} (35.5 eV) [53]. The surface W/Zr ratio increases roughly linearly as the loading of WO_3 increases. Tungsten surface enrichment

Table 1
Physicochemical characteristics and binding energies of m-WO_3/ZrO_2 samples prepared by incipient wetness impregnation.

Sample	WO_3 content/wt.%	W content/wt.%	BET[a] surface area/$m^2 \cdot g^{-1}$	W surface density/W-atom·nm^{-2}	Binding energy/eV		Atomic ratio
					Zr $3d_{5/2}$	W $4f_{7/2}$	W/Zr
1.2-WO_3/ZrO_2	1.21	0.96	46	0.7	181.9	35.4	0.03
5.1-WO_3/ZrO_2	5.09	4.04	68	2.0	182.1	35.5	0.06
9.8-WO_3/ZrO_2	9.86	7.82	86	3.0	182.3	35.6	0.10
16.8-WO_3/ZrO_2	16.85	13.36	102	4.3	182.8	36	0.15
20.9-WO_3/ZrO_2	20.93	16.60	108	5.0	182.4	35.6	0.18
ZrO_2	–		37	–			

[a] Uncertainty: ±1 $m^2 \cdot g^{-1}$.

is observed for all samples, indicating that the thermal treatment performed at 700 °C in order to activate the samples was effective in expelling tungsten from the bulk to the surface of m-WO_3/ZrO_2 catalysts, corresponding to the data reported in the literature [54].

In order to investigate the red–ox behavior of investigated solids, TPR experiments have been performed in this work (see in the Supporting Information Fig. C, the reduction profiles for pure WO_3 and the supported catalysts). As it might be expected, in the temperature region of fructose dehydration, reduction processes were not observed.

In literature [55], pure WO_3 exhibits three reduction peaks, namely, a shoulder (only for experiments performed with large amounts of sample, > 50 mg) at 638 °C ($WO_3 \rightarrow W_{20}O_{58}$), a sharp peak at 765 °C ($W_{20}O_{58} \rightarrow WO_2$) and a peak at higher temperatures ($WO_2 \rightarrow W$). On our sample we have detect only two reduction peaks for pure WO_3 centered around 800 °C and 950 °C, respectively, which can be attributed to the reduction of WO_3 to WO_2 and further to W.

In the temperature range in which features due to tungsten reduction appear (>400 °C), only the catalysts with loadings ≥5 wt.% are concerned. A reduction peak centered around 480 °C can be observed, which could be attributed to the first step of reduction $WO_3 \rightarrow WO_{2.9}$ [56,57], while the other broad reduction peak with a maximum temperature centered around 910 °C can be related to the complete reduction of WO_3 (at 700 °C $WO_{2.9} \rightarrow WO_2$, at 800–900 °C $WO_2 \rightarrow W$) [56] and at higher temperature the reduction of tetrahedrally coordinated WO_x species (amorphous and non-stoichiometric oxides) strongly anchored to the zirconia surface, as already reported in the literature [56–58].

The amount of hydrogen consumed for the first step of reduction was determined by integrating the peak at 480 °C, corresponding to 3.5% of reduction, and thus confirming the assignment of this low temperature peak to the $WO_3 \rightarrow WO_{2.9}$ partial reduction (theoretical reduction of 3.3%).

Moreover, the total H_2 consumption rises, and the peak maximum temperature shifts towards lower temperatures with increasing WO_3 loading. These findings indicate that the larger and more interconnected WO_x clusters formed at increasing WO_3 loading (W present in W–O–W groups) can be reduced more easily than the smaller and more isolated species prevailing at low WO_3 loading (W present in W–O–Zr groups) [44,53].

3.2. Acidic/basic properties

As already mentioned in the Experimental section, the acidity of the catalysts was determined by ammonia adsorption microcalorimetry. The initial heats of adsorption (denoted by Q_{init}) and the amount of ammonia adsorbed under an equilibrium pressure of 27 Pa are presented in Table 2. Fig. 2 displays the ammonia adsorption isotherms while Fig. 3 represents the differential heats as a function of coverage for m-WO_3/ZrO_2 catalysts.

According to its adsorption properties towards NH_3 and CO_2 reported in the literature [59], tungsten oxide was classified as an acidic oxide, while zirconia was assigned to the amphoteric group. However, it was observed that many oxides in the amphoteric group adsorbed more

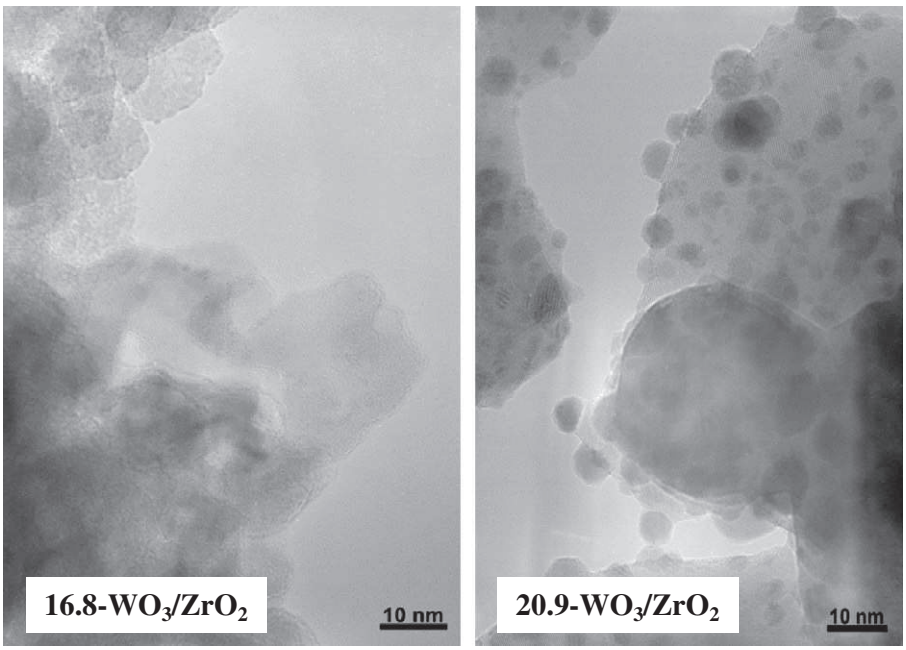

Fig. 1. TEM images of 16.8-WO_3/ZrO_2 and 20.9-WO_3/ZrO_2 catalysts.

Table 2
Initial heats of adsorption (denoted by Q_{init}), total and irreversible amounts of ammonia and sulfur dioxide adsorbed under an equilibrium pressure of 27 Pa.

Sample	Acidity/NH_3			Basicity/SO_2		
	Q_{init}/kJ·mol^{-1} [a]	V_{tot}/μmol$_{NH_3}$g^{-1} [b]	V_{irr}/μmol$_{NH_3}$g^{-1} [c]	Q_{init}/kJ·mol^{-1} [a]	V_{tot}/μmol$_{SO_2}$g^{-1} [b]	V_{irr}/μmol$_{SO_2}$g^{-1} [c]
1.2-WO_3/ZrO_2	191	171	104	198	137	120
5.1-WO_3/ZrO_2	184	204	129	186	108	84
9.8-WO_3/ZrO_2	185	263	172	158	75	33
16.8-WO_3/ZrO_2	162	259	158	108	21	6
20.9-WO_3/ZrO_2	165	289	174	104	23	5
ZrO_2	178	124	68	201	143	130

[a] Heat evolved from the first dose of NH_3 or SO_2 (±2 kJ·mol^{-1}).
[b] Total amount of NH_3 and SO_2 retained as determined at 27 Pa of equilibrium pressure.
[c] Irreversibly adsorbed amount of NH_3 and SO_2 as determined from the difference between the amounts adsorbed in the first and second adsorptions at 27 Pa.

NH_3 and with a higher heat than some of those belonging to the acidic group [60]. It has been found that as a result of ammonia adsorption on ZrO_2 a heat of 150 kJ·mol^{-1} was evolved, what is comparable to the values found for WO_3 [30,61].

The volumetric adsorption isotherms collected in this work displayed in all cases an initial vertical section at very low pressure corresponding to the amount of strongly chemisorbed NH_3 [62]. The heats of adsorption showed a decreasing trend upon increasing coverage, as usually observed for heterogeneous surfaces [60,63,64]. The heterogeneity of the studied materials is due to the presence of acidic sites of different natures (both Brønsted and Lewis sites) and presenting various strengths.

The amount of irreversibly absorbed ammonia (V_{irr}), corresponding to strong chemisorption, increased greatly with increasing WO_3 content up to the value which corresponds to the highest surface area.

Fig. 4 shows the acid site distributions of all investigated catalysts. It can be seen that for all m-WO_3/ZrO_2 samples, the population of medium strength acid sites (characterized by the values of differential heats, Q_{diff}, between 100 and 150 kJ·mol^{-1}) and weak acid sites ($50 < Q_{diff} < 100$ kJ·mol^{-1}) increased with increasing amount of WO_3 up to 16.8 wt.%; while the trend was less marked for the amount of strong acid sites with $Q_{diff} > 150$ kJ·mol^{-1}.

The basic features of the m-WO_3/ZrO_2 catalysts were studied by sulfur dioxide adsorption. Prior to the calorimetric measurements the catalysts were subjected to the same activation procedure as for ammonia adsorption. We report in Figs. 3 and 5 the differential heats of sulfur dioxide adsorption as a function of coverage, and the corresponding isotherms respectively. The initial heats of adsorption (denoted by Q_{init}) and the amount of sulfur dioxide adsorbed under an equilibrium pressure of 27 Pa are presented in Table 2. The differential heats of SO_2 adsorption on the surface of ZrO_2 show the presence of strong basic sites; this presence rapidly decreases with the increase of WO_3 content in the m-WO_3/ZrO_2 samples. These results are expected considering the acidic nature of tungsten oxide species. Sulfur dioxide can be chemisorbed on basic oxygen anions O^{2-} and on basic hydroxyl groups. Such adsorption modes lead to the formation of sulfites and hydrogenosulfites, respectively [65]. As sulfur dioxide is not chemisorbed on bulk WO_3, this probe can be used to estimate the free surface area of zirconia that is not covered by WO_3. As it was mentioned before that the monolayer can be achieved at a surface concentration of about 4 W-atom·nm^{-2}, corresponding to 15.4 wt.% of WO_3 for a 100 m^2·g^{-1} catalyst, it is expected that samples with a WO_3 loading close to this value should not adsorb any SO_2 irreversibly. Indeed, the equilibrium isotherms and irreversibly adsorbed amounts (see Table 2) show that the samples with WO_3 loading > 16 wt.% adsorb very small amounts of SO_2, corresponding to about 4% of uncovered zirconia surface. No significant differences were observed in the basic properties of the samples containing 16.8 and 20.9 wt.% of WO_3 thus confirming that the monolayer coverage was attained.

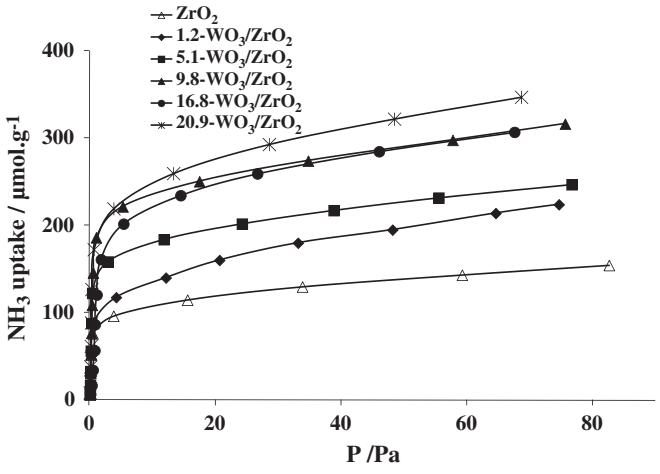

Fig. 2. Adsorption isotherms for ammonia adsorption carried out at 80 °C on m-WO_3/ZrO_2 catalysts.

3.3. Catalytic activity

As already explained in the Experimental section, the changes in fructose and product concentrations were monitored by ^{1}H liquid NMR technique (the NMR peaks used for the quantitative determination are shown on Fig. D in the Supporting Information). The product of major interest in fructose dehydration reaction is 5-HMF. However, owing to the subsequent aldehyde degradation, some unwanted chemicals, such as formic acid and levulinic acid, were also produced.

All investigated materials appear to be more or less active in dehydration of fructose and in producing 5-HMF. Fig. 6(A) and (B) shows the trend of fructose conversion as a function of reaction time and W-surface density, respectively. After 4 h of reaction, maximum conversion of fructose (66.7%) was found for 16.8-WO_3/ZrO_2, while the lowest degree of conversion (11.1%) was found for 5.1-WO_3/ZrO_2 sample. Moreover, as already shown by Soultanidis et al. [47] in the *n*-pentane isomerization reaction the maximum activity is reached for a given W-surface density that was between 4.5 and 5.5 W·nm^{-2} in their case and around 4.3 W·nm^{-2} on our catalysts in the fructose dehydration reaction.

It is well known that dehydration of hexoses is catalyzed by protonic acids as well as by Lewis acids [66,67], the same sites contributing to the formation of unwanted by-products, such as formic and levulinic acids; while isomerization between glucose and fructose is catalyzed by alkali [8]. In addition, it is known that oxidation of 5-HMF is catalyzed by alkali [8]. Hence it can be expected that samples possessing both basic and acidic sites would express different catalytic behaviors compared to mainly acidic materials (such as, accordingly to calorimetric measurements performed here, samples 16.8-WO_3/ZrO_2 and 20.9-WO_3/ZrO_2).

The insight into the results obtained in this work gives evidence that amphoteric zirconia displays activity higher than those expressed by catalysts loaded with up to 9.8 WO_3 wt.%. From the presented results

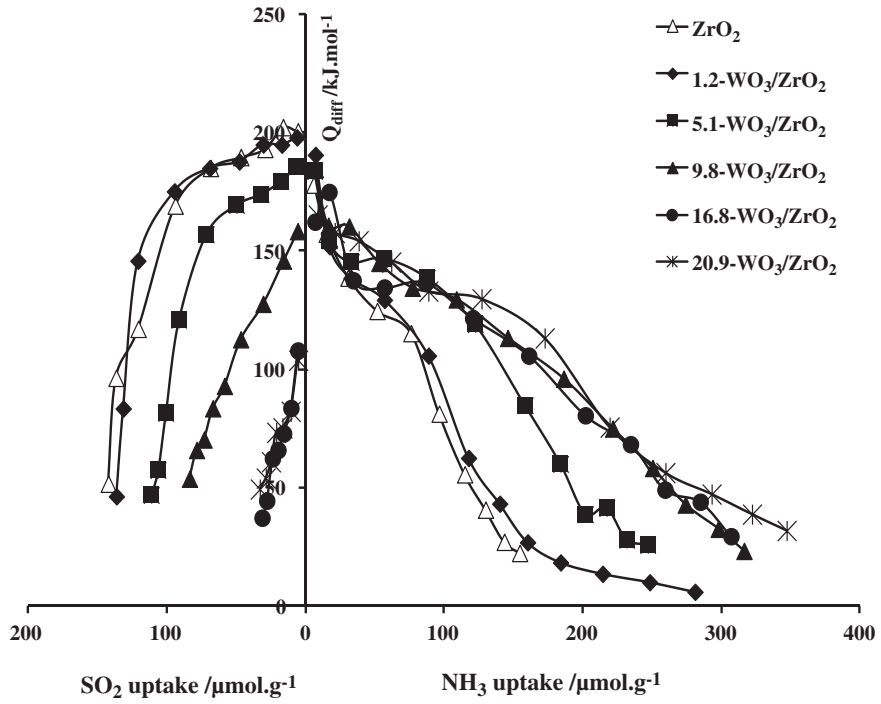

Fig. 3. Differential heats for ammonia (right), and sulfur dioxide (left) adsorptions carried out at 80 °C on m-WO_3/ZrO_2 catalysts.

it is evident that the partial coverage of active zirconia surface by monomeric WO_x species led to a loss of catalytic activity; thus indicating the importance of basic sites exposed on the surface of mixed tungstated zirconia oxides.

For higher WO_3 loadings, the potential of investigated solids to catalyze fructose dehydration increased, and overcame that of zirconia. It is known that an increased amount of WO_3 favors the formation of Brønsted acid sites, as proven by the interpretation of FTIR spectra of adsorbed pyridine [68]. The increasing fructose conversion with increasing WO_3 amount in the samples can be related to the formation (once the catalyst is put in aqueous solution) of hydroxyl groups able to further enhance the Brønsted acidity [38,63]. As already noticed, the maximum conversion of fructose was observed for the sample 16.8-WO_3/ZrO_2, which contains an amount of WO_3 close to that needed for a monolayer. A further increase in WO_3 loading (>16.8 wt.%) leads to the formation of WO_3 crystallites which resulted in a decrease in catalytic activity (decrease in fructose conversion extent).

As shown in Fig. 7, the selectivity to 5-HMF (calculated at 4 h reaction time) is represented as a function of the ratio of basic to acidic sites, as determined by adsorption calorimetry. The volcano shape curve reaches a maximum value (40.1%) for the catalyst with 9.86 wt.% of WO_3; beyond this value, it decreases with increasing WO_3 loading. This behavior could be expected, having in mind the well known reactivity of 5-HMF, its further transformation into levulinic and formic acid can be favored by the presence of very strong acidic sites [69], provided here by the presence of a high WO_3 loading. The calorimetry results obtained in this work have proved that the number of acid sites increases with the WO_3 loading,

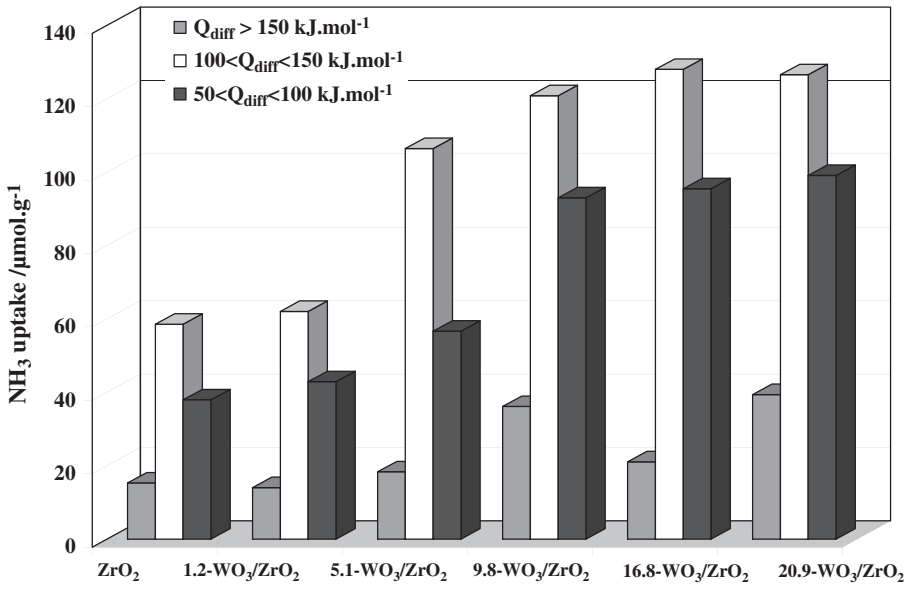

Fig. 4. Acid sites strength distribution of m-WO_3/ZrO_2 catalysts.

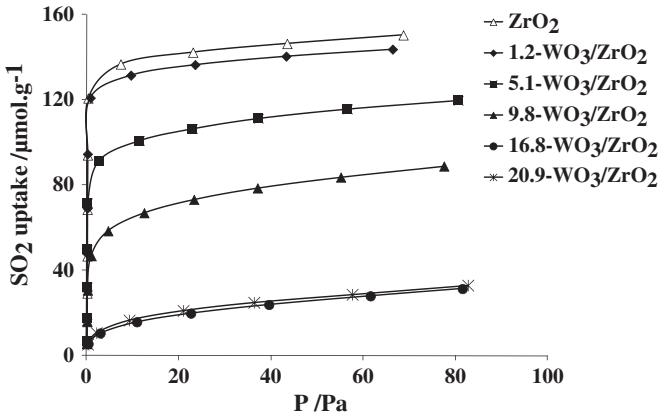

Fig. 5. Adsorption isotherms for sulfur dioxide adsorption carried out at 80 °C on m-WO_3/ZrO_2 catalysts.

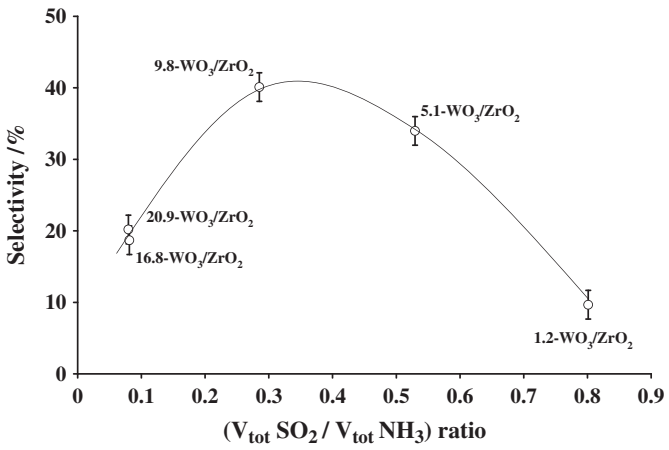

Fig. 7. Selectivity to 5-HMF as a function of the ratio of basic to acidic sites. Reaction conditions: 130 °C, 600 mg of fructose in 60 ml of water, and 80 mg of catalyst.

which explains the decrease in selectivity to 5-HMF above a certain coverage. Moreover, a too high concentration of acid sites may possibly lead to the promotion of condensation reactions which could explain the decrease in selectivity above 9.8 WO_3 wt.% [70]. The bare ZrO_2 sample is not included in the correlations, probably due to the hydration of the zirconia surface that should completely change the nature of the surface sites. It is suggested [71] that only the dehydrated surface of zirconia has Lewis acidity, but the hydrated surface, probably filled with ZrOH groups, has no or quite weak acidity. Contrarily, the Lewis acidity generated on the loaded tungsta layer is not diminished in presence of water.

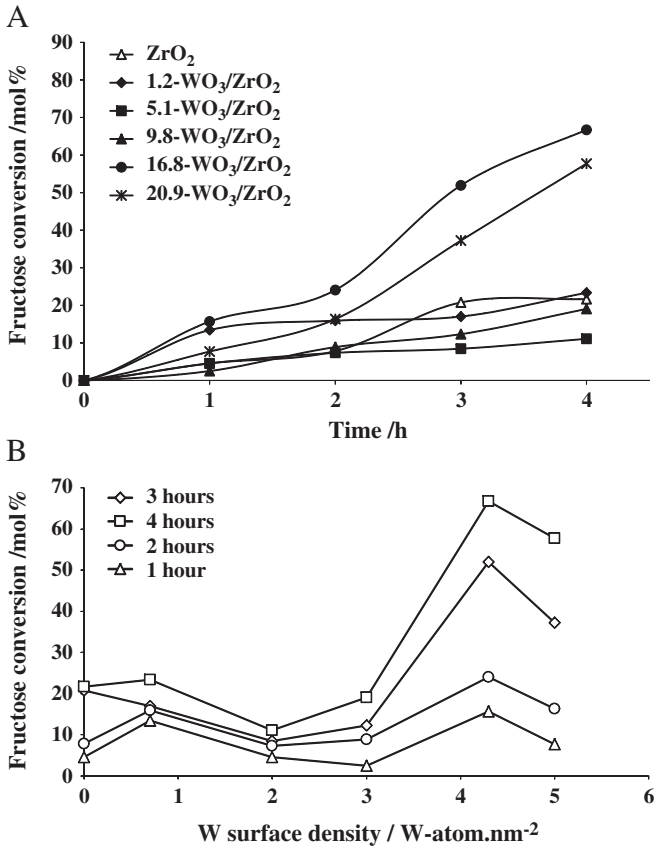

Fig. 6. Fructose conversion as a function of reaction time on m-WO_3/ZrO_2 catalysts. Reaction conditions: 130 °C, 600 mg of fructose in 60 ml of water, and 80 mg of catalyst.

Both Brønsted and Lewis acid sites are involved in the catalytic process of fructose dehydration [66,67], and are both responsible of the degradation for furfural to levulinic and formic acids.

However, it is important to notice that the formation of formic acid is different for the various samples used in this work, and seems also to depend on acidic/basic characteristics and morphology of the investigated catalysts.

Moreover, the carbon mass balance is not attainted in any of the performed experiments. This could be due to the formation of oligosaccharides, which deposited on the catalyst surface and tended to become dark brown colored (as observed on the used catalysts) [39,40].

In Fig. 8, yields of 5-HMF, are presented, together with those of formic and levulinic acids. We have observed that the formation of formic acid starts after the second hour of reaction when testing samples denoted as 9.8-WO_3/ZrO_2 and 20.9-WO_3/ZrO_2; while in the case of pure zirconia and for samples with low WO_3 contents (<10%) the formation of formic acid is evident only after the 3rd hour of reaction. Importantly, formic and levulinic acids were not formed using 1.2-WO_3/ZrO_2, which expresses moderate values of fructose conversion compared to the samples investigated here. 1.2-WO_3/ZrO_2 presents the highest amount of strong basic sites, as shown in Table 2.

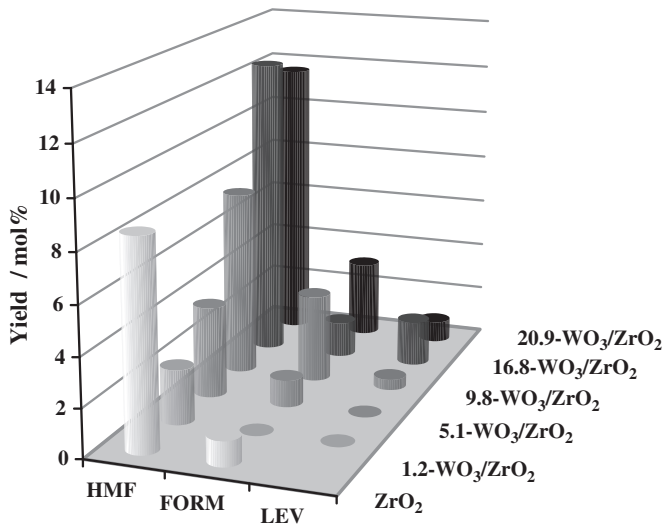

Fig. 8. Yield of 5-HMF, formic and levulinic acids at 4 h reaction time for the various samples. Reaction conditions: 130 °C, 600 mg of fructose in 60 ml of water, and 80 mg of catalyst.

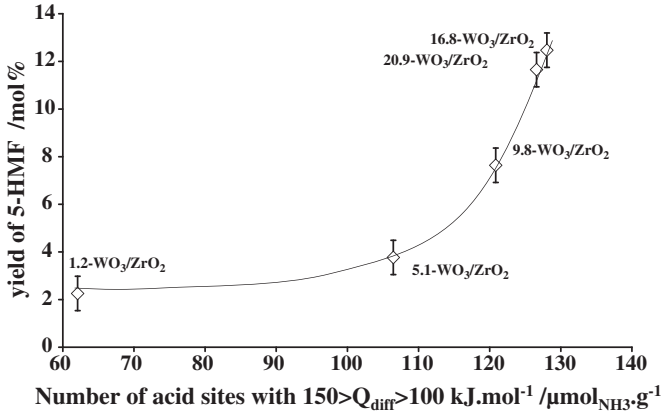

Fig. 9. Correlation between the yield of 5-HMF and the number of medium strength acid sites. Reaction conditions: 130 °C, 600 mg of fructose in 60 ml of water, and 80 mg of catalyst.

We can see that the yields of formic acid are higher than those of levulinic acid, which is common for the fructose dehydration reaction performed in an autoclave [72,73]. The decomposition of L.A and F.A into insoluble polymers [74] is the reason for not having equimolar quantities of the two acids. The difference might be due to the preferred reaction of levulinic acid with the active sites of the catalyst, with the levulinic acid molecule being larger than formic acid, which allows for a longer residence time for secondary reactions [72].

The obtained results also indicate that the amphoteric character of zirconia is important for its catalytic activity and that strong basic sites might be responsible for changes in both fructose dehydration and further 5-HMFs transformation mechanisms. However, a valuable comparison between the catalytic activities of pure zirconia (mainly present in the monoclinic phase) with tungstated zirconia samples that are presenting a zirconia phase (mainly in the tetragonal form), is difficult to establish.

It is important to point out that in acid catalysis, it is not only the number of acid sites which plays a determining role, but also the strength and nature of these sites. Fig. 9 represents the yield of 5-HMF as a function of the number of acid sites with strength between 100 and 150 kJ·mol$_{NH_3}^{-1}$, corresponding roughly to Brønsted sites [75]. This curve shows that the yield to 5-HMF is increasing with the number of medium acid strength sites, while, as seen in Fig. 7, the selectivity to 5-HMF is maximum for a ratio of basic to acid sites of about 0.3. From Fig. 9, 5-HMF yield drastically increases with the number of medium strength acid sites, reaching the maximum value for a W-surface density of 4.3 W-atom·nm^{-2}.

4. Conclusion

Materials resulting from the coupling of tungsten and zirconium oxides displayed stable structures and expressed specific acidic/basic characteristics. A calcination temperature of 700 °C has been shown to be high enough to ensure the complete elimination of the synthesis precursor, as well as the physisorbed and structural water, and low enough to avoid a predominant formation of WO_x crystallites at high surface densities (above monolayer coverage) on ZrO_2. At this high calcination temperature zirconia remained in the tetragonal phase and did not transform to the monoclinic phase, stabilized by the presence of WO_x species.

The results obtained from microcalorimetric experiments reveal the amphoteric characteristics of all the investigated samples with WO_3 content below the monolayer, as they adsorbed both ammonia and sulfur dioxide on their surface. The number of surface acid sites increased with WO_3 content in the samples, while the strength of these acid sites was rather heterogeneous. Besides, the basicity decreased with increasing WO_3 content until the zirconia surface was totally covered.

Catalytic activity for fructose dehydration is related to the presence of strong acid sites, especially for the catalysts with WO_3 loading ≥10 wt.%, while the yield to 5-HMF is associated to the medium strength acid sites. However, the influence of the amphoteric character of the investigated catalysts on the reaction mechanism is evident, and the presence of a small amount of basic sites seems to be important for an improved selectivity to 5-HMF, thus avoiding the formation of by-products,

The combination of different thermal, calorimetric, structural analyses and catalytic tests has made it possible to thoroughly analyze samples that can be potentially applied as acidic catalysts in different environmentally friendly applications such as biomass exploitation and sugar transformation to valuable products, in agreement with the requirements of modern biorefinery platforms. The results obtained in this work give evidence for the importance of the acid–base nature of active sites; further studies aimed at fine-tuning these characteristics should lead to more effective solid catalysts, that would allow higher selectivities and yield lower amounts of by-products.

Acknowledgments

The authors are thankful to the scientific services of IRCELYON for their valuable help in the characterization of the samples.

Appendix A. Supplementary data

Supplementary data to this article can be found online at http://dx.doi.org/10.1016/j.catcom.2012.10.005.

References

[1] A. Corma, S. Iborra, A. Velty, Chemical Reviews 107 (2007) 2411–2502.
[2] G.W. Huber, S. Iborra, A. Corma, Chemical Reviews 106 (2006) 4044–4098.
[3] X. Tong, Y. Ma, Y. Li, Applied Catalysis A 385 (2010) 1–13.
[4] J.N. Chheda, G.W. Huber, J.A. Dumesic, Angewandte Chemie International Edition 46 (2007) 7164–7183.
[5] B. Kamm, M. Kamm, M. Schmidt, T. Hirth, M. Schulze, in: M. Kamm, M. Schmidt, T. Hirth, M. Schulze (Eds.), Biorefineries: Industrial Process and Products, vol. 2, Wiley-VCH, Weinheim, 2006, pp. 97–149.
[6] P. Gupta, S.K. Singh, A. Pathak, B. Kundu, Tetrahedron Letters 58 (2002) 10469–10474.
[7] E.L. Kunkes, D.A. Simonetti, R.M. West, J.C. Serrano-Ruiz, C.A. Gartner, J.A. Dumesic, Science 322 (2008) 417–421.
[8] J. Lewkowski, Arkivoc 2 (2001) 17–54.
[9] B.F.M. Kuster, Starch 42 (1990) 314–321.
[10] Y. Roman-Leshkov, J.N. Chheda, J.A. Dumesic, Science 312 (2006) 1933–1937.
[11] G.W. Huber, J.N. Chheda, C.J. Barrett, J.A. Dumesic, Science 308 (2005) 1446–1450.
[12] A.A. Rosatella, S.P. Simeonov, R.F.M. Frade, C.A.M. Afonso, Green Chemistry 13 (2011) 754–793.
[13] Y. Roman-Leshkov, C.J. Barrett, Z.Y. Liu, J.A. Dumesic, Nature 447 (2007) 982–985.
[14] Y. Roman-Leshkov, J.A. Dumesic, Topics in Catalysis 52 (2009) 297–303.
[15] E.I. Gürbüz, D.M. Alonso, J.Q. Bond, J.A. Dumesic, ChemSusChem 4 (2011) 357–361.
[16] R.D. Cortright, R.R. Davda, J.A. Dumesic, Nature 418 (2002) 964–976.
[17] A.S. Amarasekara, L.D. Williams, C.C. Ebede, Carbohydrate Research 343 (2008) 3021–3024.
[18] H. Zhao, J.E. Holladay, H. Brown, Z.C. Zhang, Science 316 (2007) 1597–1600.
[19] D.A. Simonetti, J.A. Dumesic, Catalysis Reviews 51 (2009) 441–484.
[20] X. Qi, M. Watanabe, T.M. Aida, R.L. Smith Jr., Green Chemistry 10 (2008) 799–805.
[21] G. Yong, Y. Zhang, J.Y. Ying, Angewandte Chemie International Edition 47 (2008) 9345–9348.
[22] S. Hu, Z. Zhang, Y. Zhou, B. Han, H. Fan, W. Li, J. Song, Y. Xie, Green Chemistry 10 (2008) 1280–1283.
[23] X. Qi, M. Watanabe, T.M. Aida, R.L. Smith Jr., Green Chemistry 11 (2009) 1327–1331.
[24] F. Ilgen, D. Ott, D. Kralisch, C. Reil, A. Palmberger, B. Konig, Green Chemistry 11 (2009) 1948–1954.
[25] Y. Yang, X. Xiang, D. Tong, C.W. Hu, M.M. Abu-Omar, Bioresource Technology (2012), http://dx.doi.org/10.1016/j.biortech.2012.03.081.
[26] M. Watanabe, Y. Aizawa, T. Iida, R. Nishimura, H. Inomata, Applied Catalysis A 295 (2005) 150–156.
[27] F.S. Asghari, H. Yoshida, Carbohydrate Research 341 (2006) 2379–2387.
[28] F. Yang, Q. Liu, X. Bai, Y. Du, Bioresource Technology 102 (2011) 3424–3429.

[29] Y. Qu, C. Huang, J. Zhang, B. Chen, Bioresource Technology 106 (2012) 170–172.
[30] J.C. Vartuli, J.G. Santiesteban, P. Traverso, N. Cardona-Martinez, C.D. Chang, S.A. Stevenson, Journal of Catalysis 187 (1999) 131–138.
[31] F. Di Gregorio, V. Keller, Journal of Catalysis 225 (2004) 45–55.
[32] D.E. Lopez, K. Suwannakarn, D.A. Bruce, J.G. Goodwin Jr., Journal of Catalysis 247 (2007) 43–50.
[33] P. Wongmaneenil, B. Jongsomijt, P. Praserthdam, Catalysis Communications 10 (2009) 1079–1084.
[34] Y.M. Park, D.W. Lee, D.K. Kim, J.S. Lee, K.Y. Lee, Catalysis Today 131 (2008) 238–243.
[35] W. Chu, T. Echizen, Y. Kamiya, T. Okuhara, Applied Catalysis A 259 (2004) 199–205.
[36] W. Chu, Y. Ooka, Y. Kamiya, T. Okuhara, H. Hattori, Chemistry Letters 34 (2005) 642–643.
[37] E.I. Ross-Medgaarde, W.V. Knowles, T. Kim, M.S. Wong, W. Zhou, C.J. Kiely, I.E. Wachs, Journal of Catalysis 256 (2008) 108–125.
[38] J. Macht, E. Iglesia, Physical Chemistry Chemical Physics 10 (2008) 5331–5343.
[39] T. Armaroli, G. Busca, C. Carlini, M. Guittari, A.M. Raspolli Galletti, G. Sbrana, Journal of Molecular Catalysis A 151 (2000) 233–243.
[40] C. Carlini, M. Giuttari, A.M. Raspolli Galletti, G. Sbrana, T. Armaroli, G. Busca, Applied Catalysis A 183 (1999) 295–302.
[41] D.G. Barton, M. Shtein, R.D. Wilson, S.L. Soled, E. Iglesia, The Journal of Physical Chemistry. B 103 (1999) 630–640.
[42] N. Naito, N. Katada, M. Niwa, The Journal of Physical Chemistry. B 103 (1999) 7206–7213.
[43] K. Arata, Applied Catalysis A 146 (1996) 3–32.
[44] S. Kuba, P. Concepcion Heydorn, R.K. Grasselli, B.C. Gates, M. Che, H. Knozinger, Physical Chemistry Chemical Physics 3 (2001) 146–154.
[45] M. Kantcheva, C. Koz, Journal of Materials Science 42 (2007) 6074–6086.
[46] M. Scheithauer, R.K. Grasselli, H. Knozinger, Langmuir 14 (1998) 3019–3029.
[47] N. Soultanidis, W. Zhou, A.C. Psarras, A.J. Gonzalez, E.F. Iliopoulou, C.J. Kiely, I.E. Wachs, M.S. Wong, Journal of the American Chemical Society 132 (2010) 13462–13471.
[48] M. Li, Z. Feng, G. Xiong, P. Ying, Q. Xin, C. Li, The Journal of Physical Chemistry. B 105 (2001) 8107–8111.
[49] B. Zhao, X. Xu, J. Gao, Q. Fu, Y. Tang, Journal of Raman Spectroscopy 27 (1996) 549–554.
[50] N. Vaidyanathan, D.M. Hercules, M. Houalla, Analytical and Bioanalytical Chemistry 373 (2002) 547–554.
[51] M.A. Vuurman, I.E. Wachs, A.M. Hirt, Journal of Physical Chemistry 95 (1991) 9928–9937.
[52] S.T. Wong, C.C. Hwang, C.Y. Mou, Applied Catalysis B: Environmental 63 (2006) 1–8.
[53] M. Valigi, D. Gazzoli, I. Pettiti, G. Mattei, S. Colonna, S. De Rossi, G. Ferraris, Applied Catalysis A 231 (2002) 159–172.
[54] A. Martinez, G. Prieto, M.A. Arribas, P. Concepcion, J.F. Sanchez-Royo, Journal of Catalysis 248 (2007) 288–302.
[55] D.C. Vermaire, P.C. Van Berge, Journal of Catalysis 116 (1989) 309–317.
[56] M.G. Flaco, S.A. Canavese, N.S. Figoli, Catalysis Today 107–108 (2005) 778–784.
[57] D.G. Barton, S.L. Soled, G.D. Metzner, G.A. Fuentes, E. Iglesia, Journal of Catalysis 181 (1999) 57–72.
[58] A.M. Garrido Pedrosa, M.J.B. Souza, S.H. Lima, D.M.A. Melo, A.G. Souza, A.S. Araujo, Journal of Thermal Analysis and Calorimetry 87 (2007) 703–707.
[59] A. Auroux, A. Gervasini, Journal of Physical Chemistry 94 (1990) 6371–6379.
[60] A. Auroux, Topics in Catalysis 4 (1997) 71–89.
[61] W. Ji, J. Hu, Y. Chen, Catalysis Letters 53 (1998) 15–21.
[62] L. Damjanovic, A. Auroux, in: M.E. Brown, P.K. Gallagher (Eds.), Handbook of thermal analysis and calorimetry, vol. 5, Elsevier, Amsterdam, 2008, pp. 387–438.
[63] S. Bennici, A. Auroux, in: S.D. Jackson, S.J. Hargreaves (Eds.), Metal oxide catalysis, vol. 1, Wiley-VCH, Weinheim, 2009, pp. 391–442.
[64] C. Busco, A. Barbaglia, M. Broyer, V. Bolis, G.M. Foddanu, P. Ugliengo, Thermochimica Acta 418 (2004) 3–9.
[65] C. Guimon, A. Gervasini, A. Auroux, The Journal of Physical Chemistry. B 105 (2001) 10316–10325.
[66] F. Benvenuti, C. Carlini, P. Patrono, A.M.R. Galletti, G. Sbrana, M.A. Massucci, P. Galli, Applied Catalysis A 193 (2000) 147–153.
[67] R. Weingarten, G.A. Tompsett, W.C. Conner Jr., G.W. Huber, Journal of Catalysis 279 (2011) 174–182.
[68] G. Busca, Physical Chemistry Chemical Physics 1 (1999) 723–736.
[69] X. Qi, M. Watanabe, T.M. Aida, R.L. Smith, Catalysis Communications 10 (2009) 1771–1775.
[70] M. Watanabe, Y. Aizawa, T. Iida, T.M. Aida, C. Levy, K. Sue, H. Inomata, Carbohydrate Research 340 (2005) 1925–1930.
[71] N. Naito, N. Katada, M. Niwa, The Journal of Physical Chemistry. B 103 (1999) 7206–7213.
[72] K. Lourvanij, G.L. Rorrer, Industrial and Engineering Chemistry Research 32 (1993) 11–19.
[73] D. Stosic, S. Bennici, V. Rakic, A. Auroux, Catalysis Today (2011), http://dx.doi.org/10.1016/j.cattod.2011.10.040.
[74] F.S. Asghari, H. Yoshida, Industrial and Engineering Chemistry Research 46 (2007) 7703–7710.
[75] R. Kourieh, S. Bennici, M. Marzo, A. Gervasini, A. Auroux, Catalysis Communications 19 (2012) 119–126.

Publication V

Catal Lett
DOI 10.1007/s10562-012-0945-7

Influence of the Acidic Properties of ZrO_2 Based Mixed Oxides Catalysts in the Selective Reduction of NO_x with *n*-Decane

Reem Kourieh · Laurence Retailleau · Simona Bennici · Anne Giroir-Fendler · Aline Auroux

Received: 10 October 2012 / Accepted: 19 November 2012

Abstract The selective catalytic reduction of NO_x by decane ($C_{10}H_{22}$–SCR) has been studied over mixed oxides of zirconia with boria, alumina, gallia, india and tungsta. The samples were prepared by coprecipitation and thoroughly characterized using a combination of different techniques to determine their structural and surface properties. Moreover a WO_3-containing sample supported on Al_2O_3–ZrO_2 sample was prepared to verify the influence of the tungsta active phase deposited by impregnation. The surface acidity and basicity of the samples (measured by NH_3 and SO_2 adsorption microcalorimetry) varied in relation to the kind of co-oxide added to zirconia. In particular, the number of surface acid sites expressed in $\mu mol_{NH_3}\ g^{-1}$ increased in the following order WO_3–ZrO_2 > Al_2O_3–ZrO_2 > Ga_2O_3–ZrO_2 > In_2O_3–ZrO_2 > WO_3/(Al_2O_3–ZrO_2) > ZrO_2 > B_2O_3–ZrO_2. Correlations between the catalytic behaviour and the samples surface acidity were found and the results show that a moderate acidity (i.e. for Ga_2O_3–ZrO_2) is one of the key parameter for high N_2 selectivity and NO_x conversion.

Keywords Zirconia based mixed oxides · Adsorption microcalorimetry · Acidity · *n*-Decane · NO_x · HC–SCR

1 Introduction

Nitrogen oxides (NO_x) produced by internal combustion engines are still an un-solved issue. NO_x oxides are the main cause for a lot of environmental problems; such as ozone formation in the troposphere and production of acidic rains [1]. These oxides are very toxic for human health and they can provoke infections and allergies in the respiratory system [2]. Long exposure of NO_x with concentration above 0.05 ppm causes hazardous effects for human health [3]. As a result of the negative impact of NO_x, the regulation of its emission is becoming stricter, regardless of the region, including Asia, Europe and USA [4]. The next NO_x limits (Euro 6 in Europe) will require the introduction of sophisticated after-treatment techniques from the diesel manufacturers [5]. Among the different technologies existing to reduce NO_x emission from diesel engines, the selective catalytic reduction by hydrocarbons [6], HC–SCR, is a highly recommended technology, as it is a practical method to use the unburned hydrocarbons that already exist in the exhaust gas [7]. HC–SCR is more cost-effective, simpler to apply, but still higher NO_x conversion is required to find a final application [5]. Various studies have been performed using light hydrocarbons (C_1–C_4), especially methane [8, 9], ethane [10] and propane [11, 12]; however these light hydrocarbons are not usually observed in diesel engine exhaust. Gasoline is a complex mixture of different organic compounds and it is an attractive reductant to use in the SCR process due to its high reactivity and availability. Decane is one of the gasoline components and can be effectively used for selective catalytic reduction of NO_x by hydrocarbons (NO_x–HC–SCR) [13]. A suitable active commercial catalyst is needed to achieve a good NO_x conversion [14]; this catalyst should show good stability, activity and selectivity over a wide range of operation temperatures. Numerous researches upon the selective reduction of NO_x by hydrocarbons were undertaken and subsequently reported in the literature. The active catalysts can be divided into three groups:

R. Kourieh · L. Retailleau · S. Bennici · A. Giroir-Fendler · A. Auroux (✉)
Institut de recherches sur la catalyse et l'environnement de Lyon (IRCELYON), UMR 5256, CNRS, Université Lyon 1, 2 avenue Albert Einstein, 69626 Villeurbanne, France
e-mail: aline.auroux@ircelyon.univ-lyon1.fr

Published online: 08 December 2012

ion-exchanged zeolites, noble metals and metallic oxides [2]. Zeolites are not stable in presence of water vapor [15], noble metals like platinum and rhodium are expensive. Therefore, various supported mixed oxides catalysts have been developed as potential candidates for the catalytic removal of NO_x. The oxides such as Al_2O_3, SiO_2–Al_2O_3, TiO_2 and ZrO_2 are active in this selective reduction [16–19]. Despite the numerous catalysts studied for the NO_x–HC–SCR reaction, none has yet shown the required properties in terms of thermal stability, tolerance to water and high catalytic activity [20–23]. The oxides of group III elements have received much attention recently as they have been tested in various catalytic reactions of environmental interests. Ga_2O_3 and In_2O_3 supported on acidic supports (Al_2O_3–TiO_2–SiO_2/Al_2O_3) have been reported to present a remarkable de-NO_x catalytic activity [24–26].

In the present study, we investigated the effect of addition of boria, alumina, gallia, india and tungsta on the surface acidity of ZrO_2 as determined by the chemisorption of acidic and basic probe molecules (sulfur dioxide and ammonia), with the aim of gaining insight into the surface properties of the corresponding catalysts. Surface acidity was measured by means of gas phase adsorption microcalorimetry, which gives access to the number, and strength of the sites. The catalysts were tested in the *n*-decane–SCR reaction in order to establish eventual correlations between acid–base properties and catalytic behavior. The discovery of appropriate indicators of catalytic activity in $C_{10}H_{22}$–SCR of NO_x by tuning the acid–base properties of amphoteric mixed oxides being of fundamental interest.

2 Experimental

2.1 Catalyst Preparation

In this work, zirconia mixed oxides with Me_2O_3 (Me: B, Al, Ga, In, W) were prepared by coprecipitation. The compounds used as Me_2O_3 precursors were boric acid (H_3BO_3, Merck), the nitrates of aluminum, gallium, and indium: $Al(NO_3)_3{\cdot}9H_2O$ (≥99 %, Fluka), $Ga(NO_3)_3{\cdot}5H_2O$ (99.9 %, Alfa Aesar), $In(NO_3)_3{\cdot}5H_2O$ (99.9 %, Aldrich) and ammonium metatungstate $(NH_4)_6H_2W_{12}O_{40}{\cdot}nH_2O$ (≥99.0 % WO_3, Fluka). The precursor for the zirconia phase was zirconium oxychloride $ZrOCl_2{\cdot}8H_2O$ (≥99.5 %, Sigma-Aldrich). The required quantities of the group III metal oxide and zirconia precursors were dissolved in deionized water at room temperature. The solutions were mixed with a continuous monitoring of pH. Concentrated ammonia (32 % wt/wt) was added gradually dropwise to this mixture of two solutions with vigorous stirring, until the precipitation was achieved (pH 9).

Pure zirconia was obtained by precipitation from a solution of $ZrOCl_2{\cdot}8H_2O$ by ammonia in the same way. All precipitates were filtrated, washed with water and dried overnight in an oven at 100 °C and calcined at 450 °C under air flow.

WO_3/(Al_2O_3–ZrO_2) was prepared by incipient wetness impregnation on the uncalcined Al_2O_3–ZrO_2 precursor prepared as reported just above, starting from aqueous solution of ammonium metatungstate. After drying at 100 °C for 24 h and calcination at 450 °C, the tungsten oxide loading was 16.7 wt%.

The calcination temperature of 450 °C was chosen on the basis of thermogravimetry (TG) measurements, performed with a Labsys-TG from Setaram. The crude samples (~50 mg) were heated from 25 to 900 °C with a heating rate of 5 °C min^{-1} in a flow of air, which was chosen as a soft oxidizing agent for calcination.

2.2 Catalyst Characterization

The samples were dissolved by appropriate solution of NaOH + KNO_3 and the elemental analysis was performed using inductive coupled plasma optical emission spectroscopy (ICP-OES) with an ACTIVA spectrometer from Horiba Jobin–Yvon.

The surface areas, pore volumes and pore sizes were measured by nitrogen adsorption at −196 °C on a Micromeritics 2010 apparatus after heat pre-treatment under vacuum for 2 h at a temperature of 400 °C. Surface areas were determined by the BET method from the resulting isotherms.

The X-ray diffraction (XRD) measurements were carried out on a Bruker D5005 powder diffractometer scanning from 3° to 80° (2θ) at a rate of 0.02° s^{-1} using a Cu Kα radiation (λ = 0.15418 nm) source. The applied voltage and current were 50 kV and 35 mA, respectively.

The X-ray photoelectron spectra (XPS) were obtained on a KRATOS AXIS Ultra DLD spectrometer equipped with a hemispherical electron analyzer and an Al anode (Al Kα = 1486.6 eV) powered at 150 W, a pass energy of 20 eV, and a hybrid lens mode. The detection area analyzed was 700 × 300 μm. Charge neutralization was required for all samples. The peaks were referenced to the C–(C, H) components of the C 1s band at 284.6 eV. Shirley background subtraction and peak fitting to theoretical Gaussian–Lorentzian functions were performed using an XPS processing program (Vision 2.2.6 KRATOS). The residual pressure in the spectrometer chamber was 5×10^{-9} mbar during data acquisition.

The pyridine adsorption FTIR spectra were recorded at room temperature with a Bruker Vector 22 FTIR spectrophotometer (DTGS detector) operating in the 4,000–400 cm^{-1} range, with a resolution of 2 cm^{-1} and 100 acquisition scans. In each pyridine adsorption FTIR measurement, the

self-supporting wafer (about 50 mg, 18 mm diameter) was first activated in situ at 400 °C in oxygen flow for 14 h, then evacuated at the same temperature for 2 h and then exposed to pyridine (Air Liquide, 99.8 %, vapor pressure 3.3 kPa) at room temperature for 5 min. The desorption was carried out by evacuation for 30 min each at room temperature, 100, 200, 300 °C, respectively. The spectra were recorded at room temperature after adsorption and desorption at each temperature.

Adsorption microcalorimetry measurements were performed at 80 °C in a heat flow calorimeter (C80 from Setaram) linked to a conventional volumetric apparatus equipped with a Barocel capacitance manometer for pressure measurements. Ammonia used for measurements (Air Liquide, purity >99.9 %) was purified by successive freeze–pump–thaw cycles. About 100 mg of sample was pre-treated in the calorimetric quartz cell overnight at 400 °C, and then evacuated at the same temperature for 1 h prior to the measurements. The differential heats of adsorption were measured as a function of coverage by repeatedly introducing small doses of the adsorbate onto the catalyst, until an equilibrium pressure of about 66 Pa was reached. The sample was then outgassed for 30 min at the same temperature, and a second adsorption was performed at 80 °C until an equilibrium pressure of about 27 Pa was attained in order to calculate the irreversibly chemisorbed amount of the probe molecules at this pressure.

2.3 Selective Catalytic Reduction of NO_x by *n*-Decane ($C_{10}H_{22}$–SCR)

The selective catalytic reduction of NO_x is a complicated sequence of reactions, which consists of several competing parallel reactions. NO_2 and partially oxidized hydrocarbons are important intermediates in oxidizing atmosphere [27], and simplifying the global reaction equation can be written as follow [28]:

$$\mathrm{HC} + \mathrm{NO_x} + \mathrm{O_2} \rightarrow \text{intermediates} \rightarrow \mathrm{N_2} + \mathrm{CO_x} + \mathrm{H_2O}$$

The selective catalytic reduction of NO_x by *n*-decane ($C_{10}H_{22}$–SCR) was carried out in a U-shaped quartz reactor with 0.2 g of catalyst. The reactor was heated and the temperature of the catalyst was monitored using a K-type thermocouple. The reaction mixture was composed of 400 ppm NO, 240 ppm $C_{10}H_{22}$ and 9 vol% O_2 in He as carrier gas in the presence of H_2O (1.5 vol%). The total flow rate was 120 mL min^{-1}, corresponding to a space velocity of about 35,000 h^{-1}. Reaction products were analyzed by micro-gas chromatography (μGC: TCD detector) for N_2 (molecular sieve 5A), by gas chromatography (FID detector) for $C_{10}H_{22}$, and by IR–UV for CO_2, NO, NO_2 and N_2O. After stabilization, the temperature-programmed reaction began at 100 °C by increasing the catalyst temperature at a rate of 2 °C min^{-1} until 500 °C was obtained. At the end of the ramp, the temperature was maintained 30 min at 500 °C and then decreased at a rate of 1 °C min^{-1} down to 100 °C. All the data presented in this paper were recorded during the cooling ramp. The N_2, N_2O, NO_2, global NO_x, total $C_{10}H_{22}$ yields, nitrogen balance, and selectivity to N_2 were calculated by the following equations from (1) to (7):

$$Y_{\mathrm{NO_x-N_2}} = 100 \times \frac{2[\mathrm{N_2}]}{[\mathrm{NO}]_0 + [\mathrm{NO2}]_0} \quad (1)$$

$$Y_{\mathrm{NO_x-N_2O}} = 100 \times \frac{2[\mathrm{N_2O}]}{[\mathrm{NO}]_0 + [\mathrm{NO2}]_0} \quad (2)$$

$$Y_{\mathrm{NO_x-NO_2}} = 100 \times \frac{[\mathrm{NO_2}]}{[\mathrm{NO}]_0 + [\mathrm{NO2}]_0} \quad (3)$$

$$Y_{\mathrm{NO_{xglobal}}} = 100 \times \left(\frac{([\mathrm{NO}]_0 + [\mathrm{NO_2}]_0) - ([\mathrm{NO}] + [\mathrm{NO_2}])}{[\mathrm{NO}]_0 + [\mathrm{NO_2}]_0} \right) \quad (4)$$

$$Y_{\mathrm{C_{10}H_{22}}} = 100 \times \left(\frac{\frac{1}{10}[\mathrm{CO_2}]}{[\mathrm{C_{10}H_{22}}]_0} \right) \quad (5)$$

$$\text{N balance} : [\mathrm{NO}]_0 + [\mathrm{NO_2}]_0 = [\mathrm{NO}] + [\mathrm{NO_2}] + 2[\mathrm{N_2}] + 2[\mathrm{N_2O}] \quad (6)$$

$$S_{\mathrm{N_2}} = 2[\mathrm{N_2}] \,/\, 2[\mathrm{N_2}] + 2[\mathrm{N_2O}] + [\mathrm{NO_2}] \quad (7)$$

A substantial amount of NO_2 was formed in homogeneous phase in the pipes of the apparatus, before and after the reactor, as previously observed for studies on selective catalytic reduction of NO by propene in the presence of oxygen performed in the same equipment [29]. Indeed, the thermodynamic equilibrium of the following reaction leads to the formation of NO_2 at room temperature [30]:

$$\mathrm{NO} + 1/2\mathrm{O_2} \rightarrow \mathrm{NO_2}$$

The quantity of NO_2 formed in the pipes was subtracted from the total NO_2 amount before the conversion of NO_x into NO_2 was calculated.

3 Results and Discussion

3.1 Structural Properties

Table 1 presents the list of the samples synthesized in this work, their chemical compositions, obtained by ICP, and the values of BET surface areas. Higher surface areas were observed for mixed oxides in comparison with that of pure zirconia (77 $m^2\ g^{-1}$) except for B_2O_3–ZrO_2 (75 $m^2\ g^{-1}$). The increase in BET surface areas could be explained by

Table 1 Physicochemical characteristics of the catalysts

Sample calcined at 450 °C	C.A (wt%)	BET surface area ($m^2\ g^{-1}$)	Binding energy (eV)	
			Zr $3d_{5/2}$	–
ZrO_2	–	77	182.2	–
B_2O_3–ZrO_2	30.2 (B_2O_3)	75	182.2	B 1s: 191.8
Al_2O_3–ZrO_2	34.8 (Al_2O_3)	181	182.2	Al 2p: 73.9
Ga_2O_3–ZrO_2	21.3 (Ga_2O_3)	128	182.2	Ga $2p_{3/2}$: 1117.9
In_2O_3–ZrO_2	27.0 (In_2O_3)	110	182.2	In $3d_{5/2}$: 444.4
WO_3–ZrO_2	16.7 (WO_3)	218	182.8	W $4f_{7/2}$: 36.0
WO_3/(Al_2O_3–ZrO_2)	16.7 (WO_3)	178	182.1	W $4f_{7/2}$: 36.0
	34.8 (Al_2O_3)			Al 2p: 73.9

the dispersion of two oxides that happens as a result of mixed oxides forming by the coprecipitation method. The values of BET surface areas reveal that they are related to the type of guest oxide, and the highest surface area was obtained for the WO_3–ZrO_2 sample.

The XRD patterns of various mixed oxides investigated in this work are shown in Fig. 1 B_2O_3–ZrO_2, Al_2O_3–ZrO_2 and Ga_2O_3–ZrO_2 samples are poorly crystallized and contain amorphous phases, indicating that the maximum calcination temperature of 450 °C in air for 4 h was well chosen to avoid the formation of the crystalline phases of the co-precipitated oxides. Differently, diffraction peaks characteristic of tetragonal ZrO_2 (at $2\theta = 30.17°$, 35.31°, 49.79°, and 60°) [31, 32] were detected for ZrO_2, In_2O_3–ZrO_2 and WO_3–ZrO_2 samples. The monoclinic phase is observed only for pure zirconia (at $2\theta = 28.3°$ and 31.6°) [31, 33, 34]. No characteristic diffraction lines due to Al_2O_3 or ZrO_2 were observed for the WO_3/(Al_2O_3–ZrO_2) impregnated sample, which confirms that the ZrO_2–Al_2O_3 phase is amorphous or poorly crystalline even when calcined in presence of WO_3. The lines at $2\theta = 22.9°$, 23.5°, 24.1°, 33.0°, 33.6° and 34.3° can be assigned to orthorhombic WO_3 phase [35–37], and the group of small peaks between 50° and 60° 2θ belongs to the tetragonal phase of WO_3 [38].

XPS investigations were carried out in order to acquire additional data about the nature of surface-active sites. It is well-known that XPS gives information on the catalyst's surface composition and on the distribution and electronic/oxidation state of the elements in the surface layer [39]. Table 1 presents the binding energies (BE) of $Zr_{3d5/2}$, $W_{4f7/2}$, B_{1s}, Al_{2p}, $Ga_{2p3/2}$, and $In_{3d5/2}$. The BE values of $Zr_{3d5/2}$ for the catalysts are almost similar and correspond to the BE of Zr^{4+} in bulk zirconia (182.1 eV) [40]. The BE value of the $W_{4f7/2}$ for WO_3–ZrO_2 sample is close to the reported value for W^{6+} (35.5 eV) in the bulk oxide [41]. The core-level spectra of B_{1s} (191.8 eV) in the case of B_2O_3–ZrO_2 binary oxides showed a shift toward low-binding energies (BE) in comparison with pure B_2O_3 (193.5 eV) [42] indicating the interaction between the two oxides. Changes in

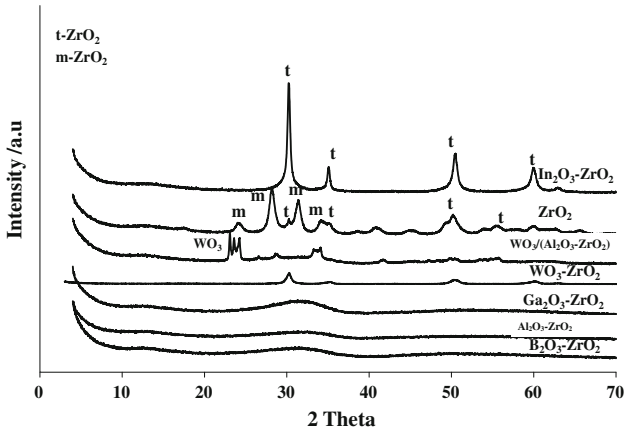

Fig. 1 XRD of the catalysts calcined at 450 °C

the BE of Al_{2p} 74.2 eV and $In_{3d2/5}$ 444.3 eV [43], were also observed for Al_2O_3–ZrO_2 (73.9 eV), WO_3/(Al_2O_3–ZrO_2) (73.9 eV), and In_2O_3–ZrO_2 (444.7 eV) indicating once again the intimate interaction between the couples of co-precipitated oxides.

3.2 Acidic/Basic Properties

The surface acidity is an important feature of a solid surface and can influence a broad range of different reactions. The amount and strength of surface acid and basic sites of the catalysts were determined respectively by ammonia and sulphur dioxide adsorption microcalorimetry.

Table 2 summarizes the data obtained by NH_3 and SO_2 adsorption on zirconia based materials: the initial heats of adsorption and the total (chemisorbed and physisorbed amounts) and irreversibly adsorbed volumes (chemisorbed amounts of gases) are reported.

According to its adsorption properties towards NH_3 and CO_2, tungsten oxide was classified as acidic oxide while zirconia and gallia were assigned to the amphoteric group [44]. Alumina is also a typical amphoteric solid which is characterized by the presence of both acidic and basic sites on its surface and presents a broad distribution of sites strength [45]. Indium oxide even if classified as amphoteric

Table 2 The initial heats of adsorption (denoted by Q_{init}), total and irreversible amounts of sulphur dioxide and ammonia adsorbed under an equilibrium pressure of 27 Pa, measured by adsorption microcalorimetry

Sample	Basicity/SO_2					Acidity/NH_3				
	Q_{init} (kJ mol^{-1})[a]	V_{tot} (μmol_{SO_2} g^{-1})[b]	V_{irr} (μmol_{SO_2} g^{-1})[c]	V_{tot} (μmol_{SO_2} m^{-2})[b]	V_{irr} (μmol_{SO_2} m^{-2})[c]	Q_{init} (kJ mol^{-1})[a]	V_{tot} (μmol_{NH_3} g^{-1})[b]	V_{irr} (μmol_{NH_3} g^{-1})[c]	V_{tot} (μmol_{NH_3} m^{-2})[b]	V_{irr} (μmol_{NH_3} m^{-2})[c]
ZrO_2	182	181	159	2.4	2.1	174	258	144	3.4	1.9
B_2O_3–ZrO_2	130	39	23	0.5	0.3	164	207	79	2.8	1.1
Al_2O_3–ZrO_2	209	303	269	1.7	1.5	164	445	285	2.5	1.6
Ga_2O_3–ZrO_2	173	294	263	2.3	2.1	179	370	236	2.9	1.8
In_2O_3–ZrO_2	222	209	191	1.9	1.7	185	324	209	2.9	1.9
WO_3–ZrO_2	160	301	240	1.4	1.1	198	508	306	2.3	1.4
$WO_3/(Al_2O_3$–$ZrO_2)$	160	416	388	2.3	2.2	147	309	181	1.7	1.0

[a] Heat evolved from the first dose of SO_2 and NH_3

[b] Total amount of SO_2 and NH_3 retained as determined at 27 Pa of equilibrium pressure

[c] Irreversibly adsorbed amount of SO_2 and NH_3 as determined from the difference between the amounts adsorbed in the first and second adsorptions at 27 Pa

can be considered as more basic than acidic [46], while boria is considered as an acidic oxide [43].

It can be concluded from the results presented in Table 2 that the group III metal oxide has a decisive role in modulating the acidic and basic properties of the investigated mixed oxides.

NH_3 adsorption isotherms of ZrO_2 based catalysts are presented in Fig. 2 the volumetric adsorption isotherms collected in this work displayed in all cases an initial vertical section at very low pressure corresponding to the amount of strongly chemisorbed NH_3, whereas the horizontal parts can be assigned to reversible adsorption [47].

As displayed in Table 2 and Fig. 2 the addition of alumina, gallia, india and tungsta to zirconia led to an increase in acid character, while the addition of acidic boria did not increase the acidity of pure zirconia as expected; quite contrarily the acidity of B_2O_3–ZrO_2 was lower than that of pure ZrO_2. Boric acid was used as a precursor for boria in order to prepare the mixed oxide of B_2O_3–ZrO_2. The transformation from boric acid to the acidic boron oxide (boria) consists of complex phenomena (metastable equilibrium) in which the intermediates can be in liquid state. This transformation depends on the heating rate during calcination: if the temperature is raised too quickly, the melting of acidic boron oxide (mp = 450 °C) can take place with the formation of a boron oxide glass of low surface area [48] and low acidity. This formation of boron oxide glass is most probably the reason of the low acidity of the B_2O_3–ZrO_2 mixed oxide.

As already mentioned, the B_2O_3–ZrO_2 surprisingly did not present the expected strong acidic properties (low NH_3 adsorption, 79 μmol_{NH_3} g^{-1} instead of 144 μmol_{NH_3} g^{-1} for the pure zirconia), associated with a very low SO_2 adsorption, nearly inexistent compared to that of pure zirconia, confirming that boric acid neutralized the basic sites of zirconia. All the other samples adsorbed significant

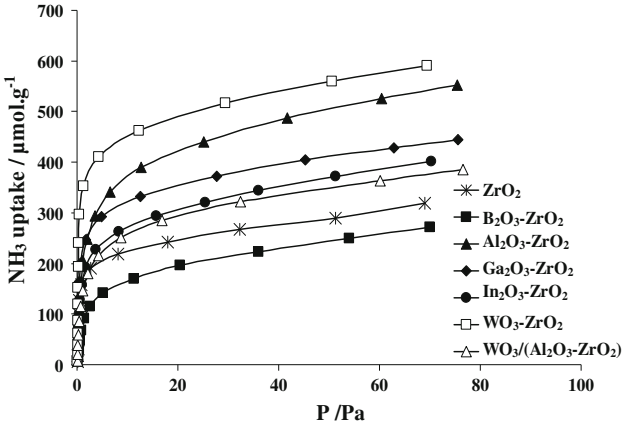

Fig. 2 Isotherms obtained from NH_3 adsorption microcalorimetry experiments carried out at 80 °C

amounts of both SO_2 and NH_3, which is a clear indication of their amphoteric nature.

Figure 3 displays the differential heats of NH_3 and SO_2 adsorption as a function of surface coverage providing information on the strength of the acid and basic sites, respectively. Furthermore, the initial heats of adsorption are characteristic of the strongest sites involved in adsorption processes. All investigated samples exhibited high initial differential heats for both ammonia and sulphur dioxide adsorption ($\geq$150 kJ mol^{-1}). It has to be noticed that WO_3–ZrO_2 displays the highest initial differential heat of NH_3 adsorption (around 198 kJ mol^{-1}), index of very strong acid sites. In each case, the heats of adsorption showed a decreasing trend upon increasing coverage, as usually observed for heterogeneous surfaces [47, 49, 50]. B_2O_3–ZrO_2 is the sample that displays the lowest acidity and basicity, in agreement with the formation of boron oxide glass, unable to adsorb any probe molecule.

Figure 4 displays the number of sites of a given strength for the various samples. Indeed strong sites with $Q_{diff} >$ 150 kJ mol^{-1} are in such greater amount for WO_3–ZrO_2 than for the other samples. Concerning the sites of medium strength, 100 $< Q_{diff} <$ 150 kJ mol^{-1}, their amount increases in the order of the figure from left to right hand side. Weak sites are mainly related to physisorption process.

FT-IR pyridine adsorption was performed to identify the type of acidic sites on the surface of catalysts. The technique of pyridine adsorption is one of the most applied methods for characterizing the nature of the surface acid sites. The band at (1,455–1,438) cm^{-1} is characteristic of Lewis acid sites, while the band at around 1,540 cm^{-1} can be attributed to Brønsted acid sites [51–53].

Figure 5 presents the IR spectra of pyridine desorption on the catalysts, after outgassing at 100 °C. Pyridine molecules bonded to Lewis acid sites and corresponding to the bands observed at 1444, 1575 and 1609 cm^{-1} were

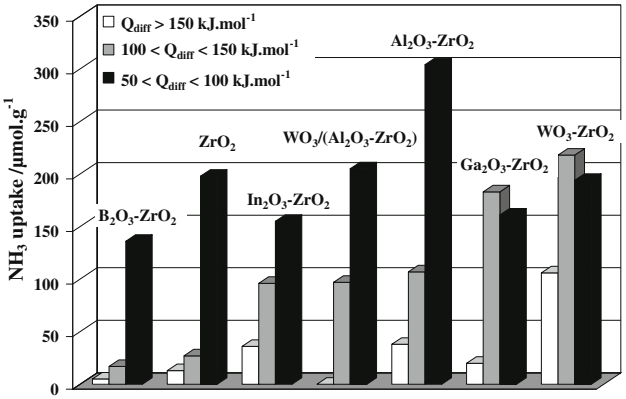

Fig. 4 Acid sites strength distribution of the catalysts

detected in all the catalysts. Only the WO_3–ZrO_2 sample displayed peaks centered at 1,540 and 1,639 cm^{-1} which correspond to pyridinium ions bonded to Brønsted acid sites. The appearance of Brönsted acid sites on the WO_3–ZrO_2 sample can be related to the presence of dispersed WO_x domains composed of two-dimensional polytungstate allowing protons to remain accessible at external surfaces [54]. The sample $WO_3/(Al_2O_3$–$ZrO_2)$ did not present this kind of Brønsted sites due to the aggregation of the WO_x clusters (source of Brønsted sites) to form WO_3 crystallites, as confirmed by the XRD results (Fig. 1). The formation of WO_3 is due to the weaker interaction between the W-phase and the Al_2O_3–ZrO_2 mixed oxide acting for this sample as support.

The band at 1,489 cm^{-1}, present for all samples, is characteristic of pyridine bonded alternatively to Brønsted and/or Lewis sites [53]. The acidity of the catalysts is mainly related to the presence of Lewis sites, and only for WO_3–ZrO_2 can be attributed also to strong Brønsted surface sites.

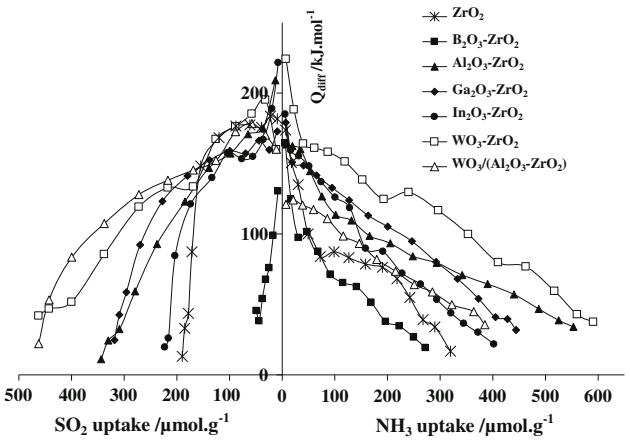

Fig. 3 Differential heats of NH_3 and SO_2 adsorption versus coverage (NH_3 and SO_2 uptakes in µmol g^{-1})

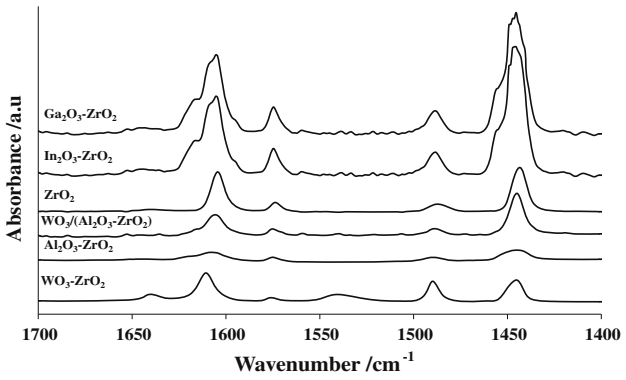

Fig. 5 FTIR spectra of pyridine after adsorption at room temperature and evacuation at 100 °C

3.3 De-NO_x Catalytic Activity

The catalytic activity of the catalysts was evaluated in the selective reduction of NO_x using *n*-decane as reducing species, in oxidant atmosphere, and in presence of water. Thanks to the analytical system employed to analyse the gas stream entering and exiting from the reactor, the $C_{10}H_{22}$ consumption, the NO_x conversion into N_2 and the evolution of N_2O and NO_2 products can be followed all over the experiment. To avoid any changes in the nature of the zirconia surface acidity by hydration (since we are working with ZrO_2 based catalysts), the water concentration used in this study (1.5 vol%) was maintained lower than that normally observed in diesel exhaust gas (~10 vol%). A fully hydrated zirconia surface (filled with ZrOH groups) presents in fact weaker acidity than dry zirconia [55] and might false the correlation between reactivity and acidity (measured by ammonia adsorption calorimetry on the dry zirconia surface). Analyzing the catalytic results, it has to be taken in account that the SCR activity in presence of long chain alkanes increases in presence of large concentrations of water due to the decrease in the concentration of carbonaceous species blocking the adsorption sites at the catalyst surface [56, 57], and that consequently the catalytic activity measured in the reported experiments might be lower than that measured in presence of higher concentration of water.

As already mentioned in the experimental part, the catalytic activity values reported in this study correspond to those recorded during the decrease of temperature after stabilization at 500 °C for 30 min. Following this procedure, the NO_x and $C_{10}H_{22}$ conversions can be correctly determined, as we assess that no reactant can be pre-adsorbed at the catalyst surface at such high temperature (500 °C). Each catalyst was activated under the reaction mixture, regardless of the support, the precursor, and the preparation procedure [29]. As previously observed on zeolitic catalysts [58, 59] this activation step increases the activity of the catalyst that otherwise, at low temperature, would probably store the hydrocarbon [58] and trap NO_x [59]. In absence of noble metals (oxidizing metal) [60] it has been observed that, analyzing the products in gas stream at increasing temperature, the CO_2 mass balance at the highest temperatures of reaction is not respected (being higher than the expected value): at high temperatures the hydrocarbon species previously adsorbed at lower temperatures can finally desorb and react to produce CO_2.

In Fig. 6 are plotted the NO_x conversion to N_2 versus *n*-decane conversion to CO_2. Each temperature, in the 450–200 °C range, is defined by a different symbol whatever the sample. This representation can be considered as an indication of the extent of reaction [61], being CO_2 the common reaction product of both NO_x reduction and *n*-decane oxidation reactions.

We can observe two groups of catalysts, the most active and selective catalysts, characterized by the curves with a high slope (high NO_x conversion for relatively low *n*-decane consumption: Ga_2O_3–ZrO_2, Al_2O_3–ZrO_2, and In_2O_3–ZrO_2, ZrO_2 and WO_3/Al_2O_3–ZrO_2), and the less active in the SCR reaction that oxidize the hydrocarbons but do not reduce NO_x (WO_3–ZrO_2, B_2O_3–ZrO_2).

Among the most active and selective catalysts, Ga_2O_3–ZrO_2 shows the best performances in all the range of investigated temperatures. At low temperature (200–250 °C), In_2O_3–ZrO_2 displays the same activity as Ga_2O_3–ZrO_2, but starting from 350 °C its selectivity towards NO_x reduction decreases, and the NO_x to N_2 conversion remains constant at around 22 %.

Temperature is indeed an important factor to understand the catalytic activity in HC–SCR. The NO_x and $C_{10}H_{22}$ conversions started simultaneously around (200–250) °C for all the catalysts, with exception only for the WO_3–ZrO_2 and B_2O_3–ZrO_2 samples that started to convert at higher temperature 300 and 350 °C, respectively.

In terms of shape the curves of Ga_2O_3–ZrO_2, Al_2O_3–ZrO_2, and In_2O_3–ZrO_2 show the same behaviour, with a high slope at low temperatures and a plateau at the maximum NO_x conversion values that are around 40, 32, and 22 % for Ga_2O_3–ZrO_2, Al_2O_3–ZrO_2, and In_2O_3–ZrO_2 respectively. Differently, for the ZrO_2 and WO_3/Al_2O_3–ZrO_2 samples the related curves in Fig. 7 increase continuously reaching the maximum values of 45 and 41 % at 450 °C for ZrO_2 and WO_3/Al_2O_3–ZrO_2 respectively.

At 400 °C all the *n*-decane is oxidized to CO_2 for WO_3–ZrO_2, and a certain activity towards the reduction of NO_x to N_2 only starts at 400 °C. For the B_2O_3–ZrO_2 sample no NO_x reduction has been observed and even a not complete oxidation of *n*-decane was detected (90 % at 450 °C), showing the global inefficiency of this catalyst.

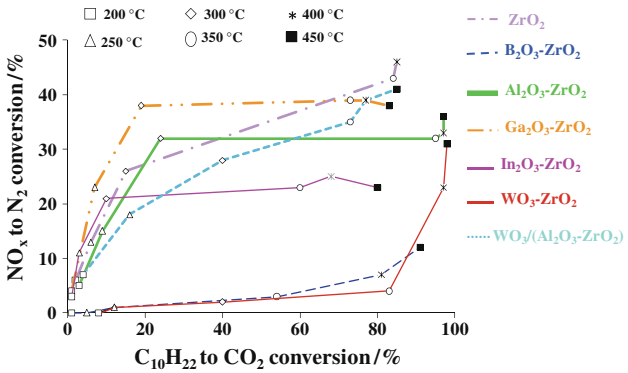

Fig. 6 Conversion of NO_x to N_2 as a function of $C_{10}H_{22}$ conversion in the $C_{10}H_{22}$–SCR reaction over the ZrO_2-based catalysts. Each marker corresponds to different reaction temperatures in the range 200–450 °C interval (reaction conditions: 0.2 g of catalyst, 400 ppm NO, 240 ppm $C_{10}H_{22}$, 9 vol% O_2 in He and 1.5 vol% H_2O)

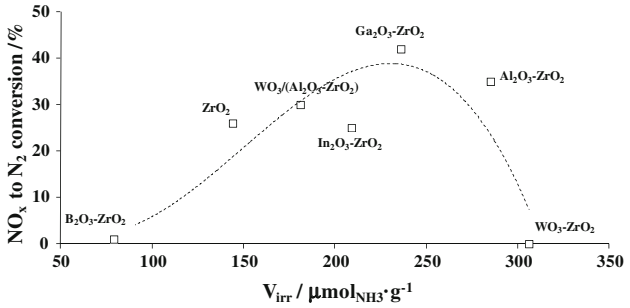

Fig. 7 Conversion of NO_x to N_2 at 300 °C over the different catalysts as a function of the irreversible adsorbed volume of NH_3 (reaction conditions: 0.2 g of catalyst, 400 ppm NO, 240 ppm $C_{10}H_{22}$, 9 vol% O_2 in He and 1.5 vol% H_2O)

Table 3 Summary of the HC–SCR by $C_{10}H_{22}$ at 300 °C over the different catalysts

Sample	300 °C conversion (%)				N_2 selectivity (%)
	n-Decane to CO_2	NO_x to NO_2	NO_x to N_2O	NO_x to N_2	
ZrO_2	15	30	11	26	59
B_2O_3–ZrO_2	12	35	2	1	–
Al_2O_3–ZrO_2	24	20	5	35	91
Ga_2O_3–ZrO_2	19	25	4	42	89
In_2O_3–ZrO_2	10	48	5	25	47
WO_3–ZrO_2	40	0	3	0	–
WO_3/(Al_2O_3–ZrO_2)	40	20	11	30	68

Unfortunately, high *n*-decane consumption does not directly correspond to higher NO_x conversion to N_2 (Table 3). It is true that the catalyst surface extent plays a key role in adsorbing higher quantities of decane, but it does not mean that the adsorbed hydrocarbon is used as reducing agent for the SCR of NO_x, and not directly oxidized to CO_2. On certain kind of catalytic sites (typically the strongest acid sites) the *n*-decane is oxidized to CO_2, as shown on WO_3–ZrO_2. For the same reason, the B_2O_3–ZrO_2 sample that possesses the lower surface area and the lowest acidity (as measured by adsorption microcalorimetry) displays a poor catalytic activity in both NO_x reduction and *n*-decane combustion reactions.

It is clear that the BET surface area is not the only parameter to be considered since the two samples WO_3–ZrO_2 and Al_2O_3–ZrO_2 that show similar BET surface (218 and 181 $m^2\ g^{-1}$, respectively) exhibit very different catalytic behaviours. Surface acidity is here the key property able to justify the catalytic behaviour in the HC–SCR of NO_x.

Figure 7 represents the NO_x to N_2 conversion versus the number of strong and medium acid sites, as given by the irreversible volume of ammonia adsorbed (V_{irr}, see Table 2). The volcano shape curve indicates that the less active samples are B_2O_3–ZrO_2 and WO_3–ZrO_2. As said before B_2O_3–ZrO_2 sample is totally inactive due to a too higher calcinations temperature, while WO_3–ZrO_2 sample possesses a high number of strong acid sites (see Fig. 4) to be efficient except in combustion reaction of decane.

The conversion of *n*-decane to CO_2 at 300 °C (reported in Fig. 8) increases with the irreversible volume of NH_3 adsorbed (corresponding to the acidity of the catalysts). Only WO_3/(Al_2O_3–ZrO_2) does not follow the trend, probably due to its different preparation route (incipient wetness impregnation (see Sect. 2.1): WO_3 seems to cover part of the acid sites of the Al_2O_3–ZrO_2 support thus diminishing the overall acidity of the sample. The most active samples at this temperature are WO_3–ZrO_2 and WO_3/(Al_2O_3–ZrO_2) with a decane conversion of 40 % (see also Table 3).

In particular, we can observe that the presence of a certain amount of acid sites of medium strength ($100 < Q_{diff} < 150$ kJ mol^{-1}) ameliorates the conversion of NO_x to N_2 (see Fig. 4). Even if for the active catalysts, the NO_x conversion to N_2 slightly increases with the number of medium strength acid sites, the only presence of this kind of sites is not sufficient to guaranty an activity in converting NO_x; the WO_3–ZrO_2 sample, that posseses the highest number of medium strength acid sites, in fact, is completely inactive at 300 °C. As shown in Fig. 4, it displays a very high amount of very strong sites on which *n*-decane is fast oxidized to CO_2, not being able to further act as NO_x reducing agent.

The samples Ga_2O_3–ZrO_2 and Al_2O_3–ZrO_2 with moderate acidity are the most selective towards N_2 (Table 3), indicating that a high surface area (allowing the adsorption of the reactants on the catalyst surface), accompanied by the presence of a certain amount of acid sites (to facilitate reactant molecule bonds activation) and by the absence of too strong acid sites (to minimize the hydrocarbon oxidation) is the right balance for a well performing catalyst in the $C_{10}H_{22}$–SCR of NO_x.

This is in agreement with the statement that the SCR of NO_x by decane follows a bi-functional path in which the limiting step is the acid-catalysed reaction at low acidity, and the oxidation on the most acidic catalysts [62, 63]. In this bi-functional mechanism a good activity and selectivity prediction is linked to the number and strength of the acid sites present on the catalyst surface. It has long been accepted that the C–H bond activation of saturated hydrocarbons can be catalyzed by solid acids, and in particular sulphate species sites [64, 65]. Strong acid sites are probably responsible of the low selectivity of WO_3–ZrO_2, since they participate in the C–H bond breaking and consequent oxidation of decane.

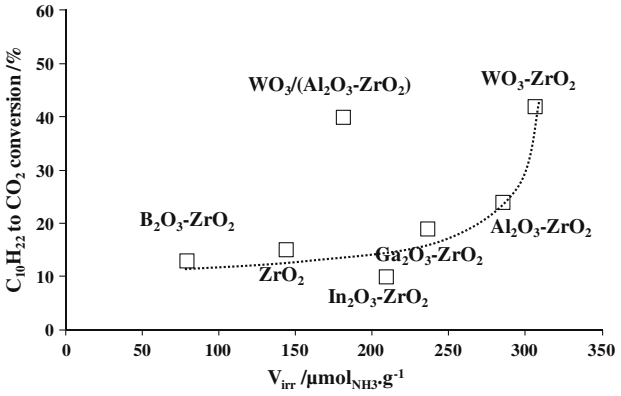

Fig. 8 Conversion of $C_{10}H_{22}$ to CO_2 at 300 °C over the different catalysts as a function of the irreversible adsorbed volume of NH_3 (reaction conditions: 0.2 g of catalyst, 400 ppm NO, 240 ppm $C_{10}H_{22}$, 9 vol% O_2 in He and 1.5 vol% H_2O)

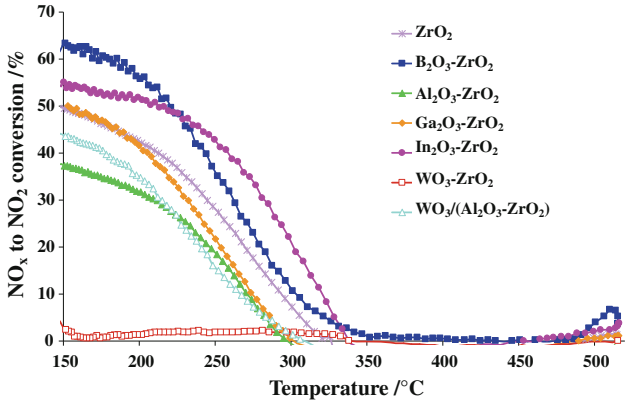

Fig. 9 Conversion of NO_x to NO_2 over the different catalysts as a function of the reaction temperature (reaction conditions: 0.2 g of catalyst, 400 ppm NO, 240 ppm $C_{10}H_{22}$, 9 vol% O_2 in He and 1.5 vol% H_2O)

Samples with moderate acidity showed higher catalytic activity for NO_x reduction to N_2. It seems that samples with strong acidity and high number acid sites lead to carbon deposition on the surface [60]. This deposition poisons the surface active sites responsible of NO_x conversion to N_2. The interest of a moderate acidity is to avoid the carbon deposition and to have a good selectivity to N_2.

Moreover, as seen in Table 2, all the mixed oxides (except B_2O_3–ZrO_2) present also a significant basicity. These base properties have an important role in the mechanism of the selective catalytic reduction of NO_x. The basic sites on the surface have a double role in the complicated mechanism of reduction:

(i) In heterogeneous catalytic oxidation, heterolytic C–H bond cleavage is considered on an acid–base pair through one of the following mechanism: (1) abstraction of a proton on a basic oxygen and formation of a carbanion on the acid metal cation. (2) or abstraction of a hydride ion and formation of a carbocation with the fragmented hydrocarbon. (3) or abstraction of a $H^{\bullet}$ atom and formation of a radical fragment [66].

(ii) The oxidation of NO to NO_2 at the metal oxides, followed by the reaction of NO_2 with an adsorbed hydrocarbon activated by the acid–base pair [67].

Looking at Fig. 9, showing the NO conversion to NO_2 as a function of the temperature, the WO_3–ZrO_2, low activity in HC–SCR can be once again justified. Many authors in fact claim the important role of NO_2 reaction with the hydrocarbon to form a radical and further transformation into HONO, playing the role of activated species [68–70]. On the WO_3–ZrO_2 sample, oxygen is principally used to oxidize the *n*-decane on the strongest acid sites and no presence of NO_2 can be detected at temperature higher than 150 °C.

The presence of WO_3 really seems to decrease the activity of the catalysts in the NO_x transformation to N_2 or NO_2: the addition of WO_3 on the Al_2O_3–ZrO_2 sample in fact results in poorer performances in the reactions involving NO transformation if compared to the bare Al_2O_3–ZrO_2.

For all the other samples the conversion of NO to NO_2 can be observed up to 300–350 °C, the NO_2 production being favoured at low temperatures.

Concerning the NO transformation to N_2O, no differences could be detected among the catalysts and the conversion values were always below 10 % (see Table 3 for the catalytic data at 300 °C).

4 Conclusions

The combination of different surface and structural analyses and catalytic tests has made possible to thoroughly analyze samples that can be potentially applied as acidic catalysts in $C_{10}H_{22}$–SCR. The results obtained in this work give evidence of the importance of the acid nature of active sites. The presence of a given number of acid sites of moderate energy plays a decisive role on the activity and selectivity in the reaction of reduction of nitrogen oxide by *n*-decane performed in lean conditions.

The selective reduction of NO_x by hydrocarbons was studied over different catalytic systems consisting of zirconia mixed oxides with boria, alumina, india, gallia and tungsta. The acidity of the catalysts was increased by adding the second component to zirconia, except with boria. A certain degree of acidity seems to be favourable for NO_x conversion and selectivity towards N_2, while too strong acid sites (as in the case of WO_3–ZrO_2) favour the oxidation of the hydrocarbons that cannot react anymore as reducing agent.

The determination of the number and strength of acid sites has shown to be an interesting tool able to address the choice between different materials towards those potentially active in HC–SCR.

Acknowledgments The authors are thankful to the scientific services of IRCELYON for their valuable help in the characterization of the samples.

References

1. Worch D, Suprun W, Glaser R (2011) Catal Today 176:309
2. Fritz A, Pitchon V (1997) Appl Catal B 13:1
3. Chiron M (1987) Stud Surf Sci Catal 30:1
4. Fischer S, Rusch K, Amon B, Asian (2004) Vehicle emission control conference, Beijing, China, 27–29 April 2004
5. Rodriguez-Fernandez J, Tsolakis A, Ahmadinejad M, Sitshebo S (2010) Energy Fuels 24:992
6. Kim MK, Kim PS, Baik JH, Nam IS, Cho BK, Oh SH (2011) Appl Catal 105:1
7. Holbrook BPM, Baylet A, Retailleau L, Boreave A, Vernoux P, Figueras F, Giroir-Fendler A (2011) Catal Today 176:48
8. Takahashi M, Inoue N, Nakatani T, Takeguchi T, Iwamoto S, Watanabe T, Inoue M (2006) Appl Catal B 65:142
9. Rodrigues A, Da Costa P, Méthivier C, Dzwigaj S (2011) Catal Today 176:72
10. Hibino T, Inoue T, Sano M (2000) J Electrochem Soc 147:3745
11. Li L, Zhang F, Guan N, Richter M, Fricke R (2007) Catal Commun 8:583
12. He C, Köhler K (2011) J Phys Chem C 115:1248
13. Houel V, Millington P, Rajaram R, Tsolakis A (2007) Appl Catal B 73:203
14. Foo R, Cortes Felix N (2009) Platin Met Rev 53:164
15. Ogura M, Kage S, Hayashi M, Matsukata M, Kikuchi E (2000) Appl Catal 27:L213
16. Kintaichi Y, Hamada H, Tabata M, Sasaki M, Ito T (1990) Catal Lett 6:239
17. Delahay G, Coq B, Ensuque E, Figueras F (1996) Catal Lett 39:105
18. Sasaki M, Hamada H, Kintaichi Y, Ito T (1992) Catal Lett 15:297
19. Yang RT, Li WB, Chen N (1998) Appl Catal A 169:215
20. Imagawa H, Tanaka T, Takahashi N, Matsunaga S, Suda A, Shinjoh H (2007) J Catal 251:315
21. Serban M, Halasz I, Datta R (1999) Catal Lett 63:217
22. Haneda M, Kintaichi Y, Hamada H (1999) Catal Today 54:391
23. Park PW, Ragle CS, Boyer CL, Balmer ML, Engelhard M, McCready D (2002) J Catal 210:97
24. Wierzchowski PT, Zatorski L (2003) Appl Catal B 44:53
25. Haneda M, Joubert E, Menezo JC, Duprez D, Barbier J, Bion N, Daturi M, Saussey J, Lavalley JL, Hamada H (2001) Phys Chem Chem Phys 3:1366
26. Petre AL, Perdigon-Melon JA, Gervasini A, Auroux A (2002) Top Catal 19:271
27. Hamada H, Kintaichi Y, Sasaki M, Ito T, Tabata T (1990) Appl Catal 64:L1
28. Maunula T, Kintaichi Y, Haneda M, Hamada H (1999) Catal Lett 61:121
29. Denton P, Giroir-Fendler A, Praliaud H, Primet M (2000) J Catal 189:410
30. Benard S, Retailleau L, Gaillard F, Vernoux P, Giroir-Fendler A (2005) Appl Catal B 55:11
31. Di Gregorio F, Keller V (2004) J Catal 225:45
32. Lopez DE, Suwannakarn K, Bruce DA, Goodwin JG Jr (2007) J Catal 247:43
33. Arata K (1996) Appl Catal A 146:3
34. Kuba S, Concepcion Heydorn P, Grasselli RK, Gates BC, Che M, Knozinger H (2001) Phys Chem Chem Phys 3:146
35. Satsuma A, Shimizu KI, Hattori T, Nishiyama H, Kakimoto S, Sugaya S, Yokoi H (2007) Sens Actuators B 123:757
36. Due-Hansen J, Kustov AL, Rasmussen SB, Fehrmann R, Christensen CH (2006) Appl Catal B 66:161
37. da Cruz JS, Fraga MA, Braun S, Appel LG (2007) Appl Surf Sci 253:3160
38. Wong ST, Li T, Cheng S, Lee JF, Mou CY (2003) J Catal 215:45
39. Galtayries A, Sporken R, Riga J, Blanchard G, Caudano R (1998) J Electron Spectrosc Relat Phenom 88–91:951
40. Wong ST, Hwang CC, Mou CY (2006) Appl Catal B 63:1
41. Valigi M, Gazzoli D, Pettiti I, Mattei G, Colonna S, De Rossi S, Ferraris G (2002) Appl Catal A 231:159
42. Rivière JP, Cahoreau M, Pacaud Y (1993) Thin Solid Films 227:44
43. Yuzhakova T, Rakic V, Guimon C, Auroux A (2007) Chem Mater 19:2970
44. Auroux A, Gervasini A (1990) J Phys Chem 94:6371
45. Gervasini A, Auroux A (1993) J Phys Chem 97:2628
46. Perdigon-Melon JA, Gervasini A, Auroux A (2005) J Catal 234:421
47. Auroux A (1997) Top Catal 4:71
48. Cucinieri Colorio G, Bonnetot B, Védrine JC, Auroux A (1994) Stud Surf Sci Catal 82:143
49. Bennici S, Auroux A (2009) In: Jackson SD, Hargreaves JS (eds) Metal oxide catalysis, vol 1. Wiley-VCH, Weinheim
50. Busco C, Barbaglia A, Broyer M, Bolis V, Foddanu GM, Ugliengo P (2004) Thermochim Acta 418:3
51. Sohn JR, Park MY (1998) Langmuir 14:6140
52. Cortés-Jacome MA, Angeles-Chaves C, Lopez-Salinas E, Navarret J, Toribio P, Toledo JA (2007) Appl Catal A 318:178
53. Busca G (1999) Phys Chem Chem Phys 1:723
54. Macht J, Iglesia E (2008) Phys Chem Chem Phys 10:5331
55. Naito N, Katada N, Niwa M (1999) J Phys Chem B 103:7206
56. Haneda M, Kintaichi Y, Hamada H (1998) Catal Lett 55:47
57. Shimizu KI, Satsuma A, Hattori T (2000) Appl Catal B 25:239
58. Na Aythaya SI, Mongkolsiri N, Praserthdam P, Silveston PL (2003) Appl Catal B 43:1
59. Brosius R, Martens JA (2004) Top Catal 28:119
60. Giroir-Fendler A, Denton P, Boreave A, Praliaud H, Primet M (2001) Top Catal 1–4:237
61. Bennici S, Carniti P, Gervasini A (2004) Catal Lett 98:187
62. Figueras F, Flores JL, Delahay G, Giroir-Fendler A, Bourane A, Clacens JM, Desmartin-Chomel A, Lehaut-Burnouf C (2005) J Catal 232:27
63. Gerlach T, Illgen U, Bartoszek M, Baerns M (1999) Appl Catal B 22:269
64. Burch R, Ottery D (1995) J Mole Catal A 100:13
65. Yao HC, Stepien HK, Gandhi HS (1981) J Catal 67:231
66. Védrine JC (2002) Top Catal 21:97
67. Gaudin C, Duprez D, Mabilon G, Prigent M (1996) J Catal 160:10
68. Kikuchi E, Yogo K (1994) Catal Today 22:73
69. Li Y, Armor JN (1994) J Catal 150:376
70. Bennici S, Gervasini A (2005) Appl Catal B 62:336

Publication VI

Tuning of the acid-base properties of primary Me_2O_3 (Me = Al, Ga, In) and binary (ZrO_2-Me_2O_3) (Me = B, Al, Ga, In) oxides by adding WO_3: a calorimetric study

Reem Kourieh, Simona Bennici, Aline Auroux*

Université Lyon 1, CNRS, UMR 5256, IRCELYON, Institut de recherches sur la catalyse et l'environnement de Lyon, 2 avenue Albert Einstein, F-69626 Villeurbanne, France

* Corresponding author: aline.auroux@ircelyon.univ-lyon1.fr,

Keywords: WO_3 based mixed oxides; microcalorimetry; acidity; basicity

Abstract:

Two series of samples were prepared by impregnation of Me (Me =Al, Ga, In) hydroxides and Zr-Me (Me = B, Al, Ga, In) mixed hydroxides with an ammonium metatungstate hydrate solution followed by calcination at 400 °C. The obtained WO_3/Me_2O_3 and $WO_3/(ZrO_2$-$Me_2O_3)$ samples have been characterized in terms of their structural, textural, and surface properties, including acid and redox features, by a variety of techniques (BET, XRD, TG, TPR) and microcalorimetry. The acid-base properties were estimated by the adsorption of NH_3 and SO_2 as probe molecules, respectively. The prepared mixed oxide catalysts showed very different properties in terms of surface area and X-ray diffractograms. TPR results were strongly dependent on the bonding nature between the oxides. All obtained mixed oxides showed a specific acid-base character influenced by the relative amounts of each oxide, the most acidic samples being WO_3/ZrO_2 and WO_3/Al_2O_3 for binary mixed oxides and $WO_3/(Al_2O_3$-$ZrO_2)$ for ternary oxides.

1. Introduction

In the last few years, a great deal of attention has been given to solids possessing both acid and base properties due to their application as catalysts for various reactions, The role of these properties for catalytic activities and selectivities has been studied extensively [1]. Nowadays, acid-base solid catalysts are considered to be important from the economic and ecological points of view, since they can eliminate the concerns caused by the use, regeneration, transportation and storage of liquid acids and bases. Such is the case of zirconium oxide and the oxides from Group III (Al, Ga, In), which display both sites in similar amounts on their surface and can be called amphoteric. In this study the oxides of group III elements were chosen as guest oxides for tungsten oxide, having in mind their catalytic activities in various important reactions: boria-based catalysts can be effectively used in the selective oxidation of hydrocarbons such as ethane [2] and acidic cracking reactions [3]. Additionally, alumina is widely used as a catalyst in the petroleum industry [4] while gallium- or indium-supported oxides are promising catalysts for combustion reactions and the selective catalytic reduction of NOx by hydrocarbons [5-9]. It was reported in literature that WO_3 supported catalysts, in particular WO_3/ZrO_2, are an alternative material for acid catalyzed reactions requiring strong acidity [10,11]. The aim of this study was to tune the acid-base properties of various single oxide (group III oxides) and zirconia-based mixed oxides (with group III oxides) by adding tungsta on their surface.

The surface properties of a solid catalyst are of primary importance in governing the energetics of the adsorption reaction and desorption steps, which represent the core of a catalytic process. These properties can be conveniently investigated by studying the adsorption of suitably chosen probe molecules on the solid. Adsorption occurs at the interface between a gas phase and a solid. The process is originated by the presence on the surface of coordinately unsaturated species able to interact with molecules from the gas phase, whose concentration at the interface results increased in comparison with that in the bulk gas phase. Microcalorimetry is one of the most reliable methods for studying the gas-solid interactions in order to characterize the acid–base features by adsorbing the corresponding probe molecule [12,13]. The acid–base features can vary with the preparation of the solid, and mixed oxides can display original features, non-linear to the bulk oxides they stem from [14].

In this work, mixed binary and ternary oxides were prepared and their acid–base features were monitored by ammonia and sulphur dioxide adsorption microcalorimetry, repectively. The

total number of acidic and basic sites and their corresponding strengths was assigned in this study. Associated with characterization by XRD and XPS analyses it brought more understanding on the nature of these mixed oxides. Besides, their redox character was determined by TPR and allowed us to determine the bifunctionality of the samples.

2. Experimental

2.1 Catalyst preparation

In this work, pure hydroxides of zirconium, aluminum, gallium and indium were obtained by precipitation. The required quantities of the nitrates of aluminum, gallium, indium: $Al(NO_3)_3 \cdot 9H_2O$ (≥99%, Fluka), $Ga(NO_3)_3 \cdot 5H_2O$ (99.9% Alfa Aesar), $In(NO_3)_3 \cdot 5H_2O$ (99.9%, Aldrich) and zirconium oxychloride $ZrOCl_2 \cdot 8H_2O$ (≥ 99.5%, Sigma-Aldrich) were dissolved in deionized water at room temperature, except in the case of gallium nitrate which was dissolved at 60 °C with stirring. The pH of the solutions was monitored during the addition of concentrated ammonia (32% wt/wt). Ammonia was added gradually dropwise to the precursor solution of with vigorous stirring, until the precipitation was complete (pH 9).

Zirconium hydroxide mixed with $Me(OH)_3$ (Me: B, Al, Ga, In) were prepared by coprecipitation. The required quantities of the group III metal and zirconium hydroxides precursor were dissolved in deionized water at room temperature. The solutions were mixed with a continuous monitoring of pH. Concentrated ammonia (32% wt/wt) was added gradually dropwise to this mixture of two solutions with vigorous stirring, until the precipitation was complete (pH 9). All precipitates (hydroxides) were filtrated, washed with water and dried overnight in an oven at 100 °C.

WO_3/Me_2O_3 and $WO_3/(Me_2O_3–ZrO_2)$ catalysts were prepared by incipient wetness impregnation on the uncalcined $Me(OH)_3$ and $Me(OH)_3$-$Zr(OH)_4$ precursors prepared as reported in the previous paragraph, starting from aqueous solution of ammonium metatungstate. After drying at 100°C for 24 h and calcination at 400 °C, the tungsten oxide loading was of ~ 6 wt.%. The preparation of WO_3/B_2O_3 by impregnation of boron hydroxide with the tungsten precursor could not be achieved, the reason being the low melting point of the boron compound (170.9 °C).

The calcination temperature of 400 °C was chosen on the basis of thermogravimetry (TG) measurements, performed using a Labsys-TG from Setaram. The crude samples (~50 mg) were heated from 25 to 900°C with a heating rate of 5 °C min^{-1} in a flow of air, which was chosen as a soft oxidizing agent for calcination.

2.2. Catalyst characterization

Elemental analysis was performed using inductively coupled plasma optical emission spectroscopy (ICP-OES) with an ACTIVA spectrometer from Horiba Jobin Yvon. The content of W was analysed after the samples were dissolved in H_2SO_4, HNO_3 and HF while the content of B, Al, Ga and In was analysed by dissolving the samples in H_2SO_4 and HNO_3. The solution was evaporated, then NaOH was added.

The surface area was measured by nitrogen adsorption at -196 °C on a Micromeritics 2010 apparatus after pretreatment under vacuum for 2 hours, at 400 °C.

The X-ray diffraction (XRD) measurements were carried out on a Bruker D5005 powder diffractometer scanning from 3° to 80° (2θ) at a rate of 0.02° s^{-1} using a Cu Kα radiation (λ = 0.15418 nm) source. The applied voltage and current were 50 kV and 35 mA, respectively.

The X-ray photoelectron spectra (XPS) were obtained on a KRATOS AXIS Ultra DLD spectrometer equipped with a hemispherical electron analyzer and an Al anode (Al Kα = 1486.6 eV) powered at 150 W, a pass energy of 20 eV, and a hybrid lens mode. The detection area analyzed was 700 μm x 300 μm. Charge neutralization was required for all samples. The peaks were referenced to the C–(C,H) components of the C 1s band at 284.6 eV. Shirley background subtraction and peak fitting to theoretical Gaussian–Lorentzian functions were performed using an XPS processing program (Vision 2.2.6 KRATOS). The residual pressure in the spectrometer chamber was 5 x 10^{-9} mbar during data acquisition.

Raman spectroscopy measurements were performed using a LabRAM HR (Jobin Yvon) spectrometer. The excitation was provided by the 514.5 nm line of an Ar^+ ion laser (Spectra physics) employing a laser power of 100 μW. The laser beam was focused through microscope objective lenses (100x) down to a 1 μm spot on the sample.

Temperature-programmed reduction (TPR) was performed using a TPD/R/O-1100 instrument (ThermoFisher). Prior to the TPR run, the fresh sample was treated in a stream of O_2/He (0.998% v/v, flowing at 20 mL min^{-1}), ramping the temperature from 40 °C to 350 °C, at 10°C $min^{-1,}$ and maintaining it for 60 min. Subsequently, the sample was cooled to RT. The TPR measurement was carried out using H_2/Ar (4.98% v/v) as reducing gas mixture, flowing at 20 mL min^{-1}. The heating rate was 10 °C min^{-1}, the temperature range used was from 40 °C to 1000°C. The masses of investigated samples were varied from 0.050 to 0.065g, in order to have approximately the same amount of WO_3 (in moles) for all the analysed samples.

Adsorption microcalorimetry measurements were performed at 80 °C in a heat flow calorimeter (C80 from Setaram) linked to a conventional volumetric apparatus equipped with a Barocel capacitance manometer for pressure measurements. The probe (ammonia) used for measurements (Air Liquide, purity > 99.9%) was purified by successive freeze–pump–thaw cycles. About 100 mg of sample was pretreated in the calorimetric quartz cell overnight at 400 °C, and then evacuated at the same temperature for 1 hour prior to the measurements. The differential heats of adsorption were measured as a function of coverage by repeatedly introducing small doses of the adsorbate onto the catalyst until an equilibrium pressure of about 66 Pa was reached. The sample was then outgassed for 30 min at the same temperature, and a second adsorption was performed at 80°C until an equilibrium pressure of about 27 Pa was attained in order to calculate the irreversibly chemisorbed amount of the probe molecule at this pressure.

In order to get additional information concerning the acidity of investigated catalysts, another probe was also used. The adsorption-desorption of pyridine was studied using FTIR spectroscopy. The spectra were recorded at room temperature with a Bruker Vector 22 FTIR spectrophotometer (DTGS detector) operating in the 4000-400 cm^{-1} range, with a resolution of 2 cm^{-1} and collecting 100 acquisitions. In each pyridine adsorption FTIR measurement, the self-supporting wafer (about 50 mg, 18 mm diameter) was first activated in situ at 400 °C in the flow of oxygen for 14 h, then evacuated at the same temperature for 2 h, and exposed to pyridine (Air Liquide, 99.8%, vapor pressure 3.3 kPa) subsequently, at room temperature for 5 min. The desorption was carried out by evacuation for 30 min each at room temperature, 100 °C, 200 °C, 300 °C, respectively. The spectra were recorded at room temperature after adsorption and desorption at each temperature. The $WO_3/(B_2O_3\text{-}ZrO_2)$ self-supported wafer was very fragile and did not endure the pretreatment conditions, while the wafers containing indium oxide (WO_3/In_2O_3 and $WO_3/(In_2O_3\text{-}ZrO_2)$) became dark after the pretreatment. Therefore it was difficult to record the spectra corresponding to these three samples.

3. Results and discussion

3.1. Chemical composition, structure and morphology of the samples

Table 1 presents the list of the samples synthesized in this work, their chemical composition, obtained by ICP, and the values of BET surface areas. Solid materials with high

specific surface areas are desirable for most catalytic applications. In general, low-temperature pretreatment processes (calcination at low temperatures) are necessary to obtain oxides with high surface areas, poor crystallinity, and small particle sizes [15].

The values of BET surface areas reveal that they are dependent on the type of group III metal oxide. Highest surface areas (207 and 328 $m^2.g^{-1}$) were observed for alumina-containing mixed oxides $WO_3/(Al_2O_3\text{-}ZrO_2)$ and WO_3/Al_2O_3, respectively. The sample containing boria has the lowest BET surface area, which can be attributed to the miss transformation of boric acid into boron oxide. This step depends on the heating rate during calcination: if the temperature is raised too quickly, the melting of metaborates can take place with the formation of a boron oxide glass of low surface area [16].

The X-ray diffraction patterns of the WO_3/ZrO_2, WO_3/Al_2O_3, WO_3/Ga_2O_3 and WO_3/In_2O_3 mixed oxides are presented in Fig. 1 (a). Diffraction peaks characteristic of tetragonal ZrO_2 (at 2θ =30.17°, 35.31°, 49.79°, and 60°) [17,18] and monoclinic ZrO_2 (at 2θ = 28.3° and 31.6°) [17,19,20] were detected for the WO_3/ZrO_2 sample. The WO_3/Al_2O_3 sample is amorphous, whereas the XRD diagram of WO_3/Ga_2O_3 shows the lines characteristic for α-Ga_2O_3 (2θ = 24.5°, 33.8°, 36.0°, 41.5°, 50.4°, 55.2°, 59.2°, 63.5°and 64.8°) [21,22]. Hence, just one phase was detected for gallia, although it is known that several phases: α-, β-, γ-, δ-, and ε-Ga2O3 can arise, depending upon the treatment conditions [23]. The WO_3/In_2O_3 sample presents very well-developed crystalline phases, the diffraction peaks were identified as characteristic of the cubic structure of In_2O_3 [9]

In Fig. 1 (b) we can see that the $WO_3/(B_2O_3\text{-}ZrO_2)$, $WO_3/(Ga_2O_3\text{-}ZrO_2)$ and $WO_3/(In_2O_3\text{-}ZrO_2)$ samples are poorly crystallized and contain amorphous phases, indicating that the calcination conditions (calcination temperature 400°C in air for 4 h) was well chosen to avoid the formation of the crystalline phases of the mixed oxides. The $WO_3/(Al_2O_3\text{-}ZrO_2)$ sample does not show the diffraction lines of Al_2O_3 or ZrO_2 which confirms that also the ZrO_2–Al_2O_3 phase is amorphous or poorly crystalline even when calcined in presence of WO_3. According to literature data, the lines at 2θ = 22.9°, 23.5°, 24.1°, 33.0°, 33.6° and 34.3° can be assigned to orthorhombic WO_3 phase [24,25,26], while the group of low-intensity lines between 50° and 60° 2θ originates from tetragonal phase of WO_3 [27].

It is well-known that XPS gives information on the catalyst's surface composition and on the distribution and electronic/oxidation state of the elements in the surface layer [28]. In XPS analysis, the peak assignment is critical for correct species identification.

The C 1s peak at 284.6 eV was used as an internal standard for the calibration of binding energies. Table 1 presents the binding energies (BE) for $W_{4f7/2}$, $Zr_{3d5/2}$, B_{1s}, Al_{2p}, $Ga_{2p3/2}$, and

$In_{3d5/2}$. The BE value of the $W_{4f7/2}$ for all samples is close to the reported value for W^{6+} (35.5 eV) in the bulk oxide [29]. The BE values of $Zr_{3d5/2}$ found for investigated catalysts are almost similar and shifted to higher BEs when compared to the BE of Zr^{4+} in bulk zirconia (182.1 eV) [30], which indicates the flow of electron density from zirconia phase into Me_2O_3 phase through Zr-O-Me linkages.

The core-level spectra of B_{1s} (192.2 eV) in the case of $WO_3/(B_2O_3\text{-}ZrO_2)$ ternary oxides showed a shift toward low-binding energies in comparison with the value published for pure B_2O_3 (193.5 eV) [31] indicating possible interaction among the three oxides.

Changes in the BEs of Al_{2p} 74.2 eV [32] were also observed for WO_3/Al_2O_3 and $WO_3/(Al_2O_3\text{-}ZrO_2)$ 74.1eV and 74.6 eV, respectively. The same behaviour for BE values of $In_{3d2/5}$ (444.3 eV) [32] in the two samples WO_3/In_2O_3 and $WO_3/(In_2O_3\text{-}ZrO_2)$ (444.4 eV and 445.0 eV respectively) indicating once again the intimate interaction between the oxides. The changes of BEs of $Ga_{2p3/2}$ 1117.75 eV [33] were observed as well for WO_3/Ga_2O_3 and $WO_3/(Ga_2O_3\text{-}ZrO_2)$.

The reduction behaviour of the catalysts was studied by TPR to locate the reduction features within the temperature range covered by the experiment (25-1000 °C). In the literature, pure WO_3 exhibits three reduction peaks, namely, a shoulder at 540 °C ($WO_3 \rightarrow W_{20}O_{58}$), a sharp peak at 765 °C ($W_{20}O_{58} \rightarrow WO_2$) and a peak at higher temperatures ($WO_2 \rightarrow W$) [34]. Pure ZrO_2, Al_2O_3 and Ga_2O_3 do not show any detectable TPR peak at temperature below 1000 °C. The reduction of bulk indium oxide is achieved completely at relatively low temperature and a single broad peak centered at 755 ◦C, incompletely finished, is obtained [9].

Fig. 2 (a). shows the reduction profiles for the impregnated binary catalysts in the temperature range in which features due to tungsten reduction appear (> 400 °C) for the samples WO_3/ZrO_2, WO_3/Al_2O_3 and WO_3/Ga_2O_3. These features are attributed to the successive reduction of WO_3 to W metallic as mentioned previously. The difference between the TPR profiles of the three samples could be attributed to the way of interaction between the WO_x species and the different supports. The TPR profile of WO_3/In_2O_3 shows two reduction features in the temperature range of 200 – 500 °C and 500 – 1000 °C; these peaks are attributed to the reduction of WO_3 and the particles of In_2O_3 of different sizes, the smallest particles are reduced at low temperature [35].

The reduction profiles for the impregnated ternary catalysts are presented in Fig. 2 (b). As observed for $WO_3/(Al_2O_3\text{-}ZrO_2)$, the reduction peaks attributed to the WO_3 reduction as mentioned previously are well defined; the reason comes from the presence of WO_3

crystallites as confirmed by the XRD analysis which is not the case for the other samples. The reduction peaks of WO_3 and In_2O_3 presented in the profile of $WO_3/(In_2O_3\text{-}ZrO_2)$ are overlapping as for WO_3/In_2O_3.

3.2. Acidic/basic properties

The acid/base properties of the catalysts were determined by ammonia and sulphur dioxide adsorption microcalorimetry. The initial heats of adsorption (denoted by Q_{init}), total and irreversible amounts of sulphur dioxide and ammonia adsorbed under an equilibrium pressure of 27 Pa are presented in Table 2.

According to its adsorption properties towards NH_3 and CO_2 reported in the literature [36], tungsten oxide was classified as an acidic oxide; while zirconia was assigned to the amphoteric group. Alumina is also a typical amphoteric solid which is characterized by the presence of both acidic and basic sites on its surface and presents a broad distribution of sites strength [37]. Indium oxide even if classified as amphoteric can be considered more basic than acidic [9], while boria is considered as an acidic oxide [32]. However, it was observed that many oxides in the amphoteric group adsorbed more NH_3 and with a higher heat than some of those belonging to the acidic group [12].

Fig. 3. (a) and (b) displays the ammonia and sulphur dioxide adsorption isotherms, respectively of the WO_3/Me_2O_3 binary oxides. The initial vertical section present in the collected volumetric adsorption isotherms at very low pressure is assigned to the amount of strongly chemisorbed probe molecule [13] while the more or less horizontal part is assigned to reversible adsorption.

The addition of acidic tungsta on amphoteric supports such as zirconia, alumina, gallia and india created a series of binary mixed oxides with different acid-base properties. The WO_3/ZrO_2 and WO_3/Al_2O_3 samples display a similar behaviour both in acidity and basicity, both catalysts presenting the highest number of acid-base sites. The two samples WO_3/In_2O_3 and WO_3/Ga_2O_3 possess a similar number of acidic sites (see Table 2) lower than the two previous samples, while they show very different basic features. WO_3/In_2O_3 sample is much more basic than WO_3/Ga_2O_3 which means that the acidic WO_3 neutralized most of the surface basic sites of amphoteric gallia.

Fig. 4. (a) and (b) show the adsorption isotherms of NH_3 and SO_2, respectively for the ternary mixed oxides. The order of the acidic properties of these ternary mixed oxides (WO_3

supported on group III oxides mixed with zirconia) is similar to the behaviour of the previous binary mixed oxides, the most acidic being $WO_3/(Al_2O_3\text{-}ZrO_2)$ followed by $WO_3/(Ga_2O_3\text{-}ZrO_2)$ and $WO_3/(In_2O_3\text{-}ZrO_2)$ with an almost similar number of acid sites (see Table 2) and then the less acidic $WO_3/(B_2O_3\text{-}ZrO_2)$ but not so different from the last two samples. The $WO_3/(Al_2O_3\text{-}ZrO_2)$ sample shows also the highest number of basic sites (see Table 2). The addition of zirconia to the sample WO_3/In_2O_3 did not change significantly the basicity of $WO_3/(In_2O_3\text{-}ZrO_2)$, the two samples showing a similar number of basic sites, while the addition of zirconia to WO_3/Ga_2O_3 increased remarkably the basicity of the $WO_3/(In_2O_3\text{-}ZrO_2)$ sample. Finally we can see that $WO_3/(B_2O_3\text{-}ZrO_2)$ shows nearly no basic features.

Comparing figs 3 and 4 show undoubtedly that the acidity and basicity of WO_3/Al_2O_3 are enhanced by the addition of zirconia. The acidic properties of WO_3/Ga_2O_3 and WO_3/In_2O_3 are slightly increased by the presence of zirconia and remain similar while the basic features, weakly enhanced for the india containing sample, are greatly affected for the gallia containing sample which becomes three times more basic than its homologue without zirconia.

Fig. 5 (a) and (b) presents the differential heats of adsorption of NH_3 and SO_2, respectively for the binary mixed oxides and fig. 6 (a) and (b) shows the same data for the ternary oxides. Differential heats of chemisorption usually fall with increasing volume adsorbed, This decrease is usually observed for heterogeneous surfaces [12,38,39]. The differential heats of SO_2 adsorption on the surface of the catalysts show the presence of strong basic sites. Sulphur dioxide can be chemisorbed on basic oxygen anions O^{2-} and on basic hydroxyl groups, such adsorption modes leading to the formation of sulphites and hydrogenosulphites, respectively [40]. At low coverage the differential heats of ammonia adsorption are not markedly different for all samples (fig 5 (a) and fig 6 (a)). Differences are more prominent at higher coverage in particular for WO_3/Me_2O_3 samples. The addition of zirconia (fig 6 (a)) seems to smooth partly the differences. Concerning the differential heats of SO_2 adsorption, the curves are well separated for all $WO_3\text{-}Me_2O_3$ samples in the whole coverage domain, the basicity of WO_3/ZrO_2 being prominent among the others. Besides, the ternary oxides present the occurrence of a plateau around 150 $kJ.mol^{-1}$ and a very weak basicity for the boria containing sample.

Using FTIR, the pyridine adsorption is one of the most applied methods for characterizing the nature of the surface acid sites. The band at (1455-1438) cm^{-1} is characteristic of Lewis acid sites, while the band at around 1540 cm^{-1} can be attributed to Brönsted acid sites [41-43]. The band centred at 1490 cm^{-1} is assigned to the hydrogen bonded pyridine to the catalyst's surface [44].

Fig. 7. presents the IR spectra of pyridine desorption in the 1700-1400 cm^{-1} range on the catalysts, after outgassing at 100 °C. The bands characteristic of pyridine adsorbed on Lewis acid sites at 1444, 1575 and 1609 cm^{-1} are observed for all samples. The position and multiplicity of the band centered at 1609 cm^{-1} of adsorbed pyridine is related to the strength and number of the different types of Lewis acid sites [45]. The doubled signal of this band in WO_3/Al_2O_3 sample indicates the presence of two different types of acidic centers on the alumina support [9]. Only the WO_3/Al_2O_3 sample displayed a broad peak centered around 1540 cm^{-1} which corresponds to pyridinium ions bonded to Brönsted acid sites. The appearance of Brönsted acid sites on the WO_3/Al_2O_3 sample can be related to the presence of dispersed WO_x domains composed of two-dimensional polytungstate species allowing protons to remain accessible at external surfaces [46]. The sample $WO_3/(Al_2O_3\text{-}ZrO_2)$ did not present this kind of Brønsted sites due to the aggregation of the WO_x clusters (source of Brønsted sites) to form WO_3 crystallites, as confirmed by the XRD results (fig. 1.). The formation of WO_3 crystallites is due to the weaker interaction between the W-phase and the $Al_2O_3\text{-}ZrO_2$ mixed oxide acting for this sample as support. The acidity of the catalysts is mainly related to the presence of Lewis sites, and only for WO_3/Al_2O_3 can be attributed also to strong Brønsted surface sites.

4. Conclusion

Coupling WO_x species with ZrO_2 and Me_2O_3 (Me=B, Al, Ga, In) gives rise to improved materials both in terms of surface acidity and structure stability. The ammonia and sulphur dioxide adsorption microcalorimetry confirmed the amphoteric character of the samples except for the boria containing sample, where we can see that the acidic features are more pronounced than the basic features. Pyridine adsorption FT-IR studies have shown that the surface acidity of the catalysts is due to the presence of Lewis acid sites and the appearance of strong Brønsted sites for tungstated alumina sample, which can be associated to the presence of WO_x clusters on the surface.

The combination of various IR, calorimetric and structural analyses has permitted to deeply characterize the binary and ternary oxides.

The addition of acidic WO_3 to the amphoteric group III permitted to obtain samples with enhanced acidity and a large panel of basic properties. The ternary zirconia containing oxides have shown a reinforced acidity, in particular in sites number, compared to their binary

homologues. The basicity is even more affected, showing the appearance of a plateau of heats at around 150 $kJ.mol^{-1}$ and a wide range in the curves. By adding WO_3 to single or mixed oxides it becomes possible to tune the acid-base properties of solids aimed to catalyze a given category of reactions, in particular in the domain of biomass conversion.

Acknowledgments

The authors are thankful to the scientific services of IRCELYON for their valuable help in the characterization of the samples.

Reference

[1] K. Tanabe, W.F. Hölderich, Industrial application of solid acid–base catalysts, Appl. Catal. A 181 (1999) 399–434.

[2] G. Cucinieri Colorio, J.C. Védrine, A. Auroux, B. Bonnetot, Partial oxidation of ethane over alumina-boria catalysts, Appl. Catal. A 137 (1996) 55-68.

[3] S.A. El-Hakam, A.A. Sharkawy, Structural characterization and catalytic properties of aluminum borates–alumina catalysts, Mater. Lett. 36 (1998) 167-173.

[4] A.L. Petre, J.A. Perdigon-Melon, A. Gervasini, A. Auroux, Acid-base properties of alumina-supported M_2O_3 (M=B, Ga, In) catalysts, Top. Catal. 19 (2002) 271-281

[5] T. Ozaki, T. Masui, K.I. Machida, G.Y Adachi, T. Sakata, H. Mori, Redox behavior of surface-modified CeO_2−ZrO2 catalysts by chemical filing process, Chem. Mater. 12 (2000) 643-649.

[6] A. Gervasini, J.A. Perdigon-Melon, C. Guimon, A. Auroux, An in-depth study of supported In_2O_3 catalysts for the selective catalytic reduction of NOx: the influence of the oxide support, J. Phys. Chem. B 110 (2006) 240-249.

[7] G. Postole, A. Gervasini, M. Caldararu, B. Bonnetot, A. Auroux, Is BN an appropriate support for metal oxide catalysts?, Appl. Catal. A 325 (2007) 227-236.

[8] Md.H. Zahir, S. Katayama, M. Awano, Synthesis and de-NO_X properties of ZnO-Ga_2O_3-Al_2O_3 spinel, Mater. Chem. Phys. 86 (2004) 99-104.

[9] J.A. Perdigon-Melon, A. Gervasini, A. Auroux, Study of the influence of the In_2O_3 loading on γ-alumina for the development of de-NO_x catalysts, J. Catal. 234 (2005) 421-430.

[10] M. Hino, M. Kurashige, H. Matsuhashi, K. Arata, The surface structure of sulfated zirconia: studies of XPS and thermal analysis, Thermochim. Acta.. 441 (2006) 35-41.

[11] S. Triwahyono, T. Yamada, H. Hattori, IR study of acid sites on WO_3-ZrO_2, Appl. Catal. A 250 (2003) 75-81.

[12] A. Auroux, Acidity characterization by microcalorimetry and relationship with reactivity, Top. Catal. 4 (1997) 71-89.

[13] L. Damjanovic, A. Auroux, Thermal analysis and calorimetric methods, In: M.E. Brown, P.K. Gallagher (Eds.), Handbook of thermal analysis and calorimetry, Vol. 5, Elsevier: Amestrdam, 2008, pp. 387-438

[14] A. Mekki-Berrada, D. Grondin, S. Bennici, A. Auroux, Design of amphoteric mixed oxides of zinc and Group 3 elements (Al, Ga, In): migration effects on basic features, Phys. Chem. Chem. Phys. 14 (2012) 4155-4161.

[15] H.H. Kung, Preparation of oxides, In Studies in Surface Science Catalysis: Transition Metal Oxides: Surface Chemistry and Catalysis, Vol. 45 Elsevier: Amsterdam, 1989, p 121-135.

[16] G. Cucinieri Colorio, B. Bonnetot, J.C. Védrine, A. Auroux, Characteristics of alumina boria catalysts used in ethane partial oxidation, Stud. Surf. Sci Catal. 82 (1994) 143-149.

[17] F. Di Gregorio, V. Keller, Activation and isomerization of hydrocarbons over WO_3/ZrO_2 catalysts: I. Preparation, characterization, and X-ray photoelectron spectroscopy studies, J. Catal. 225 (2004) 45-55.

[18] D.E. Lopez, K. Suwannakarn, D.A. Bruce, J.G. Goodwin Jr., Esterification and transesterification on tungstated zirconia: Effect of calcination temperature**,** J. Catal. 247 (2007) 43-50.

[19] K. Arata, Preparation of superacids by metal oxides for reactions of butanes and pentanes, Appl. Catal. A 146 (1996) 3-32.

[20] S. Kuba, P. Concepcion Heydorn, R.K. Grasselli, B.C. Gates, M. Che, H. Knozinger, Redox properties of tungstated zirconia catalysts: Relevance to the activation of n-alkanes, Phys. Chem. Chem. Phys. 3 (2001) 146-154.

[21] E. Gebauer-Henke, J. Farbotko, R. Touroude, J. Rynkowski, A comparative study of Ir/Ga_2O_3, Pt/Ga_2O_3, and Ru/Ga_2O_3 catalysts in selective hydrogenation of crotonaldehyde, Kinet. Catal. 49 (2008) 574-580.

[22] M. Haneda, Y. Kintaichi, T. Mizushima, N. Kakuta, H. Hamada, Structure of Ga_2O_3-Al_2O_3 prepared by sol–gel method and its catalytic performance for NO reduction by propene in the presence of oxygen, Appl. Catal. B 31 (2001) 81–92.

[23] R. Roy, V.G. Hill, E.F. Osborn, Polymorphism of Ga_2O_3 and the system Ga_2O_3-H_2O, J. Am. Chem. Soc. 74 (1952) 719-722.

[24] A. Satsuma, K.I. Shimizu, T. Hattori, H. Nishiyama, S. Kakimoto, S. Sugaya, H. Yokoi, Polytungstate clusters on zirconia as a sensing material for a selective ammonia gas sensor, Sensor. Actuator. B 123 (2007) 757–762.

[25] J. Due-Hansen, A.L. Kustov, S.B. Rasmussen, R. Fehrmann, C.H. Christensen, Tungstated zirconia as promising carrier for $DeNO_X$ catalysts with improved resistance towards alkali poisoning, Appl. Catal. B 66 (2006) 161–167.

[26] J.S. da Cruz, M.A. Fraga, S. Braun, L.G. Appel, Thermal spreading of WO_3 onto zirconia support, Appl. Surf. Sci. 253 (2007) 3160–3167.

[27] S.T. Wong, T. Li, S. Cheng, J.F. Lee, C.Y. Mou, Aluminum-promoted tungstated zirconia catalyst in *n*-butane isomerization reaction, J. Catal. 215 (2003) 45–56.

[28] A. Galtayries, R. Sporken, J. Riga, G. Blanchard, R. Caudano, XPS comparative study of ceria/zirconia mixed oxides: powders and thin film characterisation, J. Electron. Spectrosc. 88–91 (1998) 951-956.

[29] M. Valigi, D. Gazzoli, I. Pettiti, G. Mattei, S. Colonna, S. De Rossi, G. Ferraris, WO_x/ZrO_2 catalysts: part 1. preparation, bulk and surface characterization, Appl. Catal. A 231 (2002) 159-172.

[30] S.T. Wong, C.C. Hwang, C.Y. Mou, Tungstated zirconia catalyzed bromination of phenol red under nearly neutral solution, Appl. Catal. B 63 (2006) 1-8.

[31] J.P. Rivière, M. Cahoreau, Y. Pacaud, Spectroscopic studies of BN films deposited by dynamic ion mixing,Thin. Solid. Films. 227 (1993) 44-53.

[32] T. Yuzhakova, V. Rakic, C. Guimon, A. Auroux, Preparation and characterization of Me_2O_3−CeO_2 (Me = B, Al, Ga, In) mixed-oxide catalysts, Chem. Mater. 19 (2007) 2970-2981.

[33] S.C. Ghosh, M.C. Biesinger, R.R. LaPierre, P. Kruse, X-ray photoelectron spectroscopic study of the formation of catalytic gold nanoparticles on ultraviolet-ozone oxidized GaAs (100) substrates, J. Appl. Phys. 101 (2007) 114322-114322-8.

[34] D.C. Vermaire, P.C. Van Berge, The preparation of WO_3/TiO_2 and WO_3/Al_2O_3 and characterization by temperature-programmed reduction, J. Catal. 116 (1989) 309-317.

[35] P.W. Park, C.S. Ragle, C.L. Boyer, M.L. Balmer, M. Engelhard, D. McCready, In_2O_3/Al_2O_3 catalysts for NO*x* reduction in lean condition, J. Catal. 210 (2002) 97-105.

[36] A. Auroux, A. Gervasini, Microcalorimetric study of the acidity and basicity of metal oxide surfaces, J. Phys. Chem. 94 (1990) 6371-6379.

[37] A. Gervasini, A. Auroux, Thermodynamics of adsorbed molecules for a new acid-base topchemistry of alumina, J. Phys. Chem. 97 (1993) 2628-2639.

[38] S. Bennici, A. Auroux, Thermal analysis and calorimetric methods, in: S.D. Jackson, S.J. Hargreaves (Eds.), Metal oxide catalysis, Vol. 1, Wiley-VCH: Weinheim, 2009, pp. 391-442.

[39] C. Busco, A. Barbaglia, M. Broyer, V. Bolis, G.M. Foddanu, P. Ugliengo, Characterisation of Lewis and Brønsted acidic sites in H-MFI and H-BEA zeolites: a thermodynamic and ab initio study, Thermochim. Acta. 418 (2004) 3-9

[40] C. Guimon, A. Gervasini, A. Auroux, XPS study of the adsorption of SO_2 and NH_3 over supported tin dioxide catalysts used in de-NOx catalytic reaction, J. Phys. Chem. B 105 (2001) 10316-10325.

[41] J.R. Sohn, M.Y. Park, Characterization of zirconia-supported tungsten oxide catalyst, Langmuir 14 (1998) 6140-6145.

[42] M.A. Cortés-Jacome, C. Angeles-Chaves, E. Lopez-Salinas, J. Navarret, P. Toribio, J.A. Toledo, Migration and oxidation of tungsten species at the origin of acidity and catalytic activity on WO_3-ZrO_2 catalysts, Appl. Catal. A 318 (2007) 178-189.

[43] G. Busca, The surface acidity of solid oxides and its characterization by IR spectroscopic methods. An attempt at systematization, Phys. Chem. Chem. Phys. 1 (1999) 723-736.

[44] S.R.G. Carrazàn, C. Martin, G. Solana, V. Rives, A FT-IR study of the reactivity of tungsta-supported catalysts toward Butan-2-ol, Langmuir, 17 (2001) 6968-6973.

[45] M. Haneda, E. Joubert, J.C. Menezo, D. Duprez, J. Barbier, N. Bion, M. Daturi, J. Saussey, J.L. Lavalley, H. Hamada, Surface characterization of alumina-supported catalysts prepared by sol–gel method. Part I. Acid–base properties, Phys. Chem. Chem. Phys. 3 (2001) 1366-1370.

[46] J. Macht, E. Iglesia, Structure and function of oxide nanostructures: catalytic consequences of size and composition, Phys. Chem. Chem. Phys. 10 (2008) 5331-5343.

Table 1. Physiochemical characterstic of the catalysts calcined at 400 °C.

Sample calcined at 400 °C	**BET surface area $m^2.g^{-1}$**	**C.A (wt.%)**		**Binding Energy /eV**		
		WO_3		**W $4f_{7/2}$**	**Zr $3d_{5/2}$**	
WO_3/ZrO_2	158	4.3	-	35.5	182.3	
WO_3/Al_2O_3	328	6.8	-	35.7	-	**Al 2p:** 74.1
WO_3/Ga_2O_3	101	7.7	-	36.0	-	**Ga $2p_{3/2}$:** 1118.3
WO_3/In_2O_3	103	9.3	-	35.4	-	**In $3d_{5/2}$:** 444.4
$WO_3/(B_2O_3\text{-}ZrO_2)$	99	6.5	30.2 % (B_2O_3)	35.9	182.7	**B 1s :** 192.2
$WO_3/(Al_2O_3\text{-}ZrO_2)$	207	4.8	34.8 % (Al_2O_3)	36.1	182.9	**Al 2p:** 74.6
$WO_3/(Ga_2O_3\text{-}ZrO_2)$	129	5.9	21.3 % (Ga_2O_3)	35.8	182.5	**Ga $2p_{3/2}$:** 1118.0
$WO_3/(In_2O_3\text{-}ZrO_2)$	95	6.1	27.0 % (In_2O_3)	35.6	182.3	**In $3d_{5/2}$:** 445.0

Table 2. The initial heats of adsorption (denoted by Q_{init}), total and irreversible amount of ammonia and sulphur dioxide adsorbed under an equilibrium pressure of 27 Pa

Sample	Basicity			Acidity		
	Q_{init}[a] / kJ.mol^{-1}	V_{tot}[b] / µmol$_{SO2}$.g^{-1}	V_{irr}[c] / µmol$_{SO2}$.g^{-1}	Q_{init}[a] / kJ.mol^{-1}	V_{tot}[b] / µmol$_{NH3}$.g^{-1}	V_{irr}[c] / µmol$_{NH3}$.g^{-1}
WO_3/ZrO_2	208	328	296	158	425	264
WO_3/Al_2O_3	166	329	261	213	389	181
WO_3/Ga_2O_3	172	83	58	152	274	175
WO_3/In_2O_3	183	230	188	172	273	172
$WO_3/(B_2O_3\text{-}ZrO_2)$	168	72	47	164	324	198
$WO_3/(Al_2O_3\text{-}ZrO_2)$	201	416	378	177	532	342
$WO_3/(Ga_2O_3\text{-}ZrO_2)$	193	353	308	197	353	214
$WO_3/(In_2O_3\text{-}ZrO_2)$	158	247	75	171	361	235

[a] Heat evolved from the first dose of SO_2 and NH_3
[b] Total amount of SO_2 and NH_3 retained as determined at 27 Pa of equilibrium pressure.
[c] Irreversibly adsorbed amount of SO_2 and NH_3 as determined from the difference between the amounts adsorbed in the first and second adsorptions at 27 Pa.

Figure Captions

- Fig. 1 (a) and (b). XRD diagrams of the catalysts calcined at 400 °C.
- Fig. 2 (a) and (b). TPR profiles of the samples calcined at 400 °C and pretreated for 1 h at 350 °C under flow of oxygen (5 % in He)
- Fig. 3 (a) and (b). Isotherms obtained from NH_3 and SO_2 adsorption microcalorimetry experiments carried out at 80 °C on the binary mixed oxides.
- Fig. 4 (a) and (b). Isotherms obtained from NH_3 and SO_2 adsorption microcalorimetry experiments carried out at 80 °C on the ternary mixed oxides.
- Fig. 5 (a) and (b). Differential heats of NH_3 and SO_2 adsorption versus coverage (NH_3 and SO_2 uptake in $\mu mol.g^{-1}$) for the binary mixed oxides.
- Fig. 6 (a) and (b). Differential heats of NH_3 and SO_2 adsorption versus coverage (NH_3 and SO_2 uptake in $\mu mol.g^{-1}$) for the ternary mixed oxides.
- Fig. 7. FTIR spectra of pyridine after adsorption at room temperature and evacuation at 100 °C.

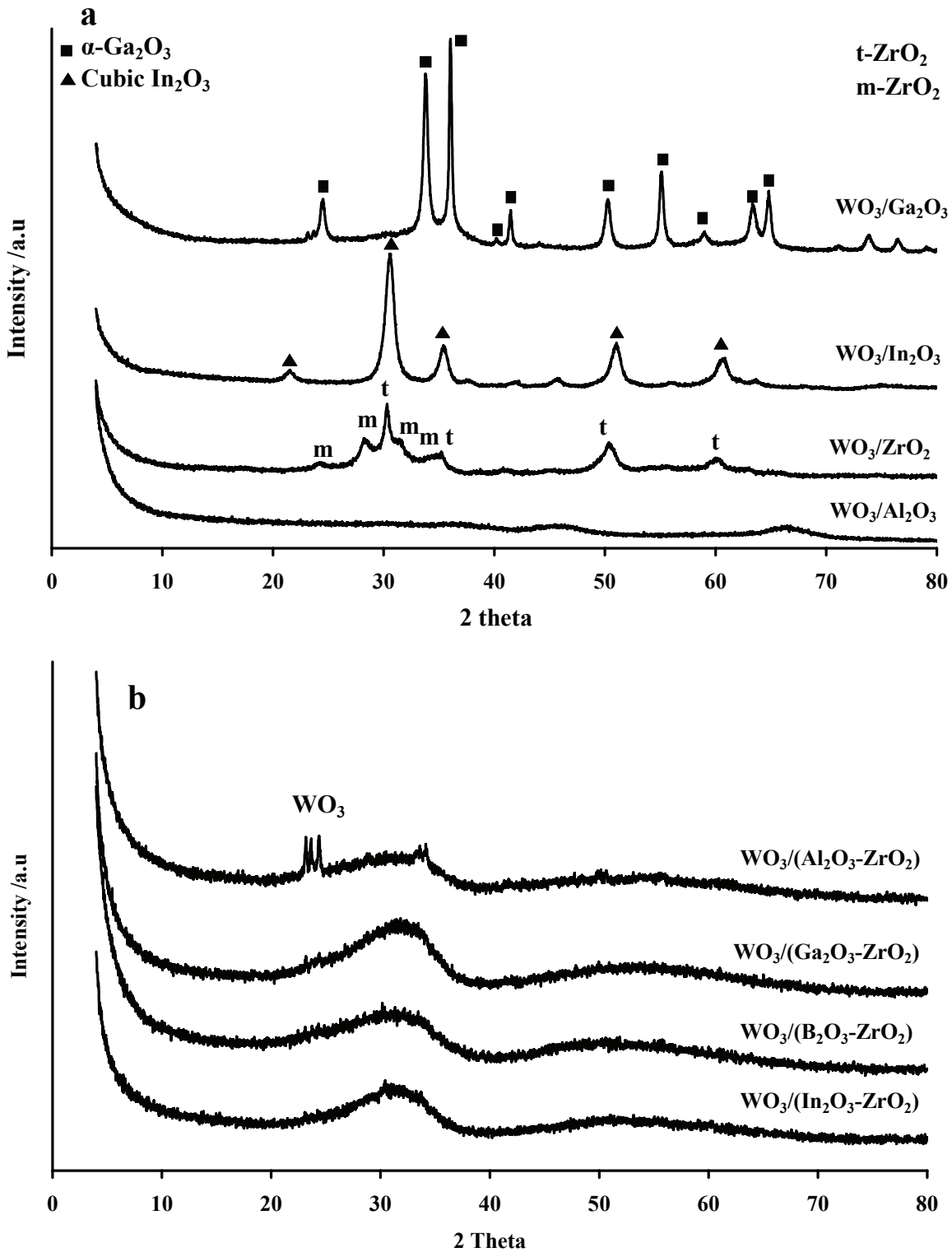
a
■ α-Ga2O3
▲ Cubic In2O3
t-ZrO2
m-ZrO2
WO3/Ga2O3
WO3/In2O3
WO3/ZrO2
WO3/Al2O3
m
m
t
m
m
t
t
t
Intensity /a.u
0
10
20
30
40
50
60
70
80
2 theta
b
WO3
WO3/(Al2O3-ZrO2)
WO3/(Ga2O3-ZrO2)
WO3/(B2O3-ZrO2)
WO3/(In2O3-ZrO2)
Intensity /a.u
0
10
20
30
40
50
60
70
80
2 Theta

Fig. 1.

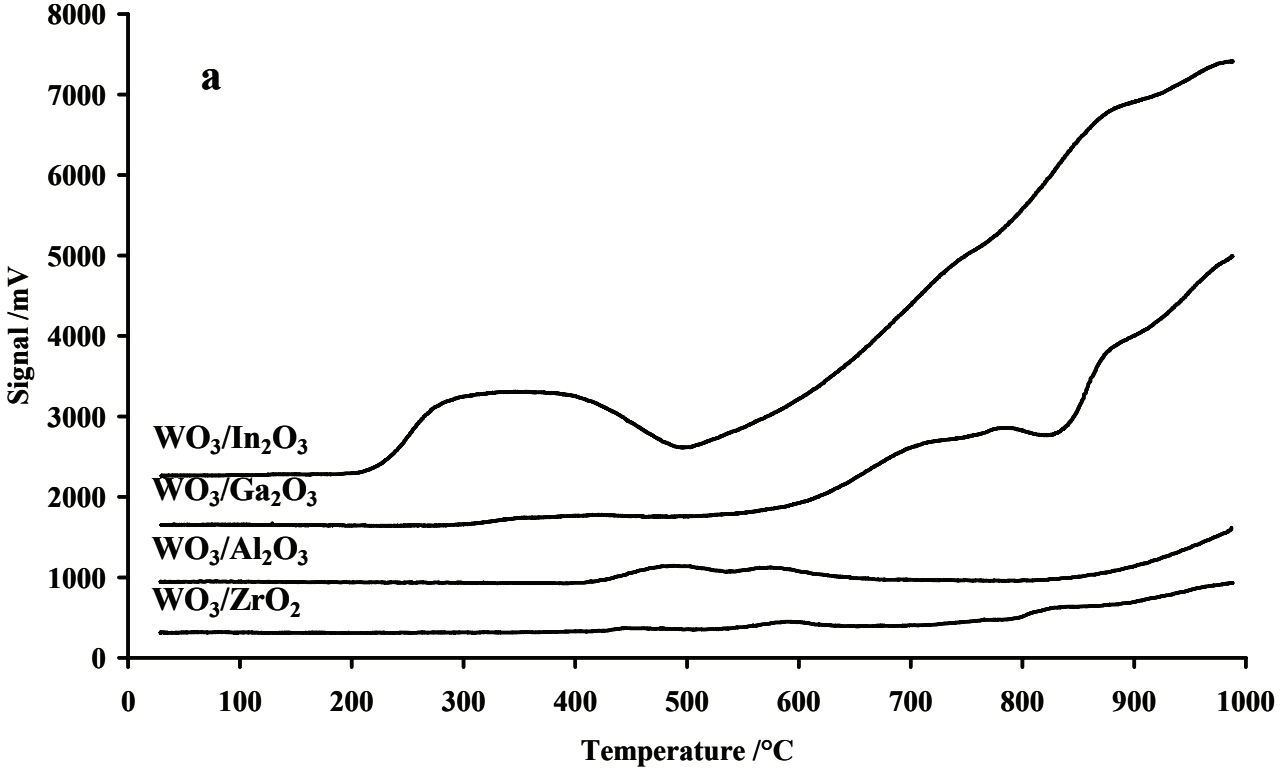
a
Signal /mV
Temperature /°C
WO3/In2O3
WO3/Ga2O3
WO3/Al2O3
WO3/ZrO2
0
1000
2000
3000
4000
5000
6000
7000
8000
0
100
200
300
400
500
600
700
800
900
1000

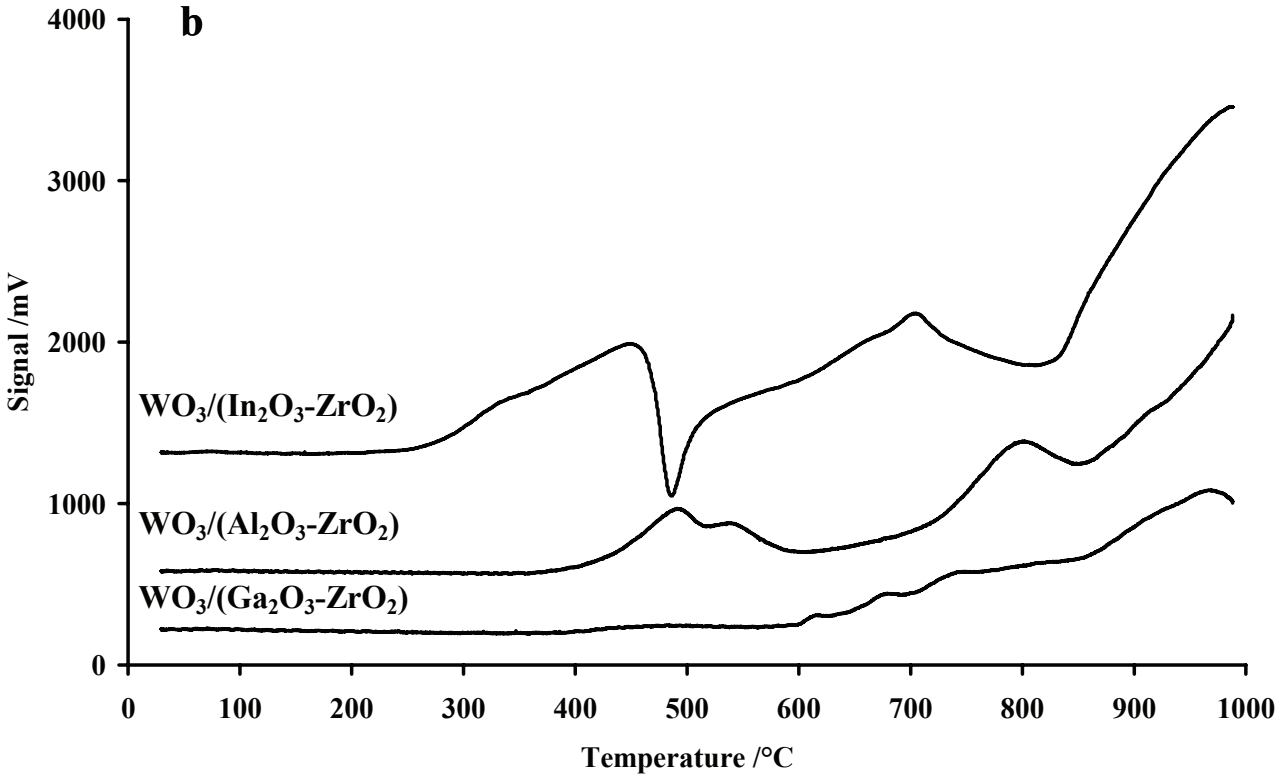
b
Signal /mV
Temperature /°C
WO3/(In2O3-ZrO2)
WO3/(Al2O3-ZrO2)
WO3/(Ga2O3-ZrO2)
0
1000
2000
3000
4000
0
100
200
300
400
500
600
700
800
900
1000

Fig. 2.

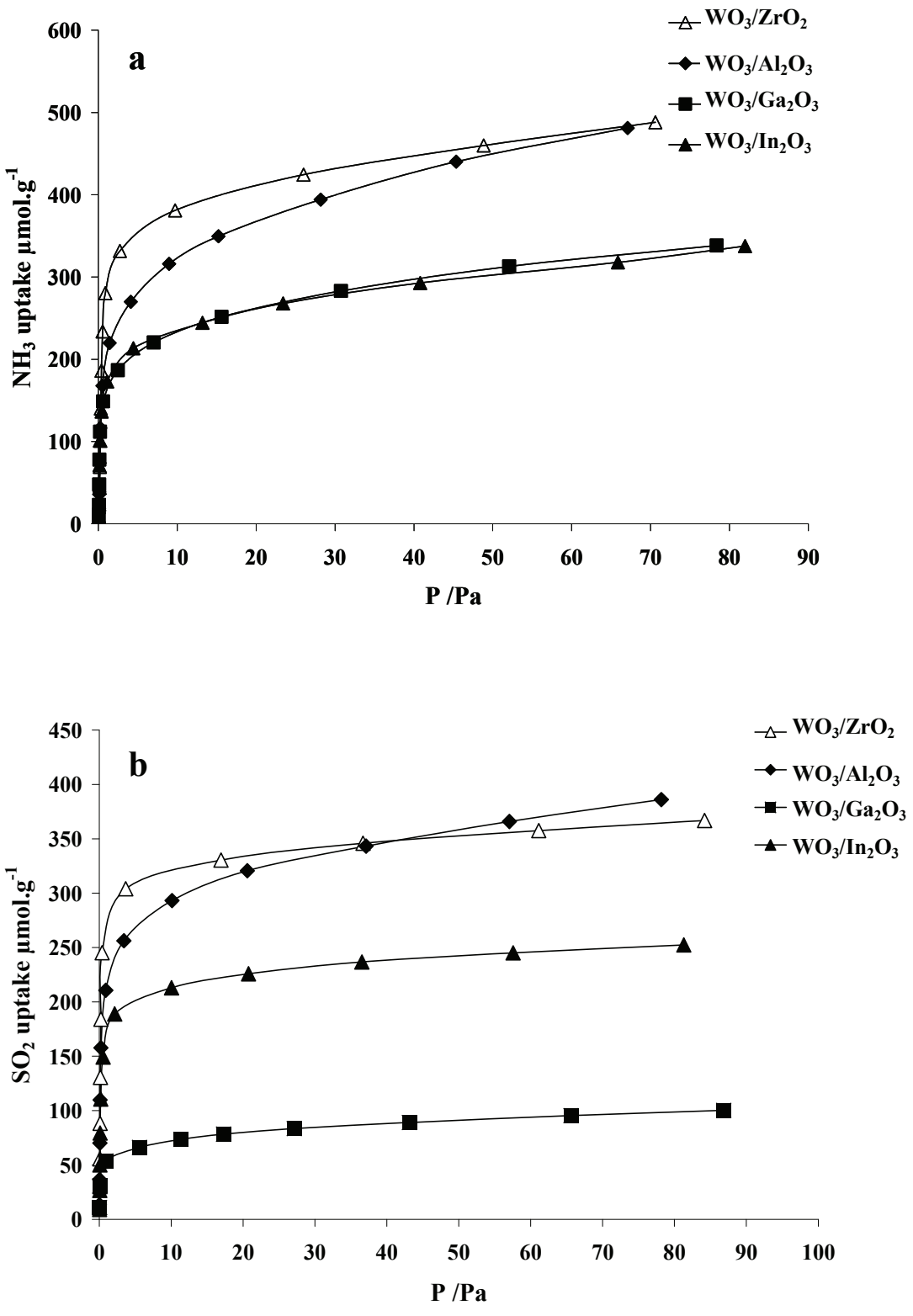
a
WO3/ZrO2
WO3/Al2O3
WO3/Ga2O3
WO3/In2O3
NH3 uptake µmol.g-1
P /Pa
b
WO3/ZrO2
WO3/Al2O3
WO3/Ga2O3
WO3/In2O3
SO2 uptake µmol.g-1
P /Pa

Fig. 3.

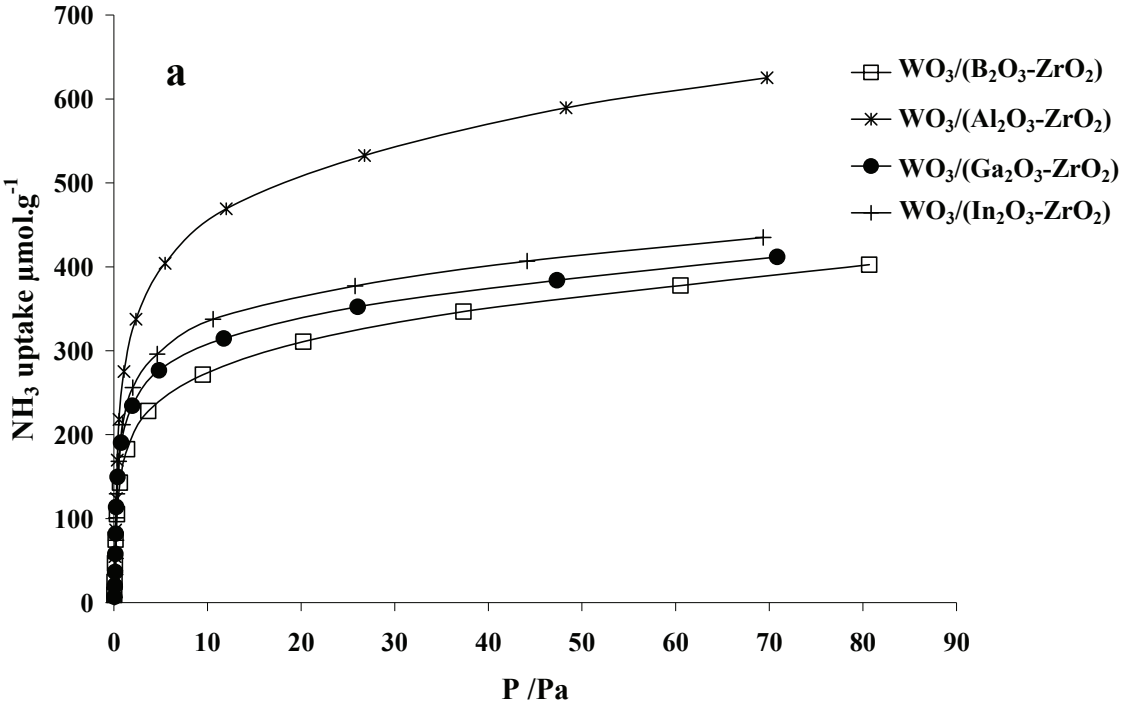
a
NH3 uptake µmol.g-1
P /Pa
WO3/(B2O3-ZrO2)
WO3/(Al2O3-ZrO2)
WO3/(Ga2O3-ZrO2)
WO3/(In2O3-ZrO2)

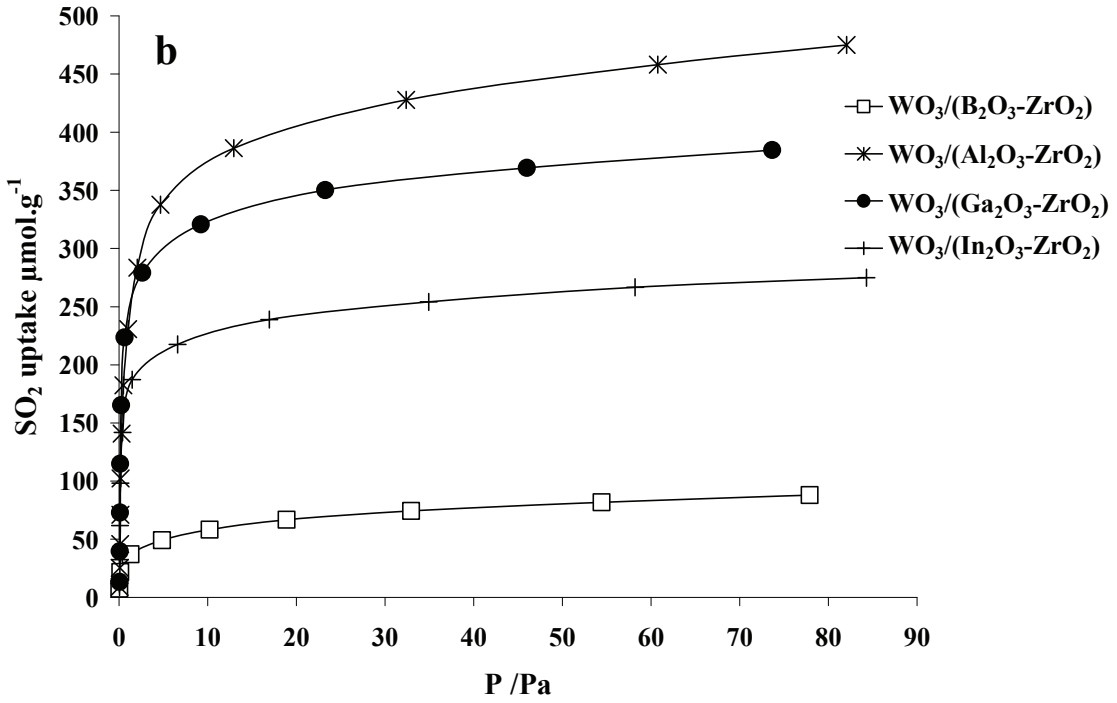
b
SO2 uptake µmol.g-1
P /Pa
WO3/(B2O3-ZrO2)
WO3/(Al2O3-ZrO2)
WO3/(Ga2O3-ZrO2)
WO3/(In2O3-ZrO2)

Fig. 4.

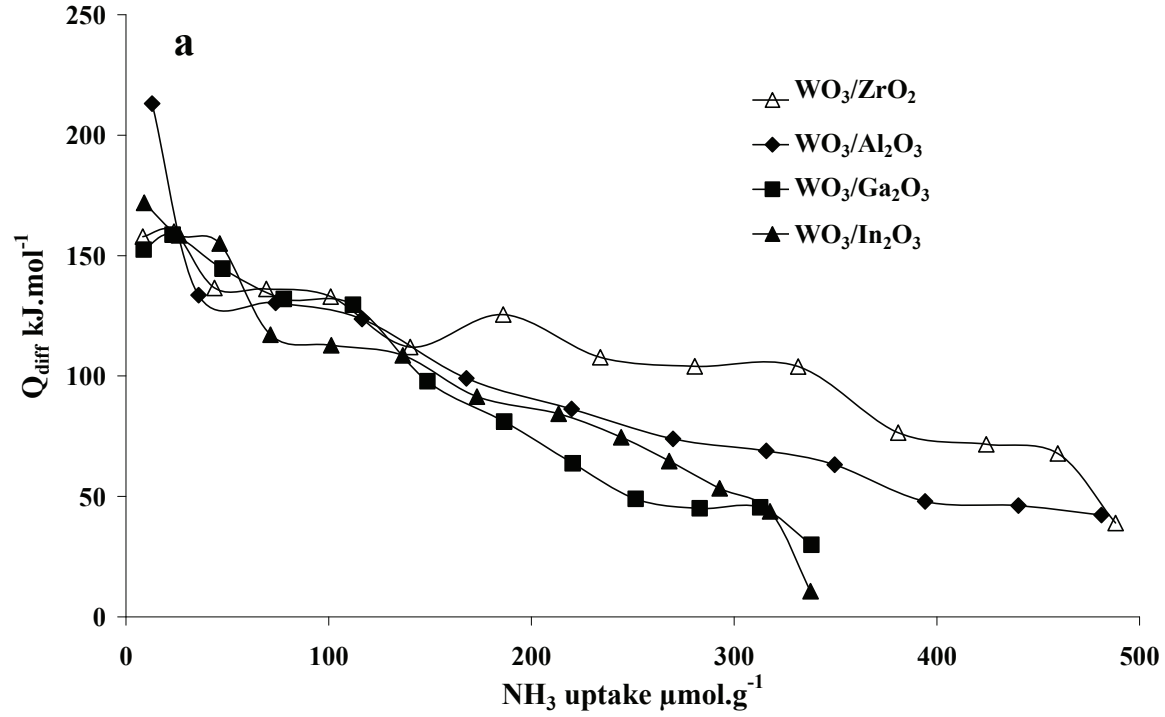
a
WO3/ZrO2
WO3/Al2O3
WO3/Ga2O3
WO3/In2O3
Qdiff kJ.mol-1
NH3 uptake µmol.g-1
0
50
100
150
200
250
0
100
200
300
400
500

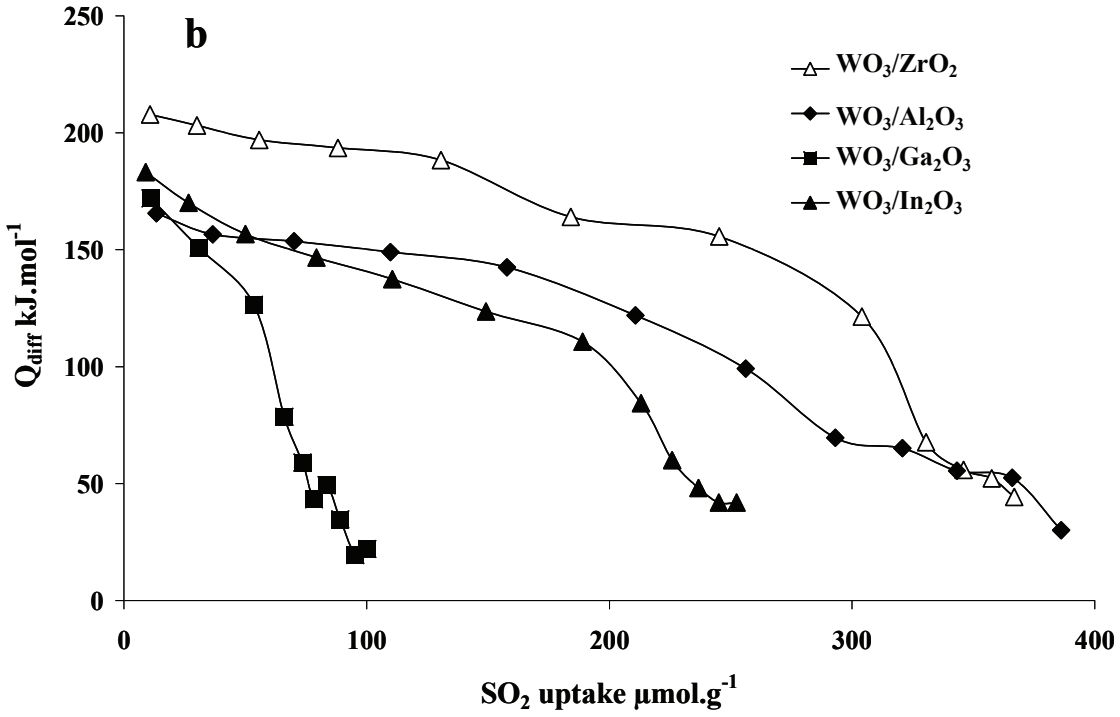
b
WO3/ZrO2
WO3/Al2O3
WO3/Ga2O3
WO3/In2O3
Qdiff kJ.mol-1
SO2 uptake µmol.g-1
0
50
100
150
200
250
0
100
200
300
400

Fig. 5.

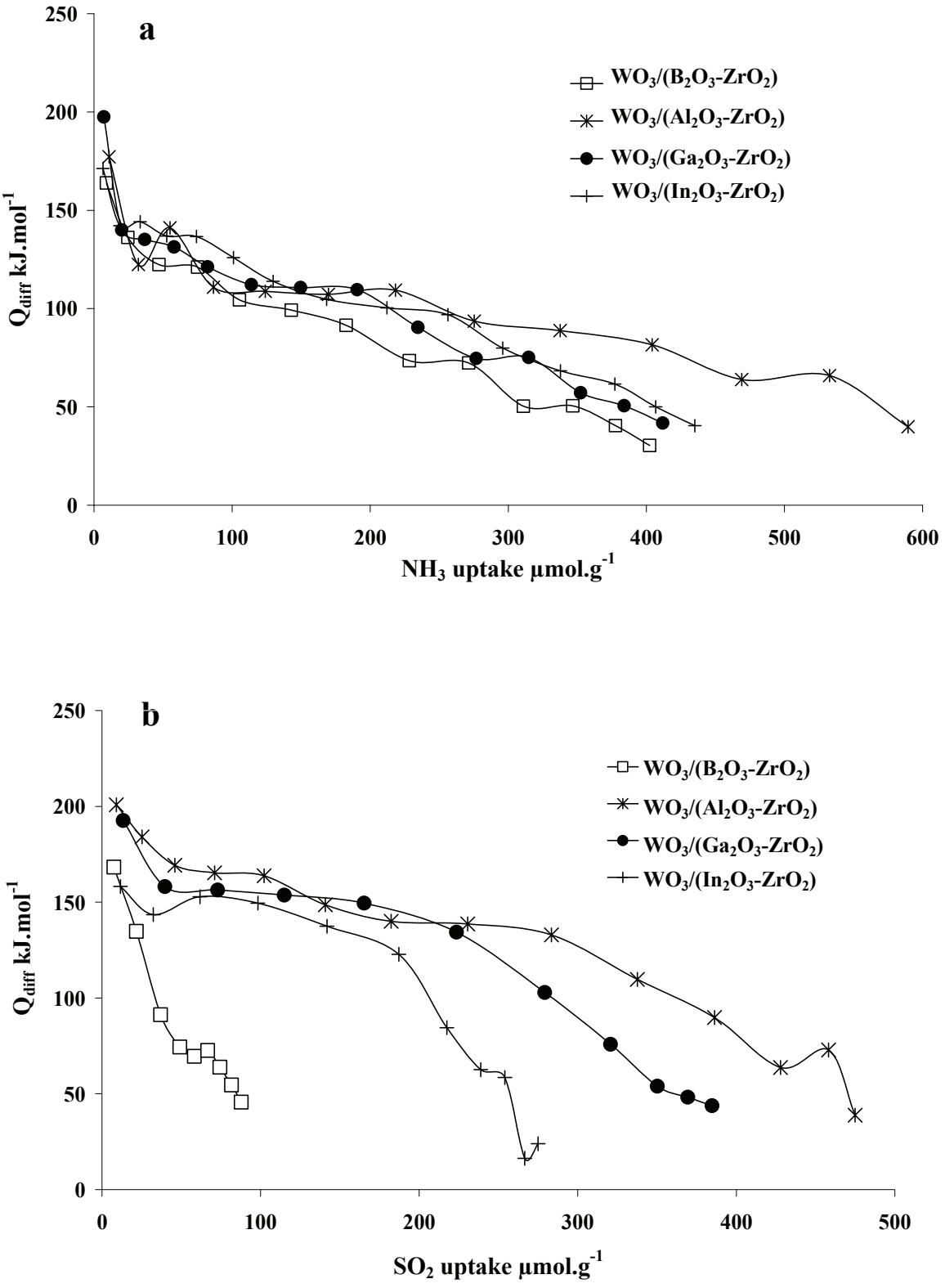
a
$WO_3/(B_2O_3-ZrO_2)$
$WO_3/(Al_2O_3-ZrO_2)$
$WO_3/(Ga_2O_3-ZrO_2)$
$WO_3/(In_2O_3-ZrO_2)$
Q_{diff} kJ.mol^{-1}
NH_3 uptake µmol.g^{-1}
0
50
100
150
200
250
0
100
200
300
400
500
600
b
$WO_3/(B_2O_3-ZrO_2)$
$WO_3/(Al_2O_3-ZrO_2)$
$WO_3/(Ga_2O_3-ZrO_2)$
$WO_3/(In_2O_3-ZrO_2)$
Q_{diff} kJ.mol^{-1}
SO_2 uptake µmol.g^{-1}
0
50
100
150
200
250
0
100
200
300
400
500

Fig. 6.

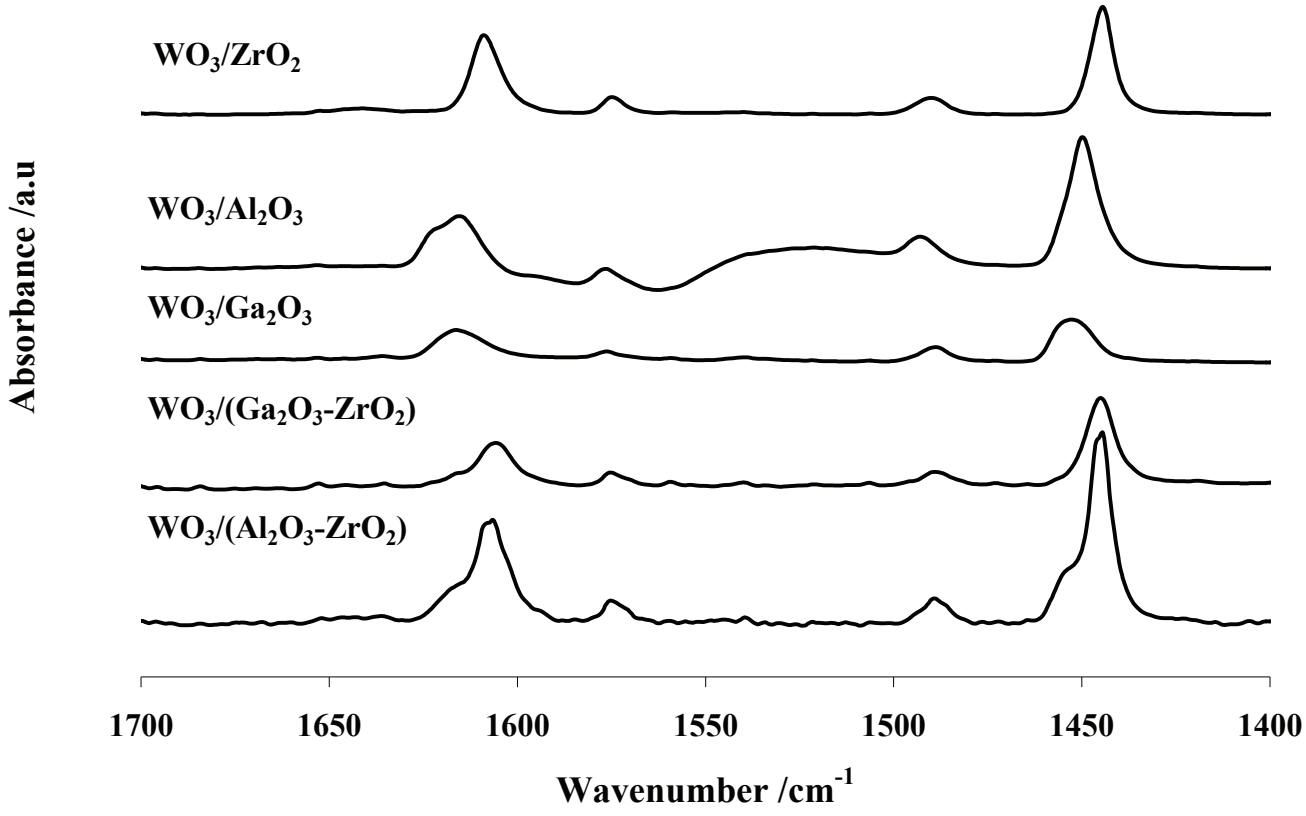
WO3/ZrO2
WO3/Al2O3
WO3/Ga2O3
WO3/(Ga2O3-ZrO2)
WO3/(Al2O3-ZrO2)
Absorbance /a.u
1700
1650
1600
1550
1500
1450
1400
Wavenumber /cm-1

Fig. 7.

Conclusions

5. Conclusions

This work is related to the application of three main principles of Green chemistry: the role of catalysts, the conversion of renewable raw materials (mainly carbohydrates) and the decrease of hazardous and toxic materials (selective catalytic reduction of NO_x by hydrocarbons).

In this work, four commercial tungstated zirconia provided by Mel-Chemicals, two series of tungstated zirconia catalysts prepared by two different methods within the range of (1-20) WO_3 wt.% loading; binary zirconia-based oxides (WO_3-ZrO_2, B_2O_3-ZrO_2, Al_2O_3-ZrO_2, Ga_2O_3-ZrO_2 and In_2O_3-ZrO_2.); binary oxides WO_3-Me_2O_3 (Me = Al, Ga and In) and ternary oxides WO_3/(Me_2O_3-ZrO_2) (Me = B, Al, Ga and In) were prepared, characterized and evaluated as catalysts in various catalytic tests. The catalysts were thoroughly characterized in terms of their acidic and redox properties in order to find correlations between the identified active sites and the catalytic properties. The structural and surface characteristics of all investigated systems have been acquired by means of XRD, BET, chemical analysis, XPS, Raman and FTIR. The acidity was characterized by ammonia adsorption microcalorimetry, adsorption-desorption of pyridine studied by FTIR, while reducibility and redox properties in general were achieved by TPR/TPO measurements.

The following is a summary of the general conclusions:

It has been proved by the results obtained in this work that the acidic properties of the prepared catalysts play a key role in the three catalytic tests chosen here (cellobiose hydrolysis, fructose dehydration and HC-SCR by n-decane). In general, we can conclude that the acidity of the catalyst (acidity represented by both Brønsted and Lewis acid sites on the catalyst's surface) is an important factor to achieve a good catalytic activity. The most selective catalysts to 5-HMF in fructose dehydration and to N_2 in NO_x conversion are those with moderate acidity.

Coupling WO_x species with ZrO_2 gave rise to improved materials both in terms of surface acidity and structure stability. In the three series of tungstated zirconia (the commercial samples, coprecipitated samples and impregnated samples) WO_x species inhibited zirconia crystallite sintering and stabilized tetragonal ZrO_2 crystallites during high-temperature oxidative treatments. The calcination at 700 °C has been shown to be high enough to ensure

the complete elimination of the synthesis precursor as well as the physisorbed and structural water, and low enough to avoid the formation of WO_x crystallites at higher surface densities near to monolayer coverage on ZrO_2. FT-IR pyridine desorption studies have shown an obvious difference of surface acidity between zirconia and tungstated zirconia samples. The appearance of strong Brønsted sites on all the tungstated zirconia samples studied in this work can be associated to the presence of WO_x clusters on the surface. The calorimetry results show that the strength of the acid sites of the catalysts was rather heterogeneous. The acidity of the studied materials is proportional to increasing WO_3 (wt.%) loading.

Concerning the activity in the cellobiose hydrolysis over the WO_3/ZrO_2 catalysts prepared by coprecipitation, the extent of reaction was not higher than 10-12% at the longer reaction times. Selectivity to glucose was total with absence of any by-products. Zirconia displayed good activity (high reaction rate and kinetic constant), higher than that of catalysts loaded with 0.9 to 9.9 WO_3 wt.%. For higher WO_3 loadings, the hydrolysis activity of the catalysts increased and overcame that of zirconia. It was confirmed that the origin of catalytic activity of cellobiose hydrolysis from the WO_3 phase is primarily associated with the presence of Brønsted sites and with a WO_3 loading close to or above the monolayer (catalysts with a WO_3 loading of 15.2 and 19.0 wt.%). The WO_x clusters of the tungstated surface which act as an entity that prevails over the Lewis acid sites of the zirconia calcined at 700 °C enable the creation of a large number of Brønsted acid sites in the direct vicinity of the disaccharide reactant, thus encouraging the adsorption of cellobiose and hydrolysis of the glycosidic bonds.

Catalytic dehydration of fructose and its conversion to 5-HMF was studied using tungstated zirconia prepared by incipient wetness impregnation. The catalytic activity is related to the presence of strong acid sites, especially for the catalysts with WO_3 loading $\geq$ 10wt.%, while the yield to 5-HMF is associated with the medium strength acid sites. However, the influence of the amphoteric character of the investigated catalysts on the reaction mechanism is evident, and the presence of a small amount of basic sites seems to be important for an improved selectivity to 5-HMF, thus avoiding the formation of by-products. The results obtained in this work give evidence for the importance of the acid-base nature of active sites; further studies aimed at fine-tuning these characteristics should lead to more effective solid catalysts, which would allow higher selectivities and yield lower amounts of by-products.

The selective reduction of NO_x by hydrocarbons was studied over different catalytic systems consisting of zirconia mixed oxides with boria, alumina, india, gallia and tungsta. The samples were prepared by coprecipitation and a WO_3-containing sample supported on Al_2O_3-ZrO_2 sample was prepared to verify the influence of the tungsten oxide active phase deposited by impregnation. The acidity of the catalysts was increased by adding the second component to zirconia, except with boria. A certain degree of acidity seems to be favourable for NO_x conversion and selectivity towards N_2, while too strong acid sites (as in the case of WO_3-ZrO_2) favour the oxidation of the hydrocarbons that cannot react anymore as reducing agent. The determination of the number and strength of acid sites has proved to be an interesting tool to choose the active materials for HC-SCR.

Binary mixed oxides WO_3-Me_2O_3 (Me = Al, Ga, In) and ternary mixed oxides WO_3/(ZrO_2-Me_2O_3) (Me = B, Al, Ga, In) were prepared by coprecipitation and incipient wetness impregnation. Coupling WO_x species with ZrO_2 and Me_2O_3 (Me=B, Al, Ga, In) gave rise to improved materials both in terms of surface acidity and structure stability. The ammonia and sulphur dioxide adsorption microcalorimetry confirmed the amphoteric character of the samples except for the boria containing sample where we observed that the acidic features were more pronounced than the basic features. Pyridine adsorption FT-IR studies have shown that the surface acidity of the catalysts was due to the presence of Lewis acid sites and the appearance of strong Brønsted sites for tungstated alumina sample, which can be associated to the presence of WO_x clusters on the surface. It has been shown that these samples can be potentially applied as acidic catalysts in different environmental friendly reactions such as the selective catalytic reduction of NO_x by hydrocarbons, the best sample being Ga_2O_3-ZrO_2.

The results obtained in this work give evidence of the importance of the acid-base nature of active sites; further studies aimed at fine-tuning these characteristics should lead to more effective solid catalysts. The combination of different thermal, calorimetric, structural analyses and catalytic tests has made it possible to thoroughly analyze the samples. These materials can be applied as acidic catalysts in different environmentally friendly applications such as biomass exploitation, sugar transformation to valuable products and the selective reduction of NO_x by hydrocarbons.

Abbreviations

XRD	X-ray diffraction
BET	Brunauer, Emmett, Teller
XPS	X-ray photoelectron spectroscopy
ICP-OES	Inductively coupled plasma optical emission spectroscopy
FTIR	Fourier transformed infrared spectroscopy
TEM	Transmission electron microscopy
SEM	Scanning electron microscopy
TPR/O	Temperature-programmed reduction/oxidation
TPD	Temperature-programmed desorption
5-HMF	5-hydroxymethylfurfural
NO_x-SCR	Selective catalytic reduction of NO_x

TITRE en français

Synthèse et caractérisation de catalyseurs de type oxydes mixtes pour des applications environnementales.

RESUME en français

Ce travail est en relation avec la thématique "Chimie Verte" en particulier, le rôle de la catalyse, l'utilisation des matières premières renouvelables et l'élimination des produits nocifs.

- Quatre échantillons commerciaux de zircone tungstatée de Mel-Chemicals.
- deux séries de zircone tungstatée préparées par deux méthodes différentes avec une teneur en WO_3 de 1 à 20 % en masse.
- des oxydes binaires tels que WO_3-ZrO_2, B_2O_3-ZrO_2, Al_2O_3-ZrO_2, Ga_2O_3-ZrO_2 et In_2O_3-ZrO_2.
- des oxydes binaires tels que WO_3-Me_2O_3 (Me = B, Al, Ga et In) et finalement des oxydes ternaires WO_3/(Me_2O_3-ZrO_2) (Me = B, Al, Ga et In) ont été étudiés et préparés lors de cette thèse.

La performance catalytique de ces catalyseurs a été évaluée dans l'hydrolyse de la cellobiose, la déshydratation du fructose et la réduction catalytique sélective des NO_x. Les propriétés acides et redox de surface ont été corrélées aux performances catalytiques. En général, la conversion totale est liée à l'acidité des catalyseurs. Les catalyseurs les plus sélectifs pour la déshydratation du fructose et en deNO_x sont ceux présentant une acidité modérée.

MOTS-CLES

Catalyseurs à base de zircone, réactions catalysées par des solides acides, propriétés acides et redox, microcalorimétrie d'adsorption d'ammoniac et de dioxyde de soufre, IRTF de pyridine

TITRE en anglais

Synthesis and characterisation of various mixed oxides catalysts for environmental applications.

RESUME en anglais

This work is related to the subject "Green Chemistry" in particular the role of the catalyst, the use of renewable raw materials and the decrease of hazardous materials.

- Four commercial tungstated zirconia provided by Mel-Chemicals.
- Two series of tungstated zirconia catalysts prepared by two different methods in a range of (1-20) WO_3 wt.% loading
- Binary zirconia-based oxides WO_3-ZrO_2, B_2O_3-ZrO_2, Al_2O_3-ZrO_2, Ga_2O_3-ZrO_2 and In_2O_3-ZrO_2.
- Binary oxides WO_3-Me_2O_3 (Me = B, Al, Ga and In) and ternary oxides WO_3/(Me_2O_3-ZrO_2) (Me = B, Al, Ga and In) were prepared and studied during my PhD thesis.

The catalytic activity of these mixed oxide catalysts was evaluated in cellobiose hydrolysis, fructose dehydration and selective catalytic reduction of NO_x. The catalysts were thoroughly characterized in terms of their acidic and redox properties in order to find correlations between the identified active sites and the catalytic properties. The total conversion is related in general to the acidity of the tested catalysts and the most selective catalysts for fructose dehydration and deNO_x are those with moderate acidity.

DISCIPLINE

Chimie, Catalyse

MOTS-CLES

Zirconia based catalysts, solid acid catalysed reactions, acidic and redox properties, NH_3 and SO_2 adsorption microcalorimetry, Pyridine FTIR

INTITULE ET ADRESSE DE L'U.F.R. OU DU LABORATOIRE :

Institut de Recherches sur la Catalyse et l'Environnement de Lyon,
UMR 5256 CNRS/Université Lyon 1,
2 avenue Albert Einstein, 69626 Villeurbanne Cedex, France